

FOR REFERENCE ONLY

41 0618177 1



ProQuest Number: 10183151

All rights reserved

INFORMATION TO ALL USERS

The quality of this reproduction is dependent upon the quality of the copy submitted.

In the unlikely event that the author did not send a complete manuscript and there are missing pages, these will be noted. Also, if material had to be removed, a note will indicate the deletion.



ProQuest 10183151

Published by ProQuest LLC (2017). Copyright of the Dissertation is held by the Author.

All rights reserved.

This work is protected against unauthorized copying under Title 17, United States Code
Microform Edition © ProQuest LLC.

ProQuest LLC.
789 East Eisenhower Parkway
P.O. Box 1346
Ann Arbor, MI 48106 – 1346

Studies on Porosity in Polymer Latex Films and Particles

Ian C Hodges

**A thesis submitted in partial fulfilment of the requirements of the
The Nottingham Trent University for the degree of Doctor of Philosophy**

March 2003

LCN= 10362529

c

S. L. C.

REF

PH. D/CP/03 HOD

Abstract

The creation of porous latex films and particles has been studied. The methods evaluated for the creation of pores in polymer latex films were; leachable additives, exceeding the critical pigment volume fraction (CPVF) of the latex and flocculation of the latex prior to film formation. Pore formation in the latex films was evaluated by specific surface area (SSA) (nitrogen adsorption) and porosimetry (mercury intrusion) determination. Successful pore formation processes were applied to a functionalised latex and its catalytic activity evaluated. It was found that up to 90% of the catalytic activity of the original latex spheres could be retained by the film. A porous latex film was coated with chitosan and its metal chelation properties were evaluated against flakes of chitosan. The chitosan on the film adsorbed more metal ions from solution and at a faster rate than the chitosan flakes. Initial studies on the transport properties of non-functionalised porous latex films were evaluated via dynamic adsorption and advantages shown. Samples of a well characterised carbon adsorbent coated by nonporous and porous latex films were compared to determine hindrance to vapour sorption.

The method evaluated for creation of pores in latex particles was based on normal macroreticular resin synthesis, but using emulsion polymerisation rather than suspension polymerisation to achieve particles in the nanometre size range. Pore formation in latex particles was evaluated by SSA (nitrogen adsorption) determination and electron microscopy studies. The theoretical SSA of the particles calculated from the particle diameters was compared with the SSA obtained from the nitrogen adsorption determination. Latex samples were made with total SSAs of $554 \text{ m}^2 \text{ g}^{-1}$, which were $373 \text{ m}^2 \text{ g}^{-1}$ higher than

predicted by electron microscopy for non porous particles of the same diameter. Clear trends were seen with the ratio of styrene to divinyl benzene having the most effect on the creation of pores. Evaluation, by t-plots, of particles with more SSA than theoretically predicted showed that the pores were all in the microporous range.

Acknowledgements

I would like to thank my supervisor John Hearn for giving me the chance to study for a PhD and his guidance throughout. Francis Karpowicz and Arthur Richards for their help in the laboratory.

Contents

1	Introduction	1
1.1	General overview	1
1.2	Polymerisation	3
1.2.1	General	3
1.2.2	Emulsion polymerisation - surfactant above its cmc.	4
1.2.3	Emulsion polymerisation - surfactant free/below its cmc.....	8
1.2.4	Shot growth polymerisation.....	10
1.3	Film formation from a Latex	12
1.3.1	Overview	12
1.3.1.1	Stage I, evaporation and particle ordering	15
1.3.1.1.1	Homogeneous drying.....	16
1.3.1.1.2	Drying lateral to film surface	17
1.3.1.1.3	Particle ordering and packing	19
1.3.1.2	Stage II, particle deformation	20
1.3.1.2.1	Water/air interfacial tension	21
1.3.1.2.2	Polymer/air interfacial tension.....	25
1.3.1.2.3	Polymer/water interfacial tension.....	27
1.3.1.3	Stage III, further coalescence	27
1.4	Fate of surfactants during and after film formation.....	30
1.4.1	Dissolution	30
1.4.2	Separation to surfaces and islets.....	30
1.4.3	Separation into a continuous phase.....	31
1.4.4	Models of surfactant distribution.	32
1.5	Barrier characteristics of porous latex films	34

1.6	Polymer supports	35
1.6.1	Pore formation	37
1.6.1.1	Non-solvating porogen	38
1.6.1.2	Solvating porogen	40
1.6.1.3	Polymeric porogen	41
1.6.2	Chemical modification	42
1.7	Emulsion crosslinking copolymerisation	45
1.8	Characterisation methods	49
1.8.1	Nitrogen adsorption	49
1.8.1.1	Quantachrome	49
1.8.1.2	Adsorption and desorption isotherm	50
1.8.1.3	Nonane pre-adsorption	55
1.8.1.4	t-plot	56
1.8.2	Mercury porosimetry	58
1.9	Aims of current work	60
1.9.1	Porous latex films	60
1.9.2	Reactive porous latex films	61
1.9.3	Porous latex particles	61
2	Experimental	62
2.1	Materials	62
2.1.1	Latices	62
2.1.2	Additives	62
2.1.3	Polymerisation materials	63
2.1.4	Other materials	63
2.2	Latex preparation	64

2.2.1	PS latex preparation	64
2.2.2	PBMA latex preparation	64
2.2.3	Sulphonated PBMA latex preparation	65
2.3	Porous latex films.....	66
2.4	Sulphonated latex films.....	68
2.4.1	Conductometric titration	68
2.4.2	Electron microscopy.....	69
2.5	Reactive latex films.....	70
2.5.1	Reactive latex films - acid catalysis.....	70
2.5.2	Reactive latex films - metal complexation by chitosan	70
2.6	Porous latex particles.....	72
2.6.1	Shaken polymerisation's	72
2.6.2	Stirred polymerisation	73
2.7	Cleaning.....	75
2.7.1	Films	75
2.7.2	Porous particles	75
2.8	Characterisation.....	76
2.8.1	Nitrogen adsorption on the Quantachrome apparatus	76
2.8.2	Mercury porosimetry	76
2.8.3	Particle sizing – transmission electron microscopy.....	76
2.8.4	Kinetics	77
2.8.5	Vacuum frame.....	78
2.8.6	t-plots.....	79
2.9	Incorporation of porous latex particles into a porous latex film.....	80
2.10	Barrier characteristics of porous latex films	81

2.11	Calculations	82
2.11.1	Calculation of a particles extra SSA.....	82
2.11.2	Calculation of the number of pores in a porous film.....	82
3	Results and discussion	84
3.1	Porous latex films.....	84
3.1.1	Specific surface area	84
3.1.2	Porosimetry.....	86
3.1.3	Electron microscopy.....	94
3.1.4	Pore closure.....	97
3.2	Reactive latex films	101
3.2.1	Sulphonated latex characterisation.....	101
3.2.2	Film characterisation.....	101
3.2.2.1	Specific surface area.....	101
3.2.2.2	Porosimetry.....	102
3.2.3	Electron microscopy.....	106
3.2.4	Suggested pore generation mechanisms.....	109
3.2.4.1	Small molecule leachable additives	109
3.2.4.2	Large particulate leachable additives.....	111
3.2.4.3	Critical pigment volume fraction.....	112
3.2.5	Temperature study.....	113
3.2.6	Surface characterisation	115
3.2.7	Reactions with porous latex films.....	117
3.2.7.1	Catalytic activity.....	117
3.2.7.2	Copper chelation.....	121
3.3	Porous latex particles.....	125

3.3.1	Systematic variation of the polymerisation components	125
3.3.1.1	Variation of surfactant concentration.....	126
3.3.1.2	Variation of initiator concentration.....	127
3.3.1.3	Variation of DVB/styrene ratio.....	128
3.3.1.4	Variation of porogen concentration	130
3.3.1.5	Variation of oil soluble initiator concentration.....	132
3.3.1.6	Maximising extra surface area	132
3.3.2	Repeatability of shaken polymerisations.....	133
3.3.3	Effect of initiator and surfactant conc' on particle number.....	133
3.3.4	Varying organic phase components in a stirred reactor	135
3.3.4.1	Comparison of shaken and stirred reactors.	140
3.3.5	Nonane pre-adsorption	142
3.3.6	t-plot.....	146
3.4	Incorporation of porous latex particles into a porous latex film.....	147
3.5	Barrier characteristics of porous latex films	148
4	Conclusion	150
5	Further work.....	152
5.1	Super water-repellent surfaces	152
5.2	Controlled release.....	152
5.3	Further understanding.....	153
6	Appendix.....	154
6.1	Abbreviations	154
7	Index.....	156
7.1	Index of figures	156
7.2	Index of charts	159

7.3 Index of tables.....	162
8 References	163
Published papers	Back

1 Introduction

1.1 General overview

Chemical reagents and catalysts attached to polymeric supports offer the prospect of cleaner, more environmentally friendly, chemistry. Corrosive, noxious and toxic species can be rendered safe, and expensively synthesised molecules and precious metal complexes can be more effectively recovered and reused when immobilised on a polymeric support¹. Activity in the commonly used coarse macroreticular resin beads is however limited, in part, by external mass transfer and intra-particle diffusion to active sites^{2,3}. Activity of non-porous polymer spheres increases as the particle size decreases because the surface area to weight ratio is inversely related to particle diameter. Colloidal sized polymer particles, such as latex particles, are promising catalyst supports because of their high specific surface area and the ability to concentrate organic reactants in the active catalyst phase by absorption from water⁴. Manufacturing processes involving aqueous colloids rather than organic solvents would also reduce the need for solvent recycling and disposal⁵.

Functionalised latex particles have proved viable catalysts⁶ for a variety of oxidation and hydrolysis reactions in which high electrolyte concentrations are not required. Functional groups have included sulphonic acids^{7,8}, a primary amine⁹ and imidazoles¹⁰ for ester hydrolysis and cobalt complexes for autoxidation of organic compounds^{11,12,13,14}. Catalysts are sought for environmental use, which would be capable of oxidising all organic compounds in industrial waste water to carbon dioxide¹⁵ as well as for use in chemical manufacturing processes.

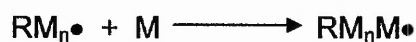
Colloidal catalysts are however, more difficult to recycle than large beads, needing to be either ultrafiltered or coagulated and redispersed for repeated use⁶. Under usual phase transfer catalytic conditions charged particles are impractical because of fast coagulation by electrolytes¹⁶. These latter disadvantages of latex catalysts, with respect to ease of recovery and sensitivity to electrolyte addition, may be overcome if the functionalised latex is presented in the form of a film. Thin polymer latex films, with glass transition temperatures close to the physiological temperature, have been shown to offer better mechanical strength, chemical and temperature stability than the more commonly employed soft gels, such as alginate or polyacrylamide, for use with trapped and immobilised viable microbial cells in biocatalytic applications¹⁷. The problems of predominantly diffusive transport of reactants and products within the gels were also overcome.

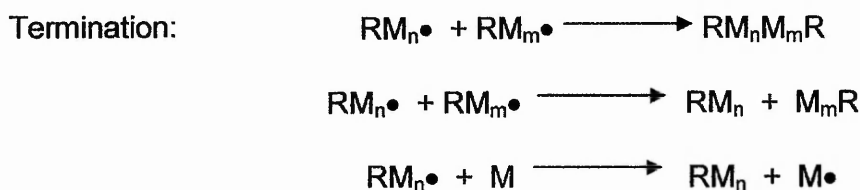
1.2 Polymerisation

1.2.1 General

An emulsion polymerisation typically consists of water, monomer and initiator, with the option of a surfactant. Other components, such as chain transfer agents, retarders and inhibitors can be incorporated to control the particle characteristics. The mixture is stirred and heated to a temperature above the decomposition temperature of the initiator, producing free-radicals, which start the polymerisation reaction.

Free-radical polymerisation can be split into three separate reactions, namely initiation, propagation and termination. Initiation begins with the thermal decomposition of the initiator forming free radicals. The free radicals quickly react with a monomer unit forming a monomer radical which continues to add more monomer, forming a growing polymeric radical. Termination of the polymeric radical can take place via 1) combination 2) disproportionation or 3) transfer reactions. Combination is the process whereby two growing polymeric radicals terminate by joining together resulting in one dead polymer chain. Disproportionation reaction proceeds by two polymeric radicals terminating, but not joining together resulting in two dead polymer chains. Chain transfer occurs when the radical is transferred to monomer, initiator or polymer, resulting in a dead polymer chain and a newly initiated radical, which can react further.





1.2.2 Emulsion polymerisation - surfactant above its cmc.

In conventional emulsion polymerisation the reaction components include a surfactant above its critical micelle concentration. The mixture is homogenised to form the emulsion resulting in monomer in three locations 1) inside micelles 2) surfactant stabilised monomer droplets 3) the aqueous phase. In 1945, Harkins¹⁸ postulated that the main locus of polymerisation is in monomer swollen polymer particles, formed from a radical entering a monomer-swollen micelle, rather than the monomer droplets. This is due to the relative large number of micelles (typically 10^{18} per gram of emulsion) and, therefore, surface area available for radical absorption compared to monomer droplets (typically 10^{12} per gram of emulsion). Nucleation begins when a z-mer, a radical which has achieved a degree of polymerisation to become surface active e.g. $z = 2-3$ for styrene¹⁹, enters a micelle. Once inside the monomer swollen micelle the radical can propagate readily in the monomer rich environment. These nuclei grow by polymerisation of monomer supplied by diffusion through the aqueous phase from monomer droplets and continue to be stabilised as they grow, by a supply of surfactant molecules obtained from uninitiated micelles. Nucleation stops when all the micelles are gone, so that no new particles are formed. This process is shown schematically in Figure 1 (adsorbed surfactant on the mature particle has been omitted for clarity).

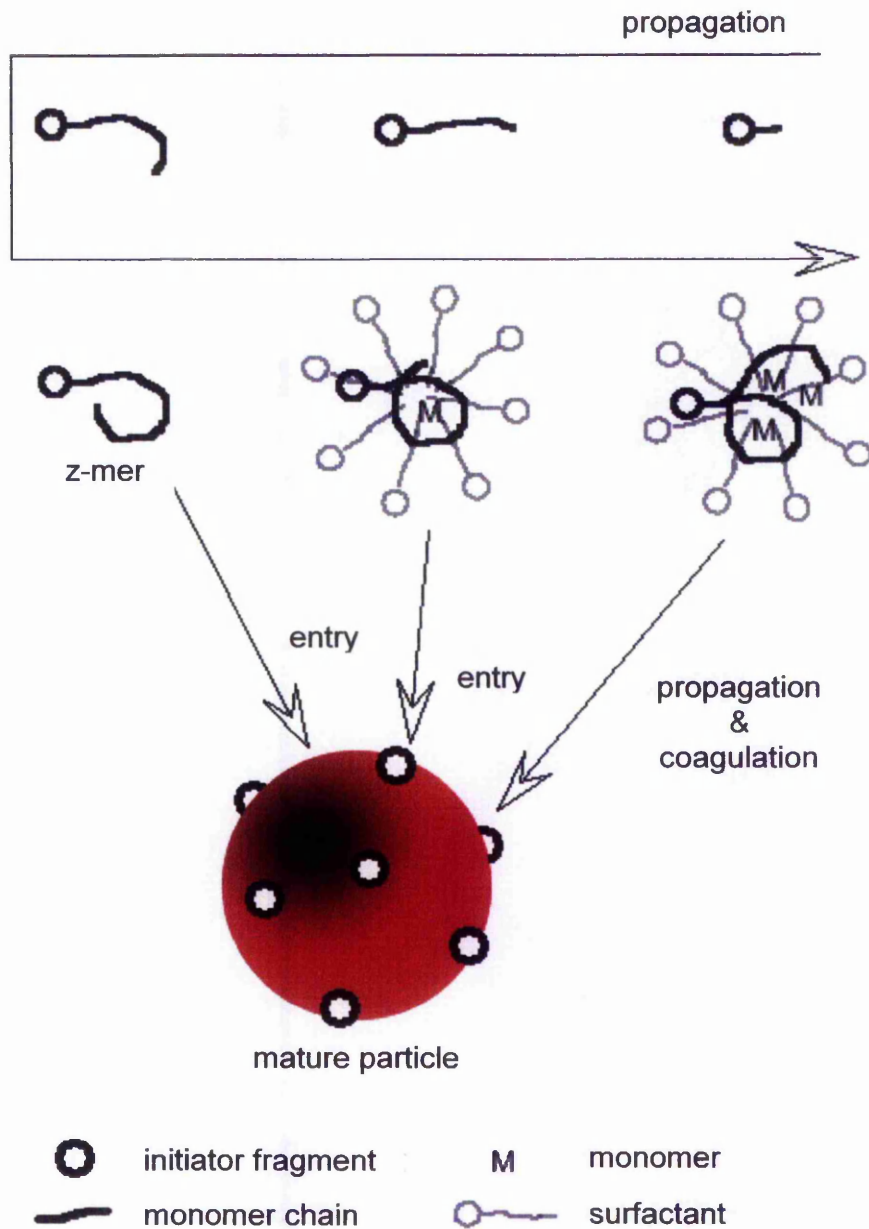


Figure 1: Particle formation in the presence of surfactant above its cmc.

In the late 1940's Smith and Ewart^{20,21,22} put Harkins picture under quantitative treatment and produced the framework for emulsion polymerisation kinetics. Subsequent research extended the treatment of the nucleation or particle formation mechanisms^{23,24,25,26,27,28,29,30}, particle growth mechanisms^{31,32,33,34,35,36,37}, determinants of particle size distribution^{38,39,40,41,42}

and particle morphology^{43,44,45,46}. It is now widely accepted that emulsion polymerisation proceeds through three main stages.

1. In this initial stage, the nucleation of latex particles takes place. The system is characterised by the presence of monomer-swollen surfactant micelles and monomer droplets, and an increase in latex particle number and particle size.

2. The second stage starts when the nucleation of the particles is complete. It is characterised by the absence of surfactant micelles, a constant number of monomer-swollen latex particles, a constant monomer concentration within the latex particles and an increasing particle size.

3. The final stage begins when the monomer droplets are all gone, and the remaining monomer is confined to the latex particles. It is characterised by a constant number of latex particles and a decreasing monomer concentration in the latex particles.

These three stages can be seen in a conversion vs time plot (Figure 2).

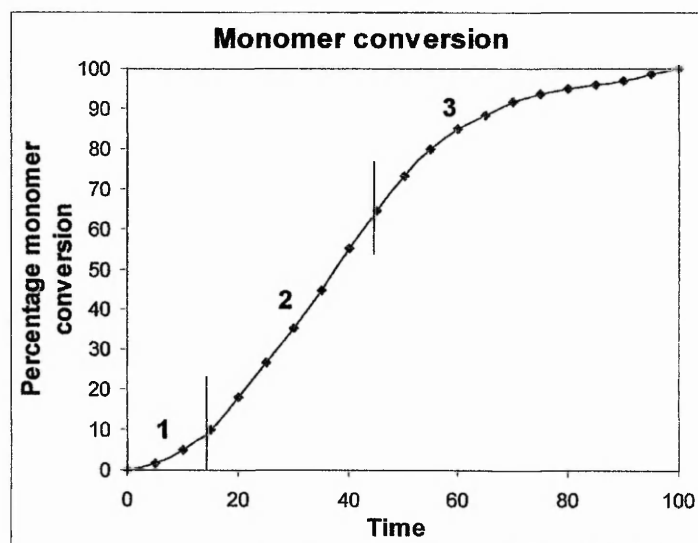


Figure 2: Monomer conversion vs. time plot for emulsion polymerisation in the presence of surfactant above its cmc.

First there is a stage of increasing rate of conversion, stage 1. This is because the free radicals generated from initiator decomposition initiate the polymerisation in the micelles thus the particle number increases during the nucleation period. The more sites of polymerisation, the more monomer that is polymerised. A point is reached where no more particles are nucleated and the rate of monomer conversion becomes constant, stage 2. This is because the particle number and monomer concentration (supplied by monomer droplets maintaining the equilibrium) within particles are constant. When the monomer droplets are used up the monomer concentration within particles starts to decrease resulting in a drop in rate of conversion, stage 3.

Control over the final particle properties can be achieved at a given temperature either by varying the initiator concentration or the surfactant concentration. By varying initiator or surfactant levels, the number of nucleated micelles produced during stage one of the polymerisation, and therefore the number of growing polymer particles, can be varied. Increasing the amount of initiator in the system increases the amount of free radicals available for absorption into monomer-swollen micelles, therefore, increasing the number of nucleated micelles. This produces more growing polymer particles, which compete for available monomer resulting in an increase in reaction rate, an increase in particle number and a decrease in particle size. Increasing the amount surfactant in the system increases the number of monomer-swollen micelles available for initiation during the nucleation stage so a larger number of nucleated micelles are formed. Again, more growing polymer particles competing for available monomer results in an increase in reaction rate, an increase in particle number and a decrease in particle size. From Smith and

Ewart's²¹ quantitative treatment it was shown that the number of particles formed is proportional to the concentration of initiator to the power 0.4 and to the concentration of surfactant to the power 0.6. Experimentally, this was found to be true for monomers of limited water solubility such as styrene.

1.2.3 Emulsion polymerisation - surfactant free/below its cmc

Surfactant free emulsion polymerisation was derived from conventional emulsion polymerisation when polymerisation was carried out in the absence of added emulsifier. This technique is ideal for preparing model colloids with narrow particle size distributions and well characterised surface properties. Surfactant free polymerisation was first described by Matsumoto and Ochi⁴⁷ for the preparation of monodisperse polystyrene latex. A number of mechanisms have been proposed for the formation of a stable latex in the absence of surfactant, including a homogenous nucleation mechanism^{48,49}, an oligomer "micellisation" mechanism⁵⁰, and the coagulation mechanism^{29,51,52}. Studies on the surfactant free polymerisation of the styrene/potassium persulphate/water system⁵⁰ found the presence of styrene oligomers in the nucleation stage suggesting that an oligomer micellation mechanism was operating. The surface active nature of the oligomers could lead to association below the cmc when, being reactive, they could terminate. However, it has been calculated that in systems with normal levels of initiator it is not possible to form a concentration of surface active species above their cmc¹⁹. Current evidence points to a joint homogeneous nucleation and coagulation mechanism⁵³ (Figure 3).

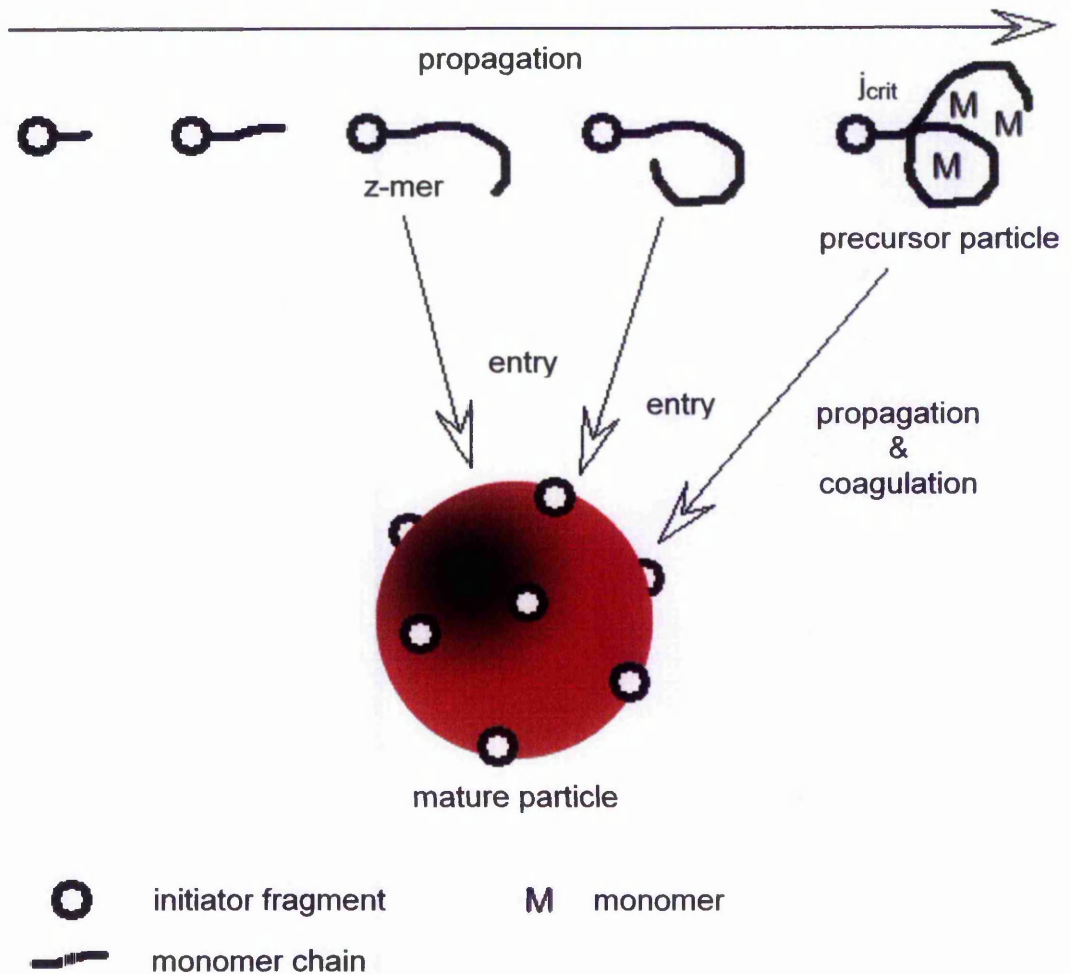


Figure 3: Particle formation in the absence/presence of surfactant below its cmc.

Once the initiator decomposes it forms a growing polymer chain. Initially, the initiator fragment is not able to enter a mature particle, but once a certain number of monomer units have combined the polymeric radical is able to enter a mature particle. Such a species is termed a z-mer and for styrene is approximately 2-3 units¹⁹. However, at the beginning of polymerisation there are no mature particles present so the polymeric radicals continue to grow until a degree of polymerisation j_{crit} (approximately 5 for styrene⁵⁴) is reached where it becomes “insoluble” and forms a coiled chain conformation which excludes water and

absorbs monomer into its interior. These precursor particles continue to grow through propagation of monomer absorbed from the aqueous phase and through coagulation with other precursor particles. Colloidal stability is achieved from surface sulphate end groups from the initiator fragments. Coagulation continues until a point where there are so many mature particles that growing polymeric chains are adsorbed as z-mers before they grow to J_{crit} -mers, and precursor particles are no longer formed. At this point nucleation stops. Polymerisation continues within the monomer swollen polymer particles and the particles growth resembles that of conventional emulsion polymerisation.

For polymer latices prepared in the absence of emulsifier, latex stability is provided by like-for-like charge repulsion by the charged end groups of polymer chains, resulting from radicals on the surface of the particles⁵⁵. As a result of this, it has been shown that the particle number density and, therefore, the final particle size can be controlled by varying the ionic strength of the aqueous medium⁵⁶. With increasing ionic strength, at constant initiator concentration, the particle size increases and the particle number decreases accordingly⁵⁷. Increasing the initiator concentration at constant ionic strength increases the particle number⁵⁶.

1.2.4 Shot growth polymerisation

Monodisperse polymer latices with high surface charge densities can be prepared via the shot-growth polymerisation method⁵⁸. Shot-growth is popular for preparing model colloids due to the control over surface properties this method provides. A polymer particle core is over coated with a polymer shell in a single stage surfactant-free polymerisation. The core is prepared by

polymerising to ~90% monomer conversion, at which point a shot of extra monomer is added to the polymerisation mixture, which binds onto the surface of the core particles. A lower number density can be used without secondary particle formation and the shell is more strongly bound to the core than in seeded-growth polymerisations⁵⁸. Initially developed to alter the mechanical properties of polymer latex films by over coating a hard polymer core with a soft polymer shell, shot-growth was further developed to control surface charge densities in model systems⁵⁹, and to prepare lattices for crystalline arrays⁶⁰.

1.3 Film formation from a Latex

1.3.1 Overview

Latices consist of small polymer spheres dispersed throughout a water medium. Stability of the spheres is preserved by surface charge repulsion or steric hindrance of adsorbed molecules on the particle surface. When water is allowed to evaporate at a sufficiently high temperature⁶¹, to exceed the minimum film forming temperature (MFFT), a fully coalesced polymer film will form. Film formation from stabiliser free latices can be described in three steps:

1. Increasing concentration of spheres as water evaporates, up to a phase ratio of 0.74 where a dense close packing order is achieved.
2. Deformation of the spheres into rhombic dodecahedra⁶². filling the interstitial voids between particles as water leaves, to form a coalesced film.
3. Further coalescence by interdiffusion of polymer chain ends between neighbouring particles to form a mechanically strong film.

This process is shown schematically in Figure 4.

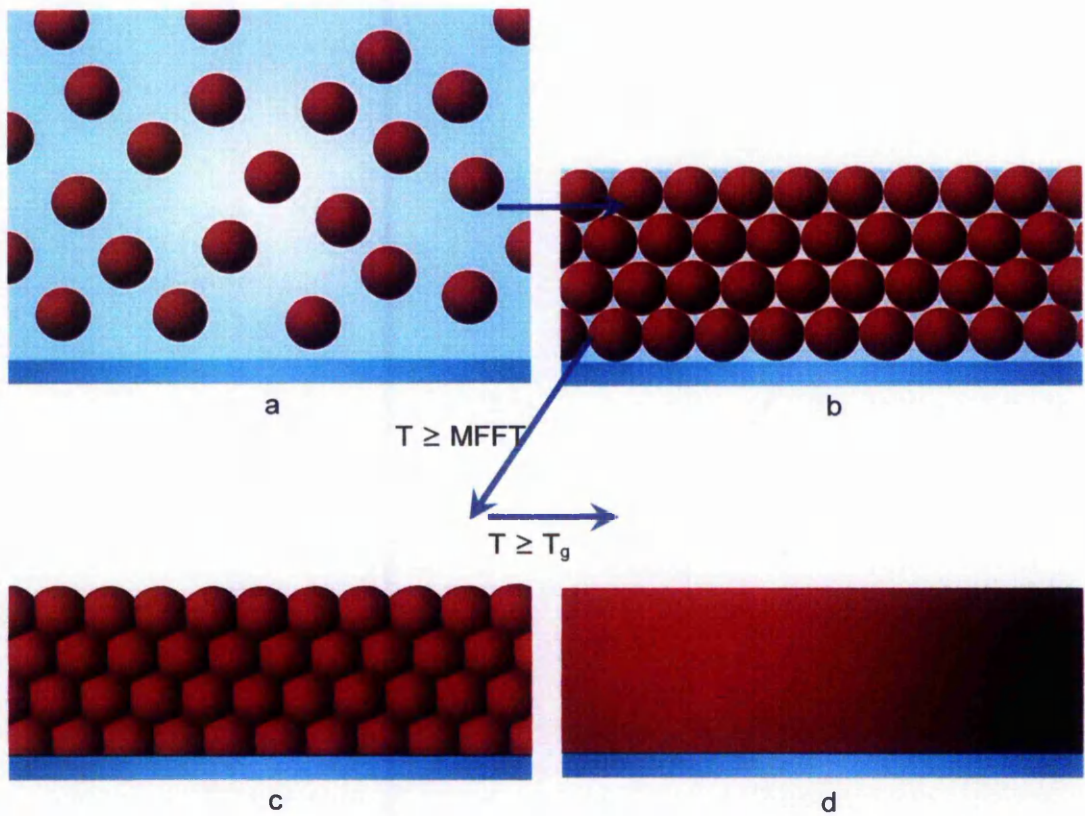


Figure 4: Film formation from a latex dispersion. a) Latex particles suspended in water. b) Latex particles close packed with water filled interstices. c) Deformed particles with no water present. d) Fully coherent polymer film.

Figure 5 is a SEM micrograph of the surface of a freeze fractured poly(butyl methacrylate) (PBMA) film cast at 50°C. Note that no trace of the original spherical particles is left (original particle diameter was 238 nm).



Figure 5: Freeze-fractured SEM photograph of a PBMA film cast at 50°C.

Measurement of MFFT is determined on a metallic bar possessing a temperature gradient along its length^{63,64}. The latex is spread on the bar and allowed to dry, and the minimum temperature at which optical clarity occurs is termed the MFFT. Far below the MFFT a typical latex forms an opaque powder, as the temperature nears the MFFT an opaque film is formed with limited mechanical strength. Just above the MFFT the latex forms a cracked optically clear⁶⁵ film with increased mechanical strength. At a higher temperature the latex film becomes continuous and free of cracks and achieves its full mechanical strength. The minimum temperature where no cracks are formed is termed the crack point, and indicates the onset of particle-particle cohesion.

1.3.1.1 Stage I, evaporation and particle ordering

Vanderhoff⁶⁶ identified three stages of water evaporation during film formation. Initially, in the diluted latex system, water evaporates at a rate comparable to that of latex serum alone. As the latex becomes so concentrated as to form a close packed structure of particles, the evaporation rate drops off as the water/air interface area decreases. In the later stages, water escapes slowly via diffusion through capillaries between particles, over time changing to diffusion through the polymer as the capillaries close up.

Croll⁶⁷ studied the drying rates of a film-forming acrylic latex and non-film-forming slurries of mica and titanium dioxide and polyester particles and suggested a two stage mechanism. Measurement of the initial rate of water loss was found to be constant and at 85% that of the serum alone, suggesting that the rate of water loss was reduced by particles reducing the water/air interface area. The rate of water evaporation from highly dilute slurries, for the first few minutes only, was equivalent to water alone. This can be explained by recent work by Sutanto *et al*⁶⁸ who showed that particles are carried to the water/air interface and form a closed packed structure during drying due to the flux of water, reducing the water/air interface even in dilute systems.

Okubo *et al.*⁶⁹ observed a skin visible with the naked eye and with enough mechanical strength to be removed. Gravimetric determination showed it to contain 5% weight of water and they postulated that skin formation was responsible for the reduced rate of water loss.

Surfactant has been shown to modify the drying mechanism⁷⁰. Surfactant free PBMA latex dried uniformly to face centred cubic (FCC) packing resulting in rhombic dodecahedron particles once deformation was complete. Addition

of sodium dodecyl sulphate (SDS) produced a drying front moving from the edge inwards and disrupted the packing of particles due to surfactant crystallites. As a general rule,⁷¹ latices with low ionic strength tend to dry homogeneous, while latices with higher ionic strength dry via a propagation front. Surfactants have been shown to hinder as well as enhance the evaporation of water from the film. Isaacs⁷² found that a fatty-acid surfactant added to styrene-butadiene rubber latex slowed the rate of water evaporation once the content was below about 5 weight percent. This was attributed to the hydrophilic surfactant retaining water. However, in the same study, addition of SDS to acrylic latices was shown to enhance the evaporation rate, ascribed to the presence of hydrophilic membranes that assist the transport of water to the surface.

1.3.1.1.1 Homogeneous drying

Under conditions of homogeneous drying, water is lost until a water saturated close packed structure is formed. Water evaporation and particle deformation occur simultaneously at the same rate across the film so deformation and water loss is complete at all points in the film at the same time.

Chevalier *et al*⁷³ studied the film formation of soft polymer latices in the absence and presence of surfactant by small angle neutron scattering (SANS). Latices in the absence of surfactant were seen to dry uniformly with equal film thickness and water content throughout the film. A schematic representation of this process is shown in Figure 7.

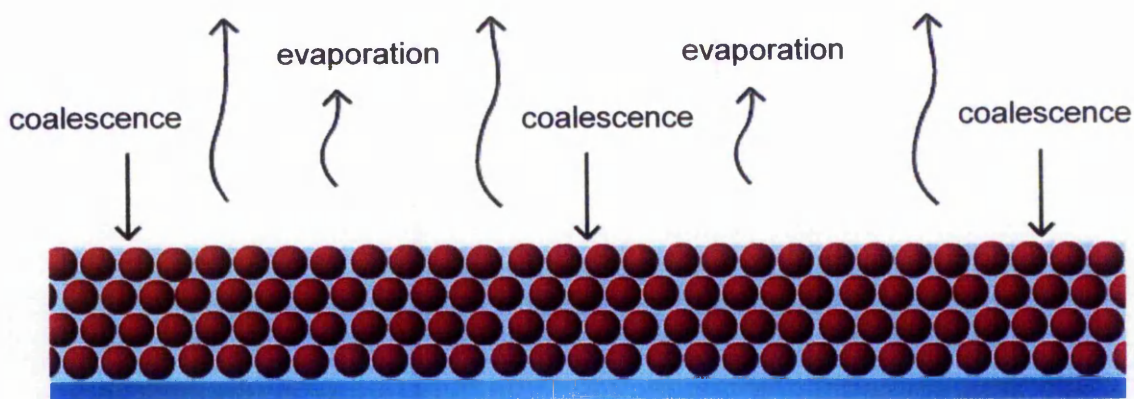


Figure 7: Schematic diagram of a drying front normal to the surface.

1.3.1.1.2 Drying lateral to film surface

Often inhomogeneous drying of latex occurs as reported by Hwa⁷⁴. The drying film consists of a turbid wet middle with a surrounding optically clear 'dry' area. Between the two is a clouded area composed of flocculated particles, which do not redisperse in water. Gravimetric analysis of the three areas showed that the dry area had 5% water, the intermediate area had 10% water and the middle had 65% water content. An explanation for this is that the edges of the latex will be thinner than the middle (true for a convex shape) so will dry sooner if there is no lateral transport of water. Likewise, if the latex is cast in a dish with vertical walls a concave shape is formed and the latex now dries from the middle (where the latex is now thinnest) outward.

Chevalier *et al*⁷³ when studying film formation of soft polymer latices, in the presence of surfactant, by SANS, noted that the convex films dried from the surface inwards with 'dry' transparent edges and a wet turbid centre. During drying the dry area moves inward and the wet area shrinks, but stays the same thickness suggesting that water is pushed from the 'dry' area into the

wet area replacing water lost by evaporation. After complete water loss the centre was found to be slightly turbid and lumpy where hydrophilic material had gathered, carried by the water flux. They found a sudden collapse from a gas-like dispersion (particles floating around) to a crystal dispersion (particles efficiently close packed) during SANS measurements. This was attributed to the dry-region/wet-region interface passing through the area under the neutron beam and they termed this interface a coalescence front. A schematic representation of this process is shown in Figure 8.

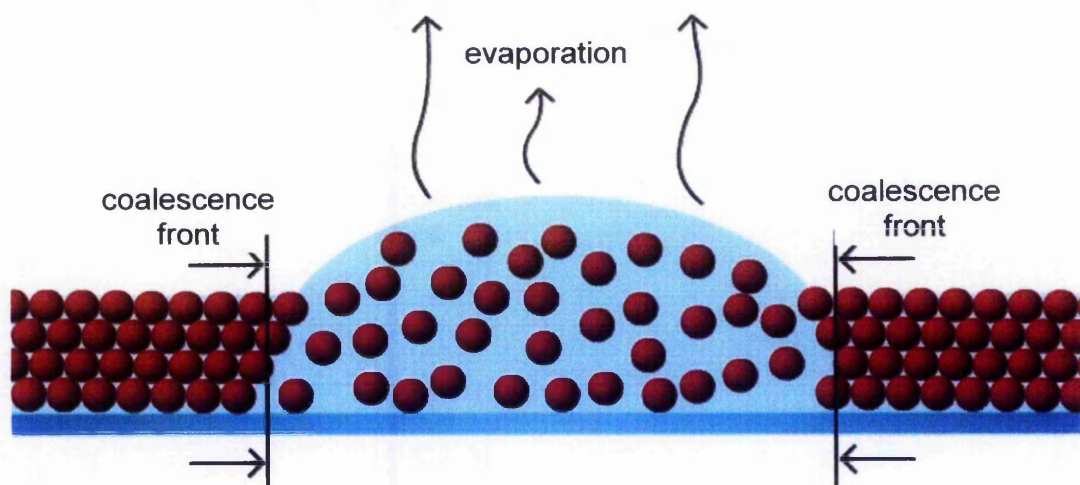


Figure 8: Schematic diagram of a drying front lateral to the surface.

Keddie *et al* followed the passage of a drying front through the film by ellipsometry⁷⁵. It found the front velocity to be temperature dependent due to the temperature dependence of water evaporation and particle deformation. Like many other workers, they found a cloudy region separating the turbid and clear regions, which might be where the drying front has moved through the film leaving an area where the particles have not fully coalesced to eliminate air voids. Cryogenic SEM⁷⁶ has similarly revealed the presence of a drying

front, where the area is void of water, and also a consolidation front where the particles have coalesced eliminating all air.

1.3.1.1.3 Particle ordering and packing

Analysis of dried latex films by light scattering⁷⁷, small angle x-ray scattering (SAXS)⁷⁸ and SANS⁷⁹ has confirmed the presence of FCC packing, forming a colloidal crystal. The evaporation rate of water and particle repulsion plays an important role in particle ordering. Fast evaporation leads to less crystalline order because the particles do not have time to arrange into a close packed order. Particles that repel each other strongly will not come into contact with each other until a later stage giving more time to allow the development of the ordered array. Melt-pressed latex films prepared from a freeze-dried latex show much less ordering than a film prepared by water evaporation at 40°C and atmospheric pressure⁸⁰.

Electrolyte added to the aqueous serum also effects packing as shown by a study of drying latex films in the chamber of an environmental scanning electron microscope⁸¹. In the absence of added salt an ordered array of particles was formed at the film surface. With addition of electrolyte into the latex, films are formed with a disordered surface. Increasing ionic strength of the serum as water evaporates causes particles to flocculate. It is these flocs, rather than individual particles⁸², that are consolidated by the drying front producing a disordered structure.

Isaacs⁸³ was the first to propose the relationship between surfactant addition and particle ordering. Particle flocculation before ordering prevents development of a close packed structure. Addition of surfactant enhances

particle stability preventing the particles from flocculating, promoting the formation of a close packed structure. Roulstone *et al*⁸⁴ studied the permeability of PBMA films with varied concentrations of post-added SDS. The permeability was found to reach a minimum when the concentration of SDS corresponded to monolayer surface coverage of the latex particles. The reduced permeability was ascribed to enhanced particle packing. At higher levels of addition, microscopy studies, showed the presence of a separate SDS phase, which lead to higher permeability.

1.3.1.2 Stage II, particle deformation

Early theories on particle deformation relied mainly on results from MFFT measurements. The polarity of the latex was found to alter the deformation properties by plasticisation of the particles by water. Brodnyan and Konen⁸⁵ found that by varying the polarity of an acrylic latex the MFFT could vary from the polymers T_g by 3°C below and 10°C above. The more polar latices having the lower MFFT.

Theoretical work by Lissant⁸⁶ predicted that particles deforming from FCC packing, to eliminate all voids, will form rhombic dodecahedra. Roulstone *et al*⁸⁷ and later Wang *et al*⁸⁸ confirmed the existence of rhombic dodecahedra via freeze-fracture transmission electron microscopy (FFTEM) studies on surfactant free PBMA films prepared under conditions where the particle boundaries were still present after film formation (Figure 9).

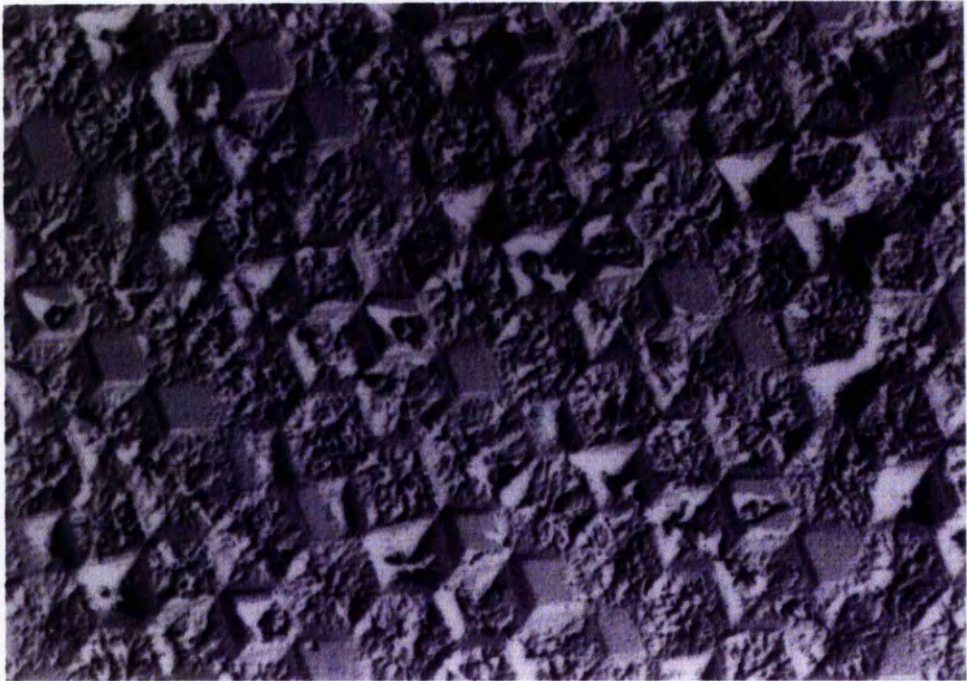


Figure 9: FFTEM photograph of a PBMA film dried at room temperature.
(Photograph courtesy of B.J. Roulstone)

The forces involved in particle deformation can arise from water/air, polymer/air and polymer/water interfacial tensions. Which is the most significant is a topic of debate, and most likely all are involved with one becoming dominant depending on the casting conditions.

1.3.1.2.1 Water/air interfacial tension

Forces arising from the water/air interface tension result from the small radii of curvature between particles as water evaporates. Deformation of the particles pushes water out reducing the radii of curvature and relieving stress at the water/air interface. Figure 10 shows the capillary force of interstitial water acting on three neighbouring particles.

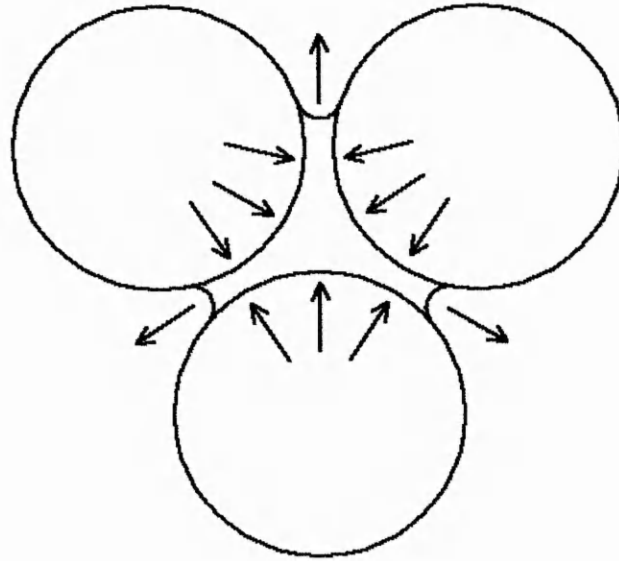


Figure 10: Capillary force of interstitial water acting on three neighbouring particles.

Brown⁸⁹ noted that film formation was complete at the same time that evaporation finished, concluding that the polymer/air interfacial tension was not significant. Slowing the evaporation rate slowed film formation and a wet latex film formed at lower temperature than dry latex, which was attributed to plasticisation by water and to capillary forces. Brown developed a formula to predict if film formation will occur. Taking capillary forces as the main force involved in deformation and the resistance to this force being the mechanical resistance of the polymer he predicted that film formation will occur when:

$$G_t < \frac{35\gamma}{r} \quad \text{Equation 1}$$

G_t being the polymers shear modulus, γ the water/air interface tension and r the particle radius. At constant G_t and γ , r must be below a certain size for film

formation to occur. At constant γ and r the temperature at which film formation occurs will depend on the temperature dependence of G_t . Vanderhoff *et al*⁶⁶ found that capillary forces are important in the early stages of film formation, although his conclusions were based on calculations assuming water evaporates from the neck region of particles in contact, not, like Brown, from the double layer surrounding each particle⁹⁰.

Objections to Brown's theory have come from many authors. Sheetz noticed that Brown had taken the contact angle between water and polymer as zero. If the angle is greater than zero then there will be a component of capillary force normal to the film and a component in the plane of the film⁹¹. Mason⁹² pointed out that Brown's assumption that capillary forces and forces of elastic resistance act over the same area is incorrect and modified for the correct areas.

Eckersley *et al*⁹³ took the viscous deformation into account, previously not considered by Brown and Mason, as well as elastic deformation. Using the time-dependent creep compliance to relate the radius of the circle of contact between two spheres to a constant capillary pressure, they derived the following criterion for film formation:

$$\frac{1}{J(t')} < \frac{34\gamma}{r} \quad \text{Equation 2}$$

Where $J(t')$ is the time-dependent compliance of the polymer. They concluded that capillary forces alone were insufficient to cause the deformation they observed, suggesting that capillary forces work together with surface forces. Eckersley and Rudin developed a two stage deformation model⁹⁴. Firstly

capillary forces deform the particles and secondly surface forces complete deformation. The surface force in operation will depend on the presence of water or not. With water present the water/polymer surface tension drives deformation and in the absence of water the polymer/air interfacial tension drives deformation.

Lin and Meier⁹⁵ studied the deformation rate of hydrophobic particles on the surface of a film with and without condensed water, providing evidence that capillary forces are the main driving force in deformation. The surface corrugation height of a PBMA film was monitored over time with atomic force microscopy and they found that the presence of water condensation reduced the time taken for particle flattening by as much as ten times.

Studies by Sperry⁹⁶ found that hydrophilic polymers had lower wet MFFT than dry MFFTs as a result of plasticisation by water and that hydrophobic polymers wet and dry MFFTs were the same. This suggested that capillary forces do not give a significant contribution to particle deformation.

More evidence against capillary forces include the limiting conditions of relative humidity and temperature for film formation for a range of latices with and without surfactant⁹⁷. It was found that the limiting conditions were the same for all the latices, irrespective of whether surfactant was present. The fact that surfactant has no effect on the limit conditions for film formation, considering addition of SDS at 1.6 g l^{-1} will reduce capillary forces by a factor of two, is evidence again that capillary forces do not play a major role.

1.3.1.2.2 Polymer/air interfacial tension

The forces necessary for deformation, arise from the favourable reduction in polymer surface area and resultant decrease in polymer surface energy. Figure 11 shows the forces acting on two particles once a neck has formed.

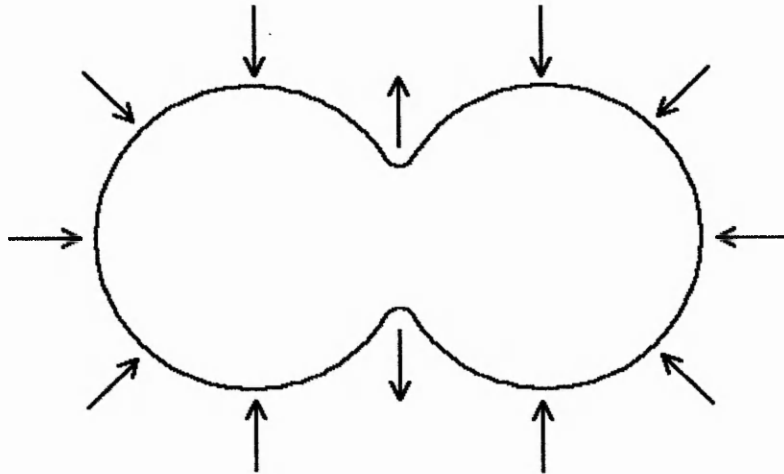


Figure 11: Polymer/air interfacial tension forces acting on two particles.

Dillon⁹⁸ adapted Frenkel's⁹⁹ theory of metal sintering to the concept of particle deformation in air. Frenkel's equation relates the area of contact between particles to time, polymer/air interfacial energy, polymer viscosity and radius of particles. Dillon found the equation to give good agreement with the sintering of poly(vinyl chloride-co-vinylidene chloride) and PS on a collodion film. They concluded that sintering of latex particles takes place by viscous flow of the polymer, the polymer/air interfacial tension providing the necessary energy. Under the conditions of these experiments the driving force could only be the polymer/air interfacial tension. However, as found by Brown and Sheetz, film formation and water evaporation finish concurrently so that the vast majority of particles will not be in contact with air.

Sperry proposed that the role of water in particle deformation depends on the temperature at which the film is cast⁹⁶. This affects the relative rate of water evaporation and particle deformation. Below a certain temperature evaporation is complete before full particle deformation. The particles will continue to film-form under the action of the polymer/air interfacial tension. Above the certain temperature water evaporation will be rate limiting and the particles will deform immediately after water evaporation. Figure 12 shows this principal schematically. At point A the particles are still immersed in water and deformation will not occur. With time the remaining water will evaporate and the particles will close pack and deform as soon as the water leaves. At point B all the water has evaporated leaving air voids in the film. With time the particles will continue to deform, filling the voids, via viscous flow of the polymer under the force of the polymer/air interfacial tension.

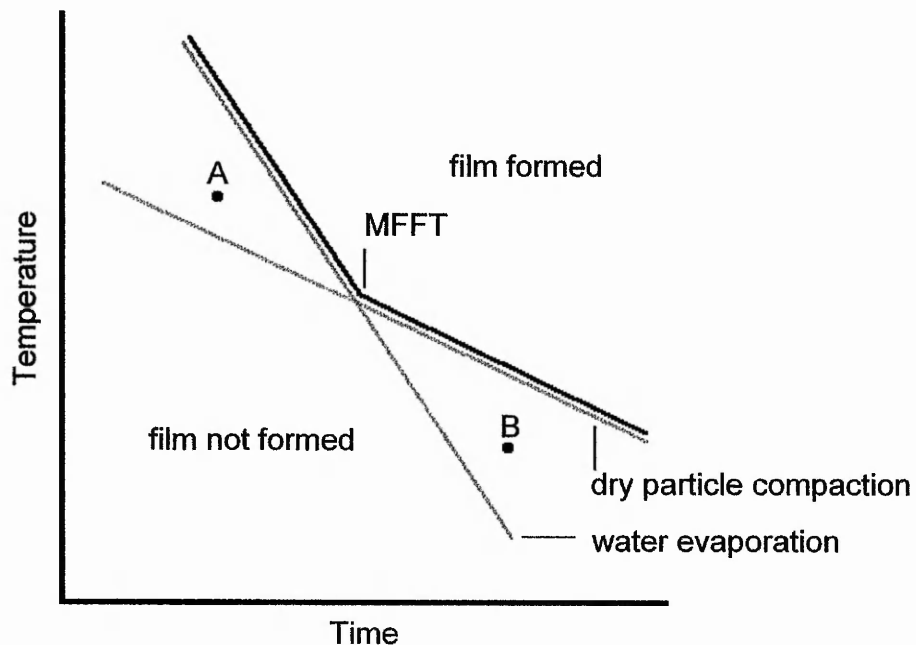


Figure 12: Limiting conditions for film formation from a latex dispersion¹⁰⁰.

1.3.1.2.3 Polymer/water interfacial tension

The forces acting on the particles are similar to those resulting from the polymer/air interfacial tension, but the interfacial surface energies of the polymer/water interface are lower.

One of the earliest papers concerning film formation attributed particle deformation to the polymer/water interfacial tension¹⁰¹. Later Vanderhoff⁹⁰ further developed the role of polymer/water interfacial tension, arguing that film formation did not show a strong particle size dependence, as predicted by Brown's model and air sintering models.

Sheetz provided evidence that the polymer/water interface can provide enough energy for particle deformation by measuring the change in solid content of wet latex agglomerates¹⁰². Dobler *et al*⁹⁷ studied the solid contents of latex agglomerates in water over time and found that the rate of solid content increase increased with increasing polymer/water interfacial tension. They concluded, however, that under normal conditions of film formation the polymer/water interfacial tension has a negligible effect on particle deformation.

1.3.1.3 Stage III, further coalescence

After deformation of the particles into a void free film, physical contact between particles will not be sufficient to form a strong film. Voyutski¹⁰³ was the first to suggest that, to obtain a mechanically strong film, interdiffusion of chain ends between particles is necessary to form a continuous material. However, mechanically strong films can result where the particles retain their identity as shown before in Figure 9. Insight into interdiffusion of polymer

between homogenous latex particles has been gathered mainly by SANS^{104,105}, and nonradiative energy transfer (NET) experiments^{106,107,108,109,110}. Using SANS measurements it was found that decreasing the polymer molecular weight (MW), increasing the temperature and polymer compatibility increased the diffusion rate¹⁰⁵. Full mechanical strength of a PS film was found to be reached after complete molecular mixing of the polymer after 48 hours at 144°C⁶⁶. Important factors were found to be the location of chain ends and the ratio of the polymer radius of gyration (R_g) to the particle diameter. NET measures the mixing of acceptor and donor chromophores, originally in separate particles, during interdiffusion. Diffusion coefficients determined by NET were in good agreement with those found via SANS. In many studies it was found that the diffusion coefficient decreased with time. This was attributed to low MW polymer localised at the surface of particles. According to the reptation model¹¹¹ diffusion in polymers varies inversely with the square of MW so the shorter polymer chains will diffuse at a faster rate. Another source of evidence for interdiffusion of chain ends comes from fracture studies of PBMA films. After annealing for 2 hours at 90°C⁸⁸ the films showed fractures that went through the particles rather than along the particle-particle boundaries indicating that interdiffusion across particle boundaries had taken place.

Interdiffusion cannot occur below the polymers T_g , because the chains are not mobile enough to move into neighbouring particles. Coalescing aids are solvents which, when added to the polymer during casting, increase the interdiffusion rate of polymer chain ends between particles. This decreases

the time taken to reach full mechanical strength and also allows polymers to film form below the polymers T_g , by increasing chain mobility.

Crosslinking of the latex particles has the effect of limiting diffusion. Work by Brown *et al*^{112,113,114} showed that lightly crosslinked latex particles will film form, but lack mechanical strength. Studies on crosslinked PBMA showed a transition from tough to brittle fracture behaviour as the chain length between crosslinks became equal to the entanglement chain length, concluding that chain entanglement is required to form a tough film.

1.4 Fate of surfactants during and after film formation.

There are three general cases for the fate of surfactants¹¹⁵ 1) the surfactant dissolves into the particles and plasticises the polymer 2) the surfactant forms a separate phase, which collects in pockets or at the polymer/air, polymer/substrate interface 3) the surfactant forms a separate phase, which is trapped between particles forming a continuous network.

1.4.1 Dissolution

This occurs when the surfactant is miscible with the polymer matrix.

Vijayendran and co-workers¹¹⁶ compared the effects of two nonyl phenol ethoxylate surfactants on the T_g of an acrylic-acetate latex. The surfactant with the higher hydrophile-lipophile balance lowered the T_g to a greater extent due to greater polymer compatibility. A FFTEM study of PBMA films prepared with the non-ionic surfactant C12E4 (tetraethyleneglycol dodecylether) showed that it dissolved into the film as there was no sign of it between particles or of it being exuded¹¹⁷. The resulting permeability of the film was higher, possibly due to the hydrophilicity of the surfactant. Polymer interdiffusion of a PBMA latex is enhanced with addition of non-ionic surfactants¹¹⁸. Polymer interdiffusion, followed by NET, was enhanced with the use of a nonyl phenol ethoxylate surfactant resulting in the surfactant being evenly distributed throughout the polymer.

1.4.2 Separation to surfaces and islets

This occurs when the surfactant is immiscible and incompatible with the polymer matrix.

Bradford and Vanderhoff¹¹⁹ conducted an electron microscopy study of the surfaces of a styrene-butadiene latex with added nonyl phenol ethoxylates. Films containing surfactants with 20 or 40 repeating ethylene oxide units formed blisters on top of the film, while films containing surfactants with 4 to 15 ethylene oxide units showed no surface exudation. This was attributed to surfactants with longer ethylene oxide units having less solubility in the polymer.

Zhao *et al*¹²⁰ studied the distribution of two anionic surfactants, SDS and sodium diphenyl ether sulphonate (SDED), in PBMA films left to coalesce over 3 days. Surfactant enrichment was found at both interfaces with the polymer/air interface containing the higher concentration due to surfactant carried by the water flux. It was found that surfactant migration was mostly established after 3 hours of coalescence, with SDS however showing a continued gradual surface enrichment due to its greater thermodynamic incompatibility with the polymer.

1.4.3 Separation into a continuous phase

This occurs when the surfactant is compatible with the polymer, but not miscible.

Poly(vinyl alcohol) is often used as a protective colloid for poly(vinyl acetate) (PVAc) and has been shown to improve mechanical strength of PVAc films¹²¹. Light scattering studies^{122,123} have shown that the stabiliser forms a continuous phase surrounding the PVAc particles.

1.4.4 Models of surfactant distribution.

Development of guidelines for predicting the distribution of surfactants in a film under known conditions of film formation has been attempted¹¹⁵. The distribution of anionic, cationic and non-ionic surfactants in a poly(2-ethylhexyl methacrylate) film as a function of ageing time, surfactant concentration and the conditions of film formation was measured by Fourier transform infrared spectroscopy (FTIR). Three major factors were found to influence the distribution of surfactant; 1) the initial distribution of surfactant in the wet latex 2) desorption of surfactant during film formation 3) the mobility of the surfactant in the drying and dried film. These are all governed by the polymer-surfactant interactions.

Urban *et al*¹²⁴ also studied surfactant exudation with FTIR attenuated total reflectance spectroscopy finding many parameters that effect the fate of surfactant. Anionic surfactants desorb to both film/substrate and film/air interfaces. Polymer-surfactant complexes occur by adsorption onto polymer segments of ethyl acrylate/methacrylic acid latices, preventing exudation. The substrate was also found to influence exudation. Surfaces with a large difference in interfacial energy compared to the surfactant, such as PTFE and mercury, promoted surfactant exudation to the film/substrate interface.

In summary there are many factors during film formation, which effect the final distribution of an additive in a dried polymer latex film:

1. Location of the additive within the latex dispersion. An additive can be freely dissolved in the aqueous medium, adsorbed on the surface of the latex particles or a combination of the two.

2. Desorption of additive from the surface of the latex particles. The adsorbed additive may or may not desorb from the surface of the polymer allowing particle-particle contact needed for polymer chain diffusion between particles. If the additive will desorb the rate at which it desorbs is important.
3. The additive mobility within the drying film. This will depend on the polymer-additive interactions, the physical mobility of the additive and the concentration at which the additive is used.

1.5 Barrier characteristics of porous latex films

Barrier characteristics of prepared films can be evaluated via dynamic adsorption. This measures the ability of a packed bed of adsorbent to adsorb a vapour from an inert gas flowing through the bed. Therefore, a sample with a slow performance will be unable to remove all the vapour from the gas stream before it has passed through the bed. A sample with faster adsorbance will remove all the vapour until a point is reached when it starts to become saturated and vapour will again escape the bed. Films can be prepared around an adsorbent whose adsorptive properties for a particular adsorbate are well known. Comparison of the dynamic adsorption profiles for the coated and uncoated adsorbent would then indicate the degree to which the polymer film hinders access of adsorbate to adsorptive sites. Figure 13 shows a schematic representation of an adsorbent packed into a VA (volume/activity) tube.

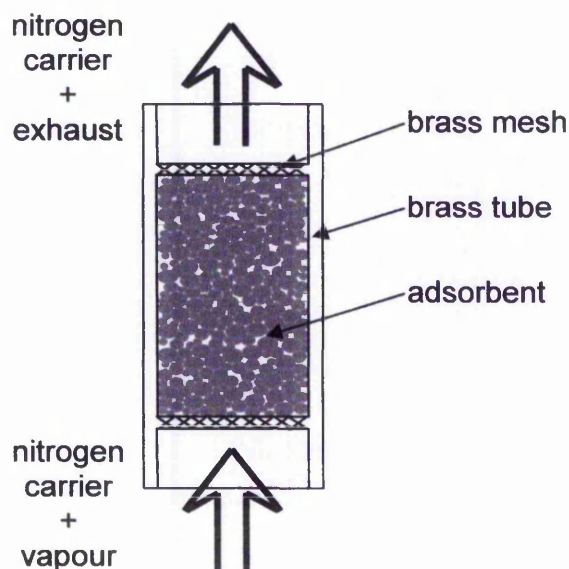


Figure 13: Schematic drawing of a packed bed of adsorbent in a VA (volume/activity) tube.

1.6 Polymer supports

Staudinger in 1935¹²⁵ found that an insoluble polymer is formed from the polymerisation of styrene and divinylbenzene (DVB). The insolubility was attributed to the bi-functionality of DVB which bridges across polymer chains forming a three-dimensional styrene-divinylbenzene (S-DVB) polymer network. D'Alelio in 1945¹²⁶ was the first to take advantage of the insoluble properties with the production of a cationic exchanger based on a sulphonated version of the S-DVB copolymer. Tailoring properties by varying S-DVB ratios was found to be insufficient for the more demanding applications proposed for ion-exchange resins. By the 1950s resins were being produced by suspension polymerisation in the presence of inert components producing macroreticular resins, possessing permanent porosity, giving a new dimension to polymer supports.

Polymer supports are now used routinely in a wide range of chemical applications^{127,128,129,130,131,132}. They come in a variety of forms ranging from hydrophobic to hydrophilic and gel-type to macroporous. Gel-type resins are generally lightly crosslinked (<4% difunctional monomer) while macroreticular resins are generally more heavily crosslinked (>20% difunctional monomer) and include a porogen during their preparation. Which type is used, depends on the application; affinity chromatography requires a hydrophobic macroporous support while racemate resolutions generally require a hydrophilic gel-type support.

The commonest supports are still the vinyl-divinyl crosslinked spheres, prepared via crosslinked suspension polymerisation, due to their chemical inertness. Suspension polymerisation involves dispersing the monomer phase

including a free radical initiator in an immiscible liquid. The monomer is kept as small droplets by stirring and the introduction of a stabiliser in the continuous phase¹³³. Initiation is usually started thermally and results in polymer 'beads', which are collected, washed, extracted and dried. The size of the beads are comparable to the size of the initial monomer droplets so varying the level of agitation gives control over the final particle size.

Kun and Kunin¹³⁴ defined ion-exchange resins as crosslinked gels of polyelectrolytes with a pore structure defined as distances between polymeric chains and referred to these structures as having gel type molecular porosity. The porosity is only present when the resin is hydrated so the polymer network is expanded, dehydration results in the collapse of the network and loss of porosity. Kun and Kunin¹³⁵ defined macroporous resins as agglomerates of randomly packed microspheres possessing a continuous gel structure permeated with holes and channels which are not part of the gel structure. The size and shape of these pores are not greatly affected by whether the resin is hydrated or not.

Minor technique modifications enable preparation of varying morphologies, from gel-type all the way through to macroporous beads. Gel-type resins expand and contract on addition and removal of a good solvent and show no tendency to imbibe bad solvents. Macroporous resins will imbibe both good and bad solvents mainly into their macropores, with little tendency to alter their overall volume. Visually gel-type resins are transparent with a glossy surface while macroporous resins are opaque with a matt surface.

Hydrophilic supports can be prepared by inverse suspension polymerisation¹³⁶. Enzymes can be immobilised in the support by including

the enzyme in the aqueous comonomer phase¹³⁷. In a similar way magnetic particles, pigments and small carbon blacks¹³⁸ can be incorporated into the support to modify the properties further and enable identification of different supports e.g. in pigmented mixed bed ion exchange systems.

1.6.1 Pore formation

Techniques for the preparation of macroporous supports were developed over 40 years ago^{139,140,141}. As stated earlier porous structures are formed during polymerisation of vinyl/divinyl monomer mixtures in the presence of an inert porogen^{139,140,141,142}. The porogen needs to be unreactive, soluble in the monomer phase and insoluble in the continuous phase. Three types of porogen produce permanent porosity:

1. A solvent for the copolymer
2. A non-solvent for the copolymer
3. Macromolecular material.

Addition of a porogen which is a good solvent for the copolymer¹⁴³ produces resins with a relatively low pore volume and high specific surface area. Such solvents for the case of S-DVB copolymer¹⁴⁴ would be toluene, xylene, and dichloroethane. Addition of a porogen which is not a solvent for the copolymer produces resins with a relatively high pore volume and low specific surface area. Such non-solvents for the case of S-DVB copolymer would be n-heptane and octane. Addition of linear polymer to the polymerisation mixture produced resins with relatively low pore volume and low specific surface area¹⁴⁵. Examples of such porogens are PS and PVAc.

At low DVB and porogen content an expanded gel-type structure is formed where the pores are found between polymer chains. The pores are lost with porogen removal as a consequence of the polymer network collapse. A macroporous polymer is only formed at high DVB and porogen content where the collapse of the internuclear chains is finished before all the porogen has been removed from the beads¹⁴³.

The crosslinking density is high at the start due to the higher reactivity of DVB compared to styrene¹⁴⁶. The DVB is polymerised at a faster rate than styrene resulting in polymer being formed with a progressively lower crosslink density as the polymerisation proceeds. This causes the formation of polymer spheres with relatively high crosslinking in the core and relatively low crosslinking at the surface.

1.6.1.1 Non-solvating porogen

When the porogen is a non-solvent, and at a sufficiently high DVB content, there are three levels of substructure. i) nuclei (5-20 nm) formed from the agglomeration of crosslinked polymer chains, ii) microspheres (60-100 nm) formed from the phase separation of nuclei and iii) agglomerates (10,000-100,000 nm) formed from agglomeration of microspheres^{139,140,142,147}. During polymerisation the solvating power of the dispersed liquid is decreasing as monomer is consumed and at a certain point the growing polymer nuclei will precipitate. The point of phase separation depends on the reaction temperature and the concentrations of crosslinker and porogen. Once phase separation occurs the remaining monomer polymerises between the

coalesced agglomerates resulting in a loss of SSA during polymerisation¹⁴⁸ due to an infilling process¹⁵¹.

Phase separation is caused by χ -induced syneresis before the gel point is reached i.e. the non-solvent porogens solvating power decreases as the polymer nuclei grow and the monomer content decreases, until the polymer is no longer soluble in the porogen and phase separation occurs.

A study by Häupke and Hoffman¹⁴⁹ looked at the effects of varying the DVB content from 5 to 50% and the porogen from 10 to 70% on the porous structure. They used a mixture of alkanes with boiling points between 150 and 200°C as porogens. From the results they were able to distinguish between four domains of structural formation.

1. Gel type polymer, translucent and non-porous, no measurable surface area – found for polymerisations with low DVB and porogen content.
2. Semi-porous polymer, semi-opaque, no measurable surface area - found for polymerisations with low DVB and intermediate porogen content and also for polymerisations with higher DVB and low porogen content.
3. Flocculent polymer, opaque powder, low surface area - found for polymerisations with a very high porogen content.
4. Macroporous polymer, opaque, measurable surface area - found for polymerisations with moderate to high DVB and intermediate porogen content.

1.6.1.2 Solvating porogen

When the porogen is a solvent, and with a sufficiently high DVB content, there are only two levels of substructure¹⁵⁰. The formation of relatively larger nuclei (20-50 nm) and their development into agglomerates, without the intermediate microspheres^{141,151}. As polymerisation proceeds phase separation occurs at a later stage and the polymer chains are no longer extended. This results in the growing chains becoming entangled inside the nuclei resulting in final nuclei which are large. At low DVB content the structure formed is an expanded gel, since the chains are fully solvated during the whole polymerisation.

Phase separation is caused by γ -induced syneresis after the gel point is reached i.e. at high DVB content due to increased crosslinking density the porogen is no longer able to fill all available volume and phase separation occurs. At low DVB content the porogen can fill all the available volume and no phase separation occurs.

Porosity in beads prepared using solvating or non-solvating porogen is formed between the particles within the bead. Micropores¹⁵² are formed between nuclei, which are responsible for most the surface area of the support. A bigger range of pore sizes are found between microspheres, and bigger pores still are found between agglomerates. When mixtures of solvating and non-solvating diluents are used, the copolymers form intermediary porous structures in relation to copolymers prepared with a single diluent¹⁵³.

Increasing the fraction of crosslinker generally leads to particles with larger surface areas and smaller pore sizes^{139,152}. The phase separation takes place at a lower monomer conversion when higher amounts of crosslinker are present. The adsorption of monomer into the nuclei and their coalescence are limited by the increased crosslinking resulting in smaller nuclei and smaller microspheres.

Rabelo *et al*¹⁵³ classified the types of pore structure found in macroreticular resins based on the uptake of heptane.

- **Gel type:** heptane does not diffuse into the beads after 24 h (heptane uptakes $<0.1 \text{ cm}^3 \text{ g}^{-1}$).
- **Collapsed:** heptane diffuses slowly into the beads opening the collapsed micropores (after 5 mins heptane uptake $<0.1 \text{ cm}^3 \text{ g}^{-1}$ and after 24 h heptane uptakes of $>0.1 \text{ cm}^3 \text{ g}^{-1}$).
- **Collapsed/macroreticular:** heptane diffuses quickly at the beginning, but the time for the equilibrium to be attained is relatively longer (after 5 mins heptane uptake $>0.1 \text{ cm}^3 \text{ g}^{-1}$).
- **Macroreticular:** heptane diffuses quickly through the fixed pores and the time for the equilibrium to be attained is very short (heptane uptakes of $>0.1 \text{ cm}^3 \text{ g}^{-1}$).

1.6.1.3 Polymeric porogen

Porosity is formed by pockets of polymeric porogen becoming trapped throughout the crosslinked bead during polymerisation. Removal of the polymeric material leaves pores which do not close due to their relatively large size and the rigid structure of the resin.

The total pore volume of the beads when PVAc is used as a porogen depends on the concentration and its MW¹⁵⁴. Increasing the concentration of PVAc increases the total pore volume. The lower the thermodynamic affinity between the polymeric porogen and the polymer network, the larger the pore size due to faster separation of the two phases during polymerisation. Generally the total pore volume is practically the same as the volume of porogen used in the polymerisation.

1.6.2 Chemical modification

Chemical modification of the support is necessary to introduce the chemical groups required, and can be approached in three ways. Firstly, a comonomer can be introduced into the polymerisation so that the functional group can be incorporated during polymerisation. Secondly, a support can be chemically modified after its initial production. Thirdly, a combination of the two.

An example of a functional polymer prepared from a functional monomer would be N-styryl proline¹⁵⁵ (Figure 14).

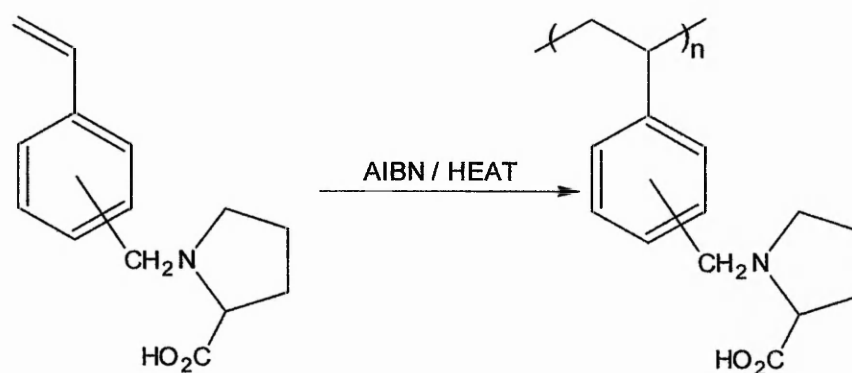


Figure 14: A functional polymer support from a functional monomer.

Chloromethylation of the benzene ring of a preformed S-DVB polymer support affords attachment of nucleophilic (Nu) species (Figure 15).

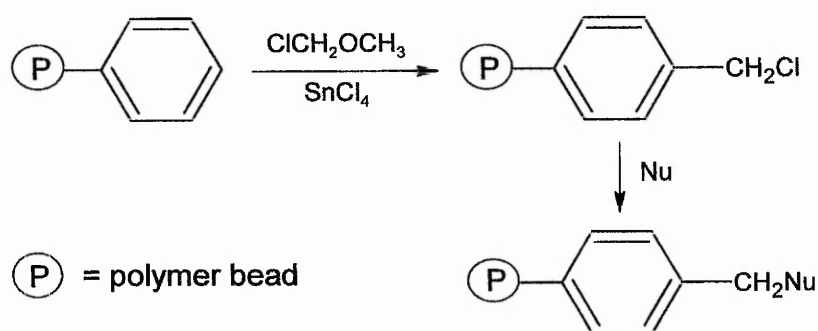
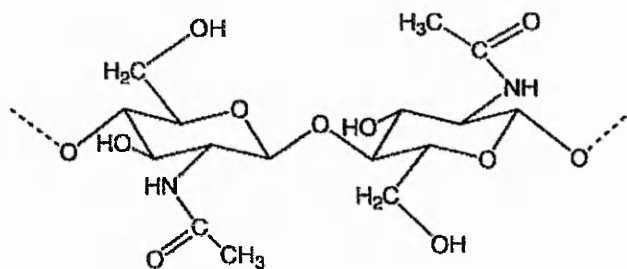


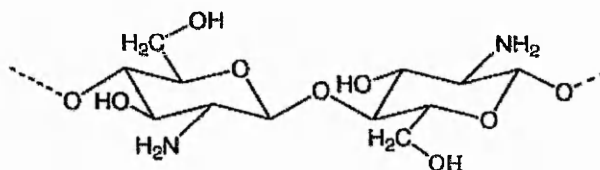
Figure 15: functionalising an initially inert polymer support.

Reactions on resins should be kept to a minimum as a build up of impurities inside the support can occur due to side reactions and incomplete transformations.

Polymer deposition can also be used to introduce chemical groups onto the surface of the film. Idealised, chitosan is a naturally occurring copolymer of poly[$\beta(1\rightarrow4)$ -2-amine-2-deoxy-D-glucopyranose], which is soluble in dilute solutions of mineral acids and some organic acids¹⁵⁶. It is prepared from the deacetylation of chitin (idealised, poly[$\beta(1\rightarrow4)$ -2-acetamido-2-deoxy-D-glucopyranose]), which is insoluble in aqueous media. In practise chitin does not exist as pure poly[$\beta(1\rightarrow4)$ -2-acetamido-2-deoxy-D-glucopyranose] and will always have some chitosan units present. Likewise, complete deacetylation of all the chitin units to chitosan is very difficult resulting in chitosan samples containing various amounts of chitin. In general, a particular sample is arbitrary designated chitin or chitosan depending on its solubility in dilute acid¹⁵⁷, with chitosan being soluble.



Chitin



Chitosan

Figure 16: Molecular structure of chitin and chitosan.

The ability of chitosan to form complexes with transition metal and post-transition metal ions has been documented in two comprehensive reviews by Muzzarelli^{158,159}. The current evidence suggests that chitosan-metal complex formation primarily occurs through the amine group acting as a ligand, therefore the degree of deacetylation will play an important role in the amount taken up.

Deposition of chitosan onto the film surface can be achieved by soaking the film in an acidified solution of chitosan followed by neutralisation.

1.7 Emulsion crosslinking copolymerisation

Emulsion crosslinking copolymerisation (ECCP) is a common method for the preparation of microgels. Microgels are used in a wide range of applications including rheology modifiers for paints, inks, and adhesives¹⁶⁰. A microgel is an intramolecularly crosslinked macromolecule, which is dispersed in normal or colloidal solutions, in which, depending on the degree of crosslinking and on the nature of the solvent, is more or less swollen. Besides linear, branched and crosslinked polymers, intramolecularly crosslinked macromolecules may be considered as a fourth class of macromolecules. Study of microgel formation by various researchers found that ECCP differs from homogeneous polymerisation in three significant ways:

1. The crosslinking density level is fairly high even from the early stages of polymerisation.
2. The weight-average MW increases linearly with monomer conversion.
3. The molecular weight distribution (MWD) is rather narrow and the distribution shifts to larger MWs while preserving the narrow profile as polymerisation proceeds.

In a typical ECCP each polymer particle consists of a single polymer molecule once stable polymer particles are formed¹⁶¹.

The reason for the crosslinking density level being fairly high even from the early stages of polymerisation can be explained by the presence of monomer droplets¹⁶¹. Because the majority of monomer resides in the monomer droplets the polymer concentration in the reaction locus, i.e. polymer particles, is higher than for bulk polymerisation. Polymer molecules formed in free-radical crosslinking polymerisation are reactive for crosslinking reactions, and

therefore, a higher polymer concentration leads to a higher probability of chain connection.

Matsumoto *et al*¹⁶² reported the weight-average MW for copolymerisation of DVB/styrene. They found that the weight-average MW tends to increase linearly with monomer conversion. This arises due to high polymer concentration in the reaction locus. The probability of a growing primary polymer chain reacting with a pendent double bond is increased resulting in all newly formed primary polymer chains connecting to the existing polymer molecule one after the other, before they grow to a significant size. There is a 97.4% chance that a chain with a degree of polymerisation of 20 is already crosslinked with the polymer molecule¹⁶³. The polymer particles essentially consist of one single crosslinked molecule.

In the case of homogeneous polymerisation only larger polymer molecules are crosslinked to grow to large species, while in emulsion polymerisation, all polymer molecules including smaller polymers are crosslinked to form larger polymer molecules. In homogeneous polymerisation the MWD becomes broader during polymerisation, while in emulsion a sharp MWD moves to larger MW during polymerisation. Again this is due to the high polymer concentration. All new polymer chains are incorporated into existing polymer molecules so the narrow distribution is retained while the MW increases.

ECCP was also found to deviate from emulsion homopolymerisation (EHP) in a significant way. Obrecht *et al*¹⁶⁴ reported that the emulsion polymerisation of DVB produced significantly more and smaller polymer particles than in the case of styrene EHP under the same emulsifier, initiator and monomer concentrations. They found that the number of particles formed in the

emulsion polymerisation of 1,4-DVB was 6-9 times higher than that formed in styrene EHP. Nomura *et al*¹⁶⁵ studied the ECCP of DVB/styrene and found that with increasing crosslinker content the overall rate of polymerisation and the rate of polymerisation per particle decreased while the number of particles increased. In emulsion polymerisation the rate of polymerisation per particle is governed by three factors, the mean propagation rate coefficient, the monomer concentration in the polymer particles and the number of radicals per particle. Nomura studied the monomer concentration in the polymer particles at various crosslinker contents and found that with increasing crosslinker content the monomer concentration within the particles decreased¹⁶⁵. He concluded that it was reasonable to assume that the decrease in the rate of polymerisation for ECCPs is mainly due to the decrease in the monomer concentration in the polymer particles. The decrease in monomer concentration with increasing crosslinker content is due to the increased crosslinking density of the polymer particles which are less swellable by the monomer.

The increase in the number of polymer particles (N_T) with increasing crosslinker content can be explained with the Smith-Ewart theory²¹:

$$N_T = k_2(I_0/\mu)^{0.4}(a_s S_m)^{0.6} \quad \text{Equation 3}$$

Where k_2 is a numerical constant, I_0 is the initial concentration of initiator, μ the volumetric growth rate per particle in interval 1, a_s the adsorption area per SDS molecule on the surface of polymer particles and S_m the amount of emulsifier forming micelles per unit volume of water. If the rate of

polymerisation per particle in interval 1 decreases, the volumetric growth rate per particle in this interval also decreases because they are proportional to each other. From the above equation it can be seen that if the value of μ becomes smaller in interval 1 the number of polymer particles will be higher. The slower growth rate in interval 1 allows the formation of more nucleated particles before all the micelles disappear and stage 1 ends. The increased number of growing polymer particles compete equally for the limited monomer resulting in a smaller final polymer particle size.

1.8 Characterisation methods

1.8.1 Nitrogen adsorption

1.8.1.1 Quantachrome

The apparent SSA of the latexes and films were measured by nitrogen adsorption on a Quantasorb detector (Quantachrome Corporation). The principal of the method is as follows: Nitrogen in a helium carrier stream is passed over the sample at various partial pressures by varying the flow rates of both gases. Immersion of the sample in liquid nitrogen promotes adsorption of nitrogen on to the accessible surface of the film until equilibrium is reached. Warming of the sample after equilibrium desorbs the adsorbed nitrogen back into the carrier stream, which passes through a thermal conductivity detector where the amount of nitrogen desorbed is determined. This process is shown schematically in Figure 17.

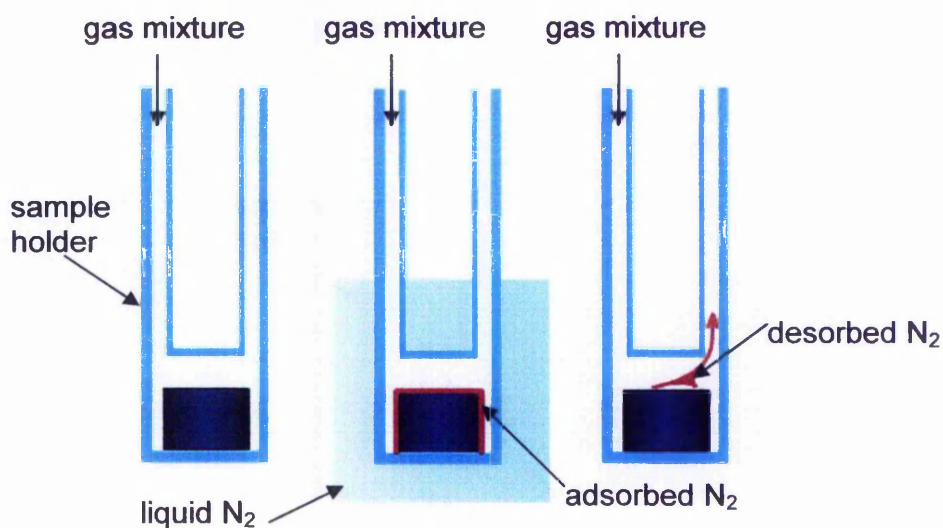


Figure 17: Schematic diagram of a nitrogen adsorption/desorption cycle.

The Quantasorb continuous flow method of surface area determination has

a high sensitivity, and avoids the dead space correction uncertainty of static methods, allowing low specific surface areas to be determined¹⁶⁶.

1.8.1.2 Adsorption and desorption isotherm

The variation in the amount of gas adsorbed on a solid with pressure, at a fixed temperature, is termed an adsorption isotherm. For a gas below its critical temperature, i.e. a vapour, then the isotherm is represented by a plot of amount of vapour adsorbed against P/P^0 , where P^0 is the saturation pressure of the vapour. Brunauer¹⁶⁷ classified adsorption isotherms into six types depending on their shape. The shape was largely dependent on the adsorbent.

A solid will have external surface, but may also have internal surface in the form of pores. Solids may have imperfections and cracks which extend deep into the solid. Internal surface can also form in agglomerates of small particles, which will have internal surface made up of the surface of the primary particles. The definition of a pore is a crack which is deeper than it is wide. Pores are classified according to their width:

- Micropores less than ~2 nm
- Mesopores between ~2 nm and ~50 nm
- Macropores more than ~50 nm

Six basic types of isotherms have been classified. The majority of adsorbate/adsorbent combinations will possess characteristics of one or more of these basic types.

Type 1: A microporous adsorbent and an adsorbate with small molecules which can readily penetrate the pores.

Type 2: A non-porous adsorbent and an adsorbate with a strong interaction with the surface.

Type 3: A non-porous adsorbent and an adsorbate with a weak interaction with the surface.

Type 4: An adsorbent with mesopores and an adsorbate with a strong interaction with the surface.

Type 5: An adsorbent with mesopores and an adsorbate with a weak interaction with the surface.

Type 6: A non-porous adsorbent with a very energetically uniform surface, resulting in a stepwise multilayer isotherm.

These isotherms are shown schematically in Figure 18.

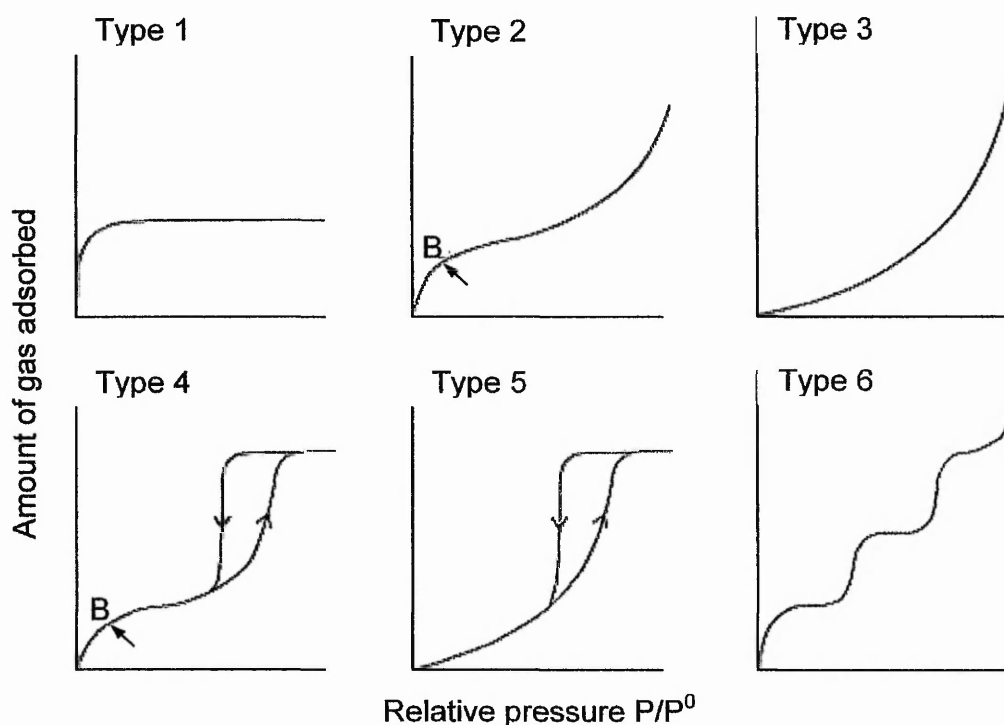


Figure 18: Schematic representation of all six standard types of adsorption isotherm.

Adsorption of a vapour onto a microporous solid is initially very strong as the vapour condenses within the pores. Once the pores are full, the vapour absorbed with increasing pressure plateau's off as very little surface is left for vapour adsorption (type 1). The volume of adsorbate sorbed, corresponding to the plateau, is the micropore volume of the adsorbent.

Adsorption of a vapour onto a non-porous adsorbent is initially onto the surface of the adsorbent until monolayer coverage is achieved. If the adsorbate has a strong interaction with the surface the point of monolayer coverage can be seen on the isotherm in the area symbolised by B. Unlike microporous samples, non-porous samples need to be highly divided for there to be any significant surface for the vapour to adsorb onto. Once monolayer coverage is achieved, subsequent vapour adsorption is on top of the existing adsorbed layer. This gives rise to the increasing amount adsorbed with increasing pressure once monolayer coverage is achieved. The specific surface area of a sample can be calculated if it has a type 2 isotherm. Langmuir's¹⁶⁸ model of adsorption regarded a solid as an array of adsorption sites. A state of dynamic equilibrium was postulated in which the rate at which molecules adsorbed on to the solid equalled the rate at which molecules desorbed from the surface. Langmuir produced the following equation for the surface area of a solid:

$$S = \frac{X_m L A_m}{M} \quad \text{Equation 4}$$

Where X_m is the monolayer capacity, L Avogadro's constant, A_m the molecular cross-sectional area and M the molar mass of adsorbent.

Langmuir's theory assumes:

1. Adsorption occurs at fixed sites, which are considered to be energetically uniform.
2. Lateral interactions between adsorbed molecules are assumed to be negligible.
3. Adsorption is assumed to be restricted to a monolayer

Langmuir¹⁶⁹ also developed an equation for multilayer adsorption, but this was complex and little used. By adopting the Langmuir equation and introducing three simplifying assumptions Brunauer, Emmett and Teller¹⁷⁰ produced the well known BET equation for multilayer adsorption. The assumptions were:

1. The first heat of adsorption is equal to the molar heat of condensation in all layers except the first.
2. The evaporation-condensation conditions are identical except in the first layer.
3. When $P=P^0$, the adsorbate condenses to a bulk liquid on the surface of the solid and the number of layers become infinite.

The application of this process to microporous solids can lead to errors. It is assumed that with increasing pressure more layers of adsorbate are condensed onto the surface of the solid. Adsorbate inside a micropore can only reach a finite number of layers before the pore is full and no more adsorption can take place within. Due to this limitation, the specific surface area of adsorbents containing micropores, obtained by the BET equation, is only apparent.

Mesoporous adsorbents exhibit a hysteresis loop in the isotherm. At any

relative pressure along the loop the desorption branch is always higher than the adsorption branch. This is shown in Figure 19. The corresponding type 2 isotherm for the sample with the absence of mesopores is shown as a broken line. The type 4 adsorption isotherm initially follows the type 2 isotherm until there is an enhanced amount of adsorption caused by condensation within the mesopores.

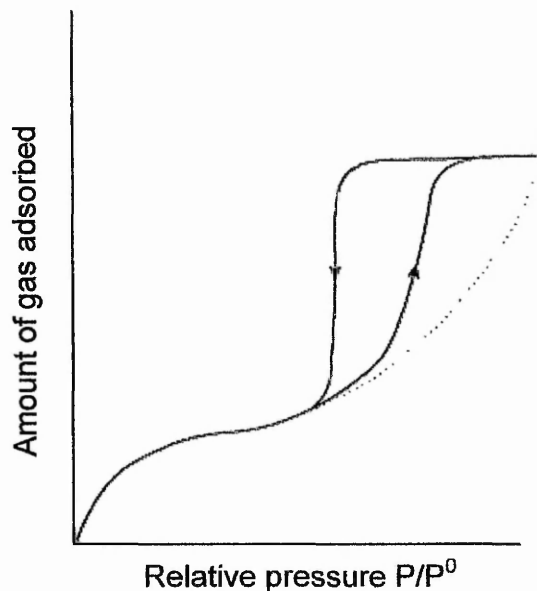


Figure 19: Schematic profile of a type 4 isotherm. The corresponding type 2 isotherm is shown as a broken line.

The hysteresis occurs due to the different processes of pore filling and pore emptying. During adsorption in a cylindrical pore, capillary condensation occurs in a cylindrical meniscus, but during desorption, capillary evaporation occurs from a hemispherical meniscus. This causes the relative pressure required for capillary evaporation from a pore to be lower than the relative pressure required for capillary condensation within the same pore.

Adsorbents with a high external area or mesoporosity, which also have

microporosity will have adsorption isotherms consisting of the two basic types of isotherm super-imposed on to each other. This is shown schematically in Figure 20.

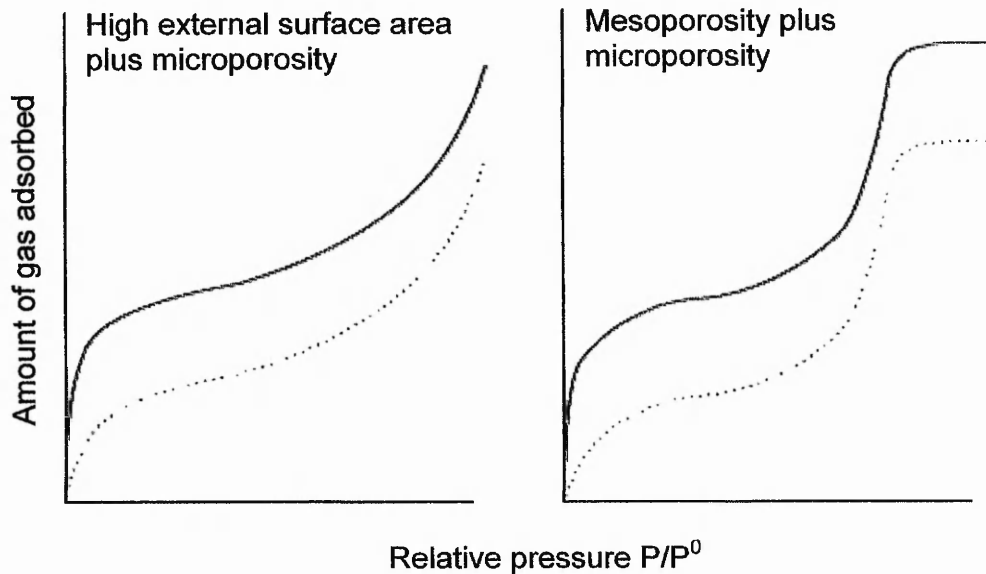


Figure 20: Schematic representation of the effect microporosity has on the adsorption isotherm. The profiles shown as broken lines are the adsorption isotherms in the absence of microporosity.

1.8.1.3 Nonane pre-adsorption

A direct method to evaluate the microporosity of a sample is to fill the micropores with an adsorbent leaving any mesopores, macropores and external surface area free. Gregg and Langford¹⁷¹ used n-nonane and showed that the rate of removal from micropores was very slow and showed that complete removal required more than 10 hours of pumping at a temperature of 450K. Thus they assumed that n-nonane would be retained within the micropores, but removed from the external surface and mesopores after 1 hour of pumping at room temperature. To test this idea they took a

sample of spherical carbon black, which had been rendered microporous by controlled oxidation. Since the particles were uniform in size the external SSA could be estimated by electron microscopy. Isotherms were generated initially from the sample with nonane filled micropores and then after with progressively emptier micropores by pumping at successive elevated temperature steps until the micropores were completely empty. It was shown that the SSA calculated from the isotherm of the initial nonane filled sample was the same as the estimated external surface area found from electron microscopy. Also with each subsequent pumping step the isotherms moved closer to the isotherm of the original sample until there was no difference.

The presence of micropores in a sample can be found by first generating a normal nitrogen adsorption isotherm for a sample. The sample is exposed to n-nonane vapour at RT until equilibrium adsorption is obtained. The vapour is removed and the sample pumped down, removing the adsorbed n-nonane from the external surface, macropores and mesopores. If any micropores exist, they will still be filled with n-nonane. A repeat nitrogen adsorption isotherm is carried out on the modified sample. If micropores are present, subtraction of the nonane pre-adsorbed isotherm from the original sample isotherm will result in a type I isotherm. This can be evaluated to find the micropore volume of the sample.

1.8.1.4 t-plot

The task of detecting deviation from the standard isotherm is essentially of comparing the shape of the isotherm under test with that of a standard, by finding whether the two can be brought into coincidence by mere adjustment

of the scale of ordinates. The t-plot of Lippens and de Boer¹⁷² is a means of comparing a sample to see if it deviates from a standard non porous sample. It is based on the t-curve, which is a plot of the standard isotherm with t, the statistical thickness of the adsorbed film, rather than x/x_m as the dependent variable. t is calculated using the following formula:

$$t = (x/x_m)\sigma \quad \text{Equation 5}$$

Where x is the weight of vapour adsorbed at pressure P, x_m is the weight of vapour at monolayer capacity and σ is the height of a single layer of molecules. Lippens, Linsen and de Boer¹⁷³ put $\sigma=3.54 \text{ \AA}$ assuming that the arrangement of molecules within the film is hexagonal close packing. The value of x_m can be obtained from the BET¹⁷⁰ equation.

The isotherm under test is drawn using the amount adsorbed against the t values of the standard sample rather than against p/p^0 . If the isotherm under test is the same shape as the standard then the t-plot must be a straight line passing through the origin. If the isotherm under test is from a sample with no porosity, but has a higher SSA then the t-plot will be a straight line with a bigger gradient passing through the origin. If the isotherm under test is from a sample that has mesoporosity then a deviation from a straight line will be seen at higher pressures as a consequence of capillary condensation. If the isotherm under test is from a sample that has microporosity then a straight line will result with a positive intercept as a consequence of the extra adsorption of vapour by the micropores.

The effect of mesopores and micropores on the shape of the t-plot are shown schematically in Figure 21.

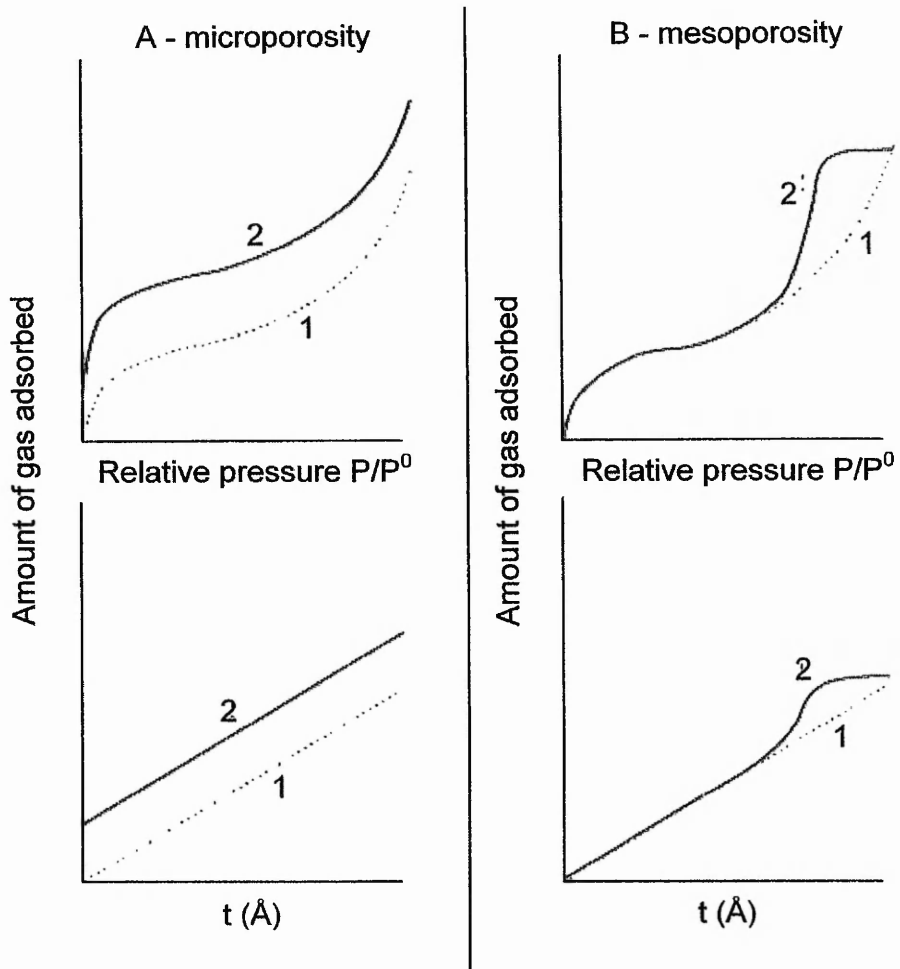


Figure 21: (A) effect on microporosity on the isotherm and t-plot of a sample. (1) is the standard sample (2) is the same sample with micropores. (B) effect of mesoporosity on the isotherm and t-plot of a sample. (1) is the standard sample (2) is the same sample with mesopores.

1.8.2 Mercury porosimetry

Pore size distributions and pore volumes can be determined by mercury porosimetry. Film samples are placed in a dilatometer and firstly evacuated of air and then filled with mercury. Mercury is non-wetting and does not enter

pores until a threshold pressure is reached relative to the pore diameter; smaller pores requiring higher pressures for mercury to enter them. The filled dilatometer is placed in an oil filled autoclave and the pressure increased and the mercury intrusion volume noted for each pressure point. A plot of the pore radius against the change in volume of mercury intruded with change in pore radius, gives the pore size distribution.

A schematic representation of a mercury porosimetry run is shown in Figure 22.

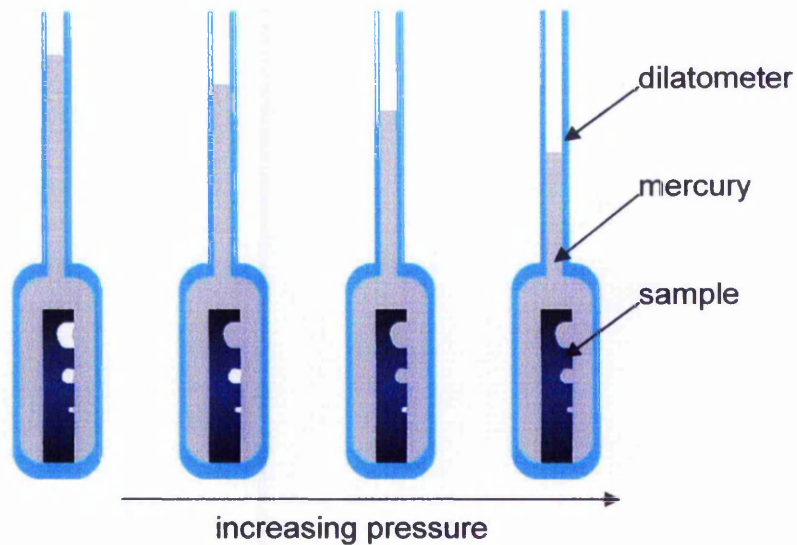


Figure 22: Schematic diagram of a mercury porosimetry run.

1.9 Aims of current work

1.9.1 Porous latex films

Steward¹⁷⁴ has shown that water leachable materials added to polymer latex films can be used to control solute permeability. This was attributed to water filled pores, but when films having MFFT's below room temperature were allowed to dry, porosity was lost as a consequence of further film formation processes. The aim of this study is to extend this approach to the creation of permanent porosity in latex films by additive leaching and to explore other possible routes to pore creation by deliberate reductions in latex stability prior to film formation and by exceeding the CPVF of a binder. Destabilising the latex will prevent close packing of the latex spheres during water evaporation resulting in a disordered arrangement in the final film. The disordered arrangement will hinder full coalescence of the polymer leaving voids available for possible mass transport. Exceeding CPVFs is a method used in the coating industry to prepare 'breathable paint'. This involves adding excess pigment or filler so that there only is enough binder to glue the particles together, but not enough to completely fill interstitial voids.

Barrier characteristics of porous latex films covering an absorbent can be evaluated via dynamic adsorption. Dynamic adsorption measures the ability of a packed bed of adsorbent to adsorb a vapour from an inert gas flowing through the bed. If the kinetics of vapour sorption are inhibited by the presence of the latex film then the adsorbent may not be able to utilise its full capacity before vapour breaks through the packed bed. Comparison of the dynamic adsorption profiles for the coated and uncoated adsorbent would then

indicate the degree to which the polymer film hinders access of adsorbate to adsorptive sites.

1.9.2 Reactive porous latex films

Evaluation of methods for the incorporation of functionality on to a porous latex film for use as a catalytic/reactive membrane. Evaluation of the catalytic/reactive membrane to determine its effectiveness.

1.9.3 Porous latex particles

Also of interest is production of novel colloidal porous particles, based on production of macroreticular resins, for potential use as additives in reactive films. Macroreticular beads are commonly produced by suspension polymerisation of styrene and divinyl benzene in the presence of a porogen (usually an organic solvent) producing millimetre size beads. Adaptation of this process to emulsion polymerisation is to be evaluated for the production of macroreticular particles with diameters in the nanometre range. This would facilitate their incorporation into a porous polymer film, which could then be utilised for its high surface area. Previous studies on emulsion polymerisation of vinyl and divinyl monomers have been carried out, but without the incorporation of porogens at high DVB content¹⁷⁵.

Preparation of porous latex particles via ECCP in the presence of a porogen. The porosity produced should be permanent and not lost upon removal of porogen or during work-up of the latex. This will facilitate their use as additives, which can be incorporated into porous latex films to enhance their surface area and reactivity.

2 Experimental

2.1 Materials

2.1.1 Latices

- poly(styrene), 527 nm diameter - prepared in-house via surfactant-free free-radical emulsion polymerisation. Further details are given in section 2.2 "Latex preparation".
- poly(butyl methacrylate), 238 nm diameter - prepared in-house via surfactant-free free-radical emulsion polymerisation. Further details are given in section 2.2 "Latex preparation".
- Eudragit® L30D - ethyl acrylate/methacrylic acid latex, 131 nm diameter, 30% aqueous dispersion, Röhm Pharma, GmbH Weiterstadt Germany.
- Eudragit® NE30D - ethyl acrylate/methylmethacrylate latex, 160 nm diameter, 30% aqueous dispersion, Röhm Pharma, GmbH Weiterstadt Germany.
- Sulphonate poly(butyl methacrylate), 501 nm diameter - prepared in-house via surfactant-free free-radical shot-growth polymerisation. Further details are given in section 2.2 "Latex preparation".

2.1.2 Additives

- sucrose - GPR Grade, Merck, Poole Dorset UK.
- glycerol - >99%, Avocado Research Chemicals Ltd., Heysham Lancashire UK.
- hydroxypropyl methyl cellulose - Celacol, Courtaulds Chemicals.
- sodium dodecyl sulphate - >97%, Sigma-Aldrich Co. Ltd., Gillingham Dorset UK.

- sodium diphenyl ether disulphonate - Dowfax 2A1, 55% solution GPR grade, Univar PLC, Croydon UK.
- polyvinyl pyrrolidone - 40,000 MW, Sigma-Aldrich Co. Ltd., Gillingham Dorset UK.
- sodium chloride - >99.9%, Fisher Scientific Limited, Loughborough UK)

2.1.3 Polymerisation materials

- butyl methacrylate - 99%, distilled under reduced pressure, Sigma-Aldrich Co. Ltd., Gillingham Dorset UK.
- sodium styrene sulphonate - Polysciences Inc., Warrington PA USA.
- styrene - 99%, distilled under reduced pressure, Sigma-Aldrich Co. Ltd. Gillingham UK.
- divinylbenzene - 80% mixture of isomers, distilled under reduced pressure, Sigma-Aldrich Co. Ltd., Gillingham Dorset UK.
- toluene - 99%, Sigma-Aldrich Co. Ltd., Gillingham Dorset UK.
- doubly distilled water - distilled from an all Pyrex glass still.
- potassium hydrogen carbonate - >99% SLR Grade, Fisher Scientific UK, Loughborough UK.
- potassium persulphate - >98% SLR Grade recrystallised twice from doubly distilled water, Fisher Scientific UK, Loughborough UK.
- Octane - >99.5% GPR grade, BDH, Poole Dorset England.

2.1.4 Other materials

- ethyl methanoate - 97%, Lancaster, Eastgate Morecombe UK
- chitosan - 98% deacetylated, kindly donated by Prof GAF Roberts, Fashion and Textiles TNTU.

2.2 Latex preparation

To achieve good reproducibility between polymerisation runs the polymerisation conditions must be closely controlled and followed meticulously for each run. Repeated trial runs were carried out to tailor the reaction parameters to the reaction vessels and reaction materials being used. Only after this initial tailoring of the polymerisation were latices prepared for use in this study.

2.2.1 PS latex preparation

Materials used were styrene, doubly distilled water (DDW), sodium chloride (NaCl), potassium persulphate (KPS). The polymerisation type was by surfactant-free emulsion.

A stirred mixture of 95 cm³ styrene, 150 cm³ DDW, and 0.24 g NaCl was initiated with 0.041 g of KPS at 65°C for 24 hours. The reaction was carried out under a nitrogen atmosphere. After reaction the latex was cleaned by repeated ultracentrifugation¹⁷⁶/decantation steps with DDW until the wash water was the same conductivity as DDW.

2.2.2 PBMA latex preparation

Materials used were butyl methacrylate (BMA), DDW, potassium hydrogen carbonate (KHCO₃), KPS. The polymerisation type was by surfactant-free emulsion.

A stirred mixture of 170 cm³ BMA, 1350 cm³ DDW, and 0.6 g KHCO₃ was initiated with 2.55 g of KPS at 60°C for 12 hours. The reaction was carried out under a nitrogen atmosphere. After reaction the latex was cleaned by

repeated ultracentrifugation/decantation steps with DDW until the wash water was the same conductivity as DDW.

2.2.3 Sulphonated PBMA latex preparation

Materials used were BMA, DDW, KHCO_3 , KPS, and sodium styrene sulphonate (NaSS). The polymerisation type was by surfactant-free shot-growth polymerisation¹⁷⁷.

A stirred mixture of 150 cm³ BMA, 1350 cm³ DDW, and 0.6 g KHCO_3 was initiated with 2.55 g of KPS at 60°C. Between 90-95% monomer conversion a shot consisting of 18 cm³ BMA, 9 g NaSS (dissolved in 70 cm³ DDW) was added, along with 1.5 g KPS, and allowed to react further. This resulted in a high concentration of functional groups on the surface of the particles. After reaction the latex was cleaned by repeated ultracentrifugation/decantation steps and sodium ions were exchanged for protons by acid-washing. The name used to refer to this latex throughout this study is "SLATEX".

2.3 Porous latex films

Latex films were formed from four main base latices, which were PS, PBMA, Eudragit® L30D (L30D) and Eudragit® NE30D (NE30D). L30D is water soluble at pH's greater than 7 and NE30D has a T_g below room temperature. Water soluble additives investigated were sucrose, glycerol, hydroxypropyl methyl cellulose (HPMC), SDS, sodium diphenyl ether disulphonate (SDED), poly(vinyl pyrrolidone) (PVP), and NaCl. The additive was mixed into the latex prior to film casting by gentle agitation. Films were cast at 40°C on Pyrex glass plates in rings sealed with silicone grease and produced coherent transparent films (although the films were not fully coalesced the additives trapped within them did not have significantly differing refractive indices, compared to the polymer, to scatter light). Films incorporating water soluble additives were soaked in DDW to leach out the additive. Films containing L30D were washed with sodium hydroxide solution, at pH12, followed by DDW. During the leaching process the films turned opaque, then white, as a consequence of light scattering from the pores as the additive was replaced with water. Washing was continued until no residue was detectable in the evaporated wash water.

A cross-section of the ring and plate casting container is shown in Figure 23.

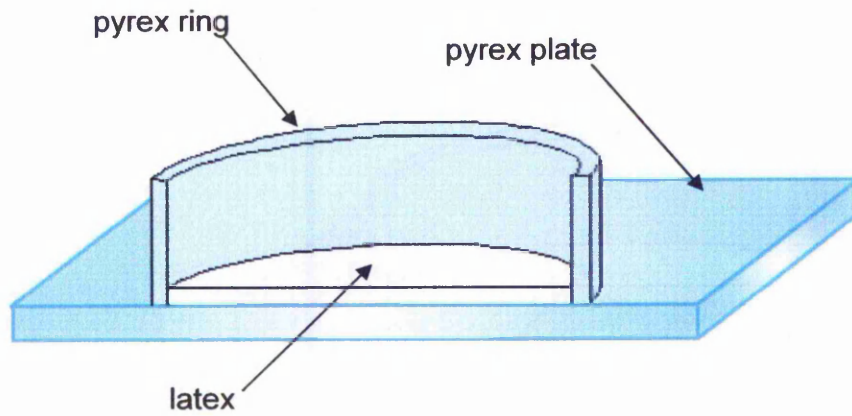


Figure 23: Cross-section through the ring and plate used for latex film casting.

2.4 Sulphonated latex films

Latex films were formed from one base latex, which was the sulphonated functionalised poly(butyl methacrylate), SLATEX, prepared in house. The additives investigated were sucrose, glycerol and L30D.

The additive was mixed into the latex, prior to film casting by gentle agitation. Films were cast at 60°C in 75 mm diameter glass rings on plates sealed with silicone grease, producing 230 µm thick, coherent transparent films. As before, films incorporating water soluble additives were soaked in DDW to leach out the additive. Films containing L30D were washed with sodium hydroxide solution, at pH12, followed by DDW. Washing was continued until the wash water had the same conductivity as fresh DDW. Surface charge characterisation and catalytic activity were evaluated while the films were still immersed in water. SSA and porosimetry measurements were carried out on films whose water was removed by freeze drying. Freeze drying eliminates any pore closure caused by drying the films by liquid water evaporation¹⁷⁸.

2.4.1 Conductometric titration

The concentration of accessible sulphonate groups was evaluated by conductometric titration. 25 cm³ of 6% w/w dispersion of protonated latex was titrated with 0.01M sodium hydroxide and back titrated with 0.01M hydrochloric acid, under a nitrogen blanket. The surface charge was calculated in the same manner as Chainey *et al*¹⁷⁹. Surface charge determinations of porous films were carried out on a sample of wet film (weight of polymer ~2 grams) in

25 cm³ of DDW. The exact weight of film was found after the titration by weighting the sample after drying in an oven.

2.4.2 Electron microscopy

Electron micrographs of the films prepared from PBMA were obtained from gold-coated freeze-fractured samples on a Joel JSM-840A scanning electron microscope.

Electron micrographs of the films prepared from SLATEX were obtained from gold-coated freeze-fractured samples on a Phillips XL30 scanning electron microscope.

2.5 Reactive latex films

2.5.1 Reactive latex films - acid catalysis

The catalytic properties of the SLATEX and films prepared from SLATEX were evaluated by their ability to catalyse the hydrolysis of ethyl methanoate catalysed by the sulphonate groups on the polymer surface. The production of methanoic acid from the hydrolysis can be followed conductometrically and the relative rates of reaction found.

One gram of polymer sample was mechanically stirred with 200 cm³ of DDW at 25°C in a 250 cm³ round bottom flask. At thermal equilibrium 1 cm³ of ethyl methanoate was added and the change in conductance with time recorded.

2.5.2 Reactive latex films - metal complexation by chitosan

Chitosan was dissolved in 0.1M acetic acid producing a 1% w/v solution. The porous films were immersed in the chitosan solution. After 12 hours the films were removed and any excess solution allowed to drain off before immersing the film in 0.1M NH₄OH. The neutralisation step precipitates the chitosan out of solution onto the walls of the pores within the film and also renders the chitosan water insoluble (except in acid media). The film was further washed in DDW until the wash water had the same conductance as DDW.

The amount of chitosan adsorbed onto the films was determined by dye adsorption. Maghami and Roberts¹⁸⁰ have shown that certain anionic dyes, such as C.I. Acid Orange 7, adsorb onto the protonated amine groups of chitosan with a 1:1 stoichiometry. Determining the concentration of amine

groups and knowing the sample to be 98% deacetylated, the amount of chitosan present can be calculated. A 0.87 g l^{-1} solution of C.I. Acid Orange 7 in 0.1M acetic acid was prepared. Each sample was placed in 100 cm^3 of the dye solution for 48 hours after which the polymer film or chitosan residue was removed. The resulting dye solutions were analysed via UV absorption at 484 nm to calculate the amount of dye adsorbed, the amount of amine groups present and finally the amount of chitosan in the sample.

The ability of the chitosan coated porous film to uptake copper ions from solution was measured compared to chitosan flakes. To evaluate the uptake of Cu ions each sample was placed in a 250 cm^3 conical flasks with 150 cm^3 of 6.3 ppm CuSO_4 solution and gently agitated on a shaker throughout the determination. The changing concentration of Cu ions in solution was followed by atomic absorption spectroscopy (Perkin Elmer, Atomic Absorption Spectrometer 3110).

2.6 Porous latex particles

Porous colloidal particle production was based on macroreticular resin preparation with modification of the polymerisation type to ECCP. The organic phase consisted of styrene, DVB, and toluene, which was emulsified in water containing the surfactant SDS.

Two types of reaction vessel/agitation systems were used. To optimise on time and components during the systematic variation of the components, small scale polymerisation's were carried out in jars, with agitation attained by shaking. Once the polymerisation recipe had been optimised all subsequent reactions were run in a three necked Pyrex round bottom flask with agitation attained by stirring with a PTFE paddle to allow sampling of the polymerisation mixture for kinetic studies.

2.6.1 Shaken polymerisation's

All components were thoroughly out-gassed with nitrogen prior to preparation. Preparation of the polymerisation mixture and the polymerisation was carried out under a nitrogen atmosphere at all stages. Surfactant and buffer in powder form were added to 6oz jars followed by DDW and swirled to aid dissolution, forming a single aqueous mixture. The organic components were mixed together to form a single organic mixture before addition to the surfactant solution. The organic phase was added to the aqueous phase and mechanically homogenised, with a Silverson mixer, to form an emulsion. Initiator was added and the jar sealed with a PTFE seal inserted into the jars lid so the reaction mixture was only in contact with glass and PTFE and not the plastic of the lid. Each step of the preparation of the polymerisation

mixture was completed for all samples before moving on to the next step. This helped ensure that all samples had identical preparation conditions. The jars were transferred to a shaking water bath at 80°C and allowed to react for 12 hours. Each run involved up to 9 samples being polymerised at one time.

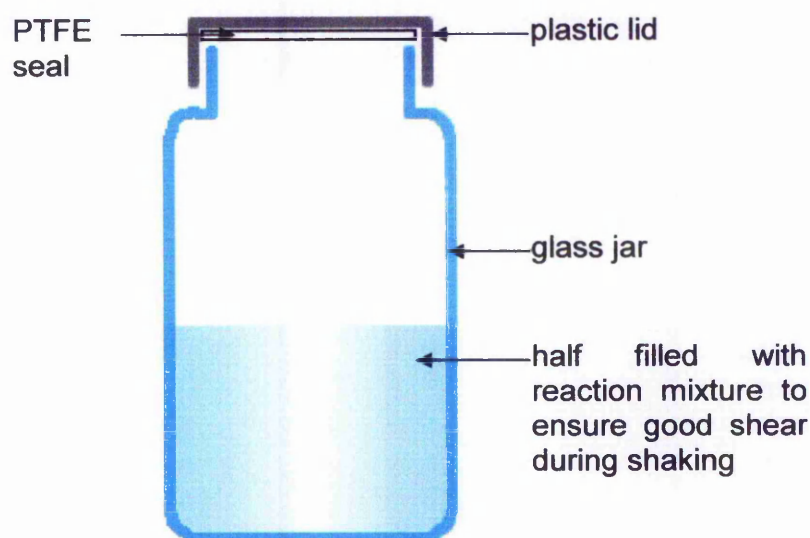


Figure 24: Diagram of “shaken” reaction vessel.

2.6.2 Stirred polymerisation

All components were thoroughly out-gassed with nitrogen prior to preparation to remove O_2 . O_2 is a free-radical scavenger, which will retard the progress of a free-radical polymerisation. Preparation of the polymerisation mixture and the polymerisation were carried out under a nitrogen atmosphere at all stages. Surfactant and buffer in powder form was added to a conical flask followed by DDW and swirled to aid dissolution, forming a single aqueous mixture. The organic components were mixed together to form a single organic mixture before addition to the surfactant solution. The organic phase was added to the aqueous phase and mechanically homogenised, using a

Silverson mixer, to form an emulsion. The emulsion was transferred to a four necked Pyrex round bottom flask with a nitrogen inlet, water cooled condenser and a PTFE paddle stirrer, held in a water bath at 80°C. The fourth neck was stoppered and was used to introduce the reaction components to the reaction vessel. Once the emulsion had reached thermal equilibrium the initiator was added to the flask and allowed to react for 12 hours.

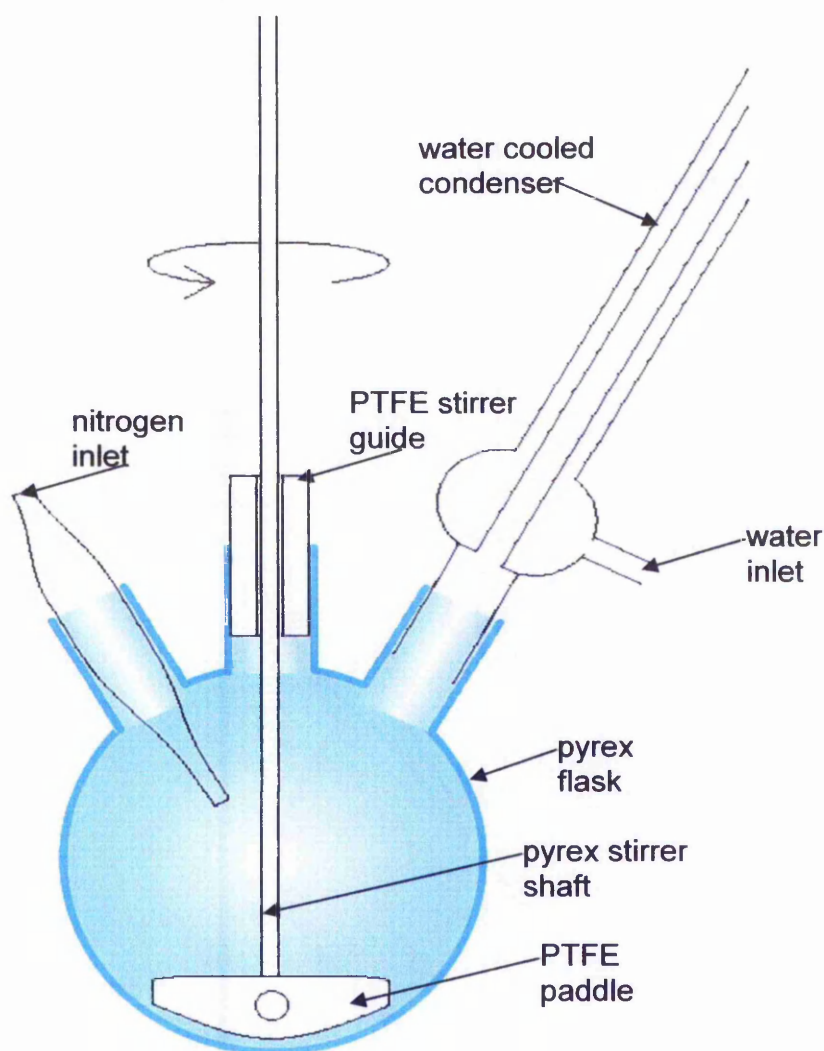


Figure 25: Diagram of “stirred” reaction vessel.

2.7 Cleaning

2.7.1 Films

The leaching steps used to prepare the film were also essentially cleaning steps. Leaching additive from the films involved numerous baths in DDW until the bath water was the same conductivity as the original DDW. This removed all the additive and any contaminants from the film. In cases where electrolyte solutions were used in film preparation i.e. HCl acid for acid washing and NaOH for leaching L30D, the samples were cleaned by bathing in DDW until the bath water was the same conductivity as the original DDW.

2.7.2 Porous particles

Cleaning the samples was achieved by flocculating the particles with 0.5M HCl, followed by repeated centrifugation/decantation steps until the waste water was the same conductivity as the original DDW. This is a relatively quick method of cleaning and also removes the soluble polyelectrolytes that dialysing does not remove. The particles were easily re-suspended by ultrasonification. For SSA determinations the dispersions were freeze-dried obtaining a free-flowing powder.

2.8 Characterisation

2.8.1 Nitrogen adsorption on the Quantachrome apparatus

Prior to a SSA measurement the sample was placed in a sample holder with a dynamic flow of helium across it until the thermal detector response settled back to zero. The sample, in its holder, was transferred to the Quantachrome detector and two adsorption/desorption cycles were carried out. The SSA of the sample was determined only after this initial cleaning.

The amount of nitrogen adsorption at five partial pressures, between P/P^0 values of 0.1 and 0.3, were taken and incorporated into the BET equation and the SSA calculated.

2.8.2 Mercury porosimetry

Pore size distributions and pore volumes were determined by mercury porosimetry on a Porosimeter 2000 series mercury porosimeter (Carlo Erba Strumentazione). Film samples were placed in a dilatometer and firstly evacuated of air and then filled with mercury. The dilatometer was placed in an oil filled autoclave and the pressure continuously increased at a steady rate. At predefined pressure values the mercury intrusion volume was recorded and used to generate the pore radius profile.

2.8.3 Particle sizing – transmission electron microscopy

Samples of latex were diluted and dried onto a sample grid. The sample was evaluated on a Joel JEM 2010 transmission electron microscope and photographs taken.

The transmission electron microscopy (TEM) micrographs were blown up to A4 size and lines drawn across the middle of the particles. All the lines drawn were parallel to each other. The lines were measured in millimetres and converted to nanometres with the aid of the sizing bar. Approximately 300 particles were measured per sample and the diameters entered into a spreadsheet and the average particle diameter determined.

2.8.4 Kinetics

The kinetics of the porous latex particle polymerisations was determined from the plot of monomer conversion against time. The polymerisation kinetics were evaluated for polymerisations carried out in the stirred reaction vessel. The monomer conversion was evaluated at various points during the polymerisation by removing 0.5 cm³ of the reaction mixture, via the fourth stoppered neck. The positive pressure supplied from the nitrogen inlet prevented oxygen from entering the reaction vessel. The sample was removed by a syringe equipped with a long, 3 mm bore, PTFE tube. The tube had enough internal volume that the sample of reaction mixture did not reach the actual plastic syringe where contamination from the lubricating grease could result. The sample was transferred to a watch glass, weighed and placed in an oven at 80°C for 1 hour. The resulting residue was weighed and the contribution from surfactant, initiator and buffer was subtracted to find the percent weight of polymer present. A previous study¹⁷⁸ has proven that the residual monomer in the sample does not effect the result of the gravimetric determination. Monomer deliberately added to the sample was shown to

evaporate off in the oven rather than polymerise and give a false value of the percent solids.

2.8.5 Vacuum frame

Nitrogen adsorption and desorption isotherms of samples were carried out in a vacuum frame. A vacuum frame consists of a glass-enclosed microbalance, which can be evacuated of air. The sample was suspended on the microbalance so that it hangs at the bottom of a drop tube facilitating its cooling by liquid nitrogen (Figure 26).

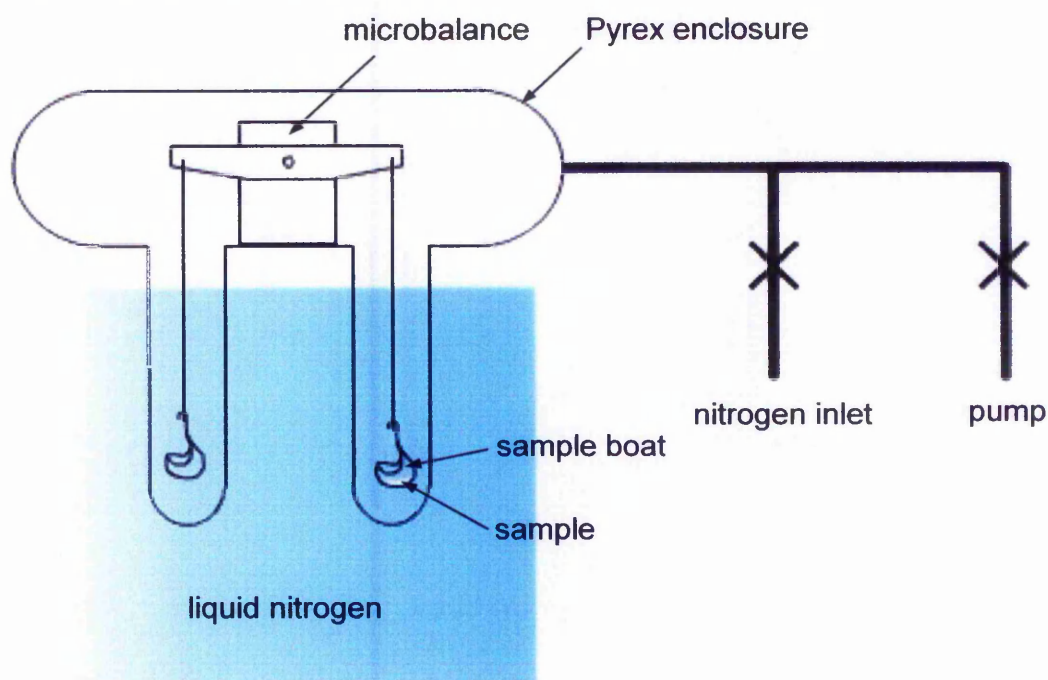


Figure 26: Schematic diagram of a vacuum frame.

Once the sample had reached thermal equilibrium and constant weight, nitrogen was let into the system in pressure steps and the weight of nitrogen adsorbed at each step was recorded. A plot of P/P^0 against weight of nitrogen adsorbed produced the adsorption isotherm. Once the saturation pressure of

nitrogen had been reached, the pressure was reduced in steps and the new weight of nitrogen adsorbed at each step recorded. Using the new values and plotting P/P^0 against weight of nitrogen adsorbed produced the desorption isotherm.

2.8.6 t-plots

t-plots were carried out in a vacuum frame. The standard sample was polymerised in the same manner as the porous latex particles, but using no toluene or DVB, to form a non porous material. An isotherm of the standard sample was generated and the t values calculated for each pressure point. An isotherm for each sample under investigation was generated and the amount adsorbed at each pressure point was plotted against the corresponding t value to form the t-plot. The theory behind the t-plot is described in section 1.8.1.4 t-plot.

2.9 Incorporation of porous latex particles into a porous latex film

Porous latex particles, dispersed in water, were incorporated into the porous latex film prior to casting. The wet PBMA latex, pore forming additive and porous latex particles were all mixed together and cast in the usual manner. The removal of pore forming agent and cleaning of the film was the same as that for films prepared without the incorporation of porous latex particles.

2.10 Barrier characteristics of porous latex films

The barrier characteristics of the latex films were evaluated by dynamic adsorption of methanol on a base carbon adsorbent coated in latex film. The dynamic adsorption apparatus has been described previously¹⁸¹. 12-30 mesh granules of steam activated coal based carbon BPL (Chemviron) were dip coated in latex. Methanol was carried through a volume activity tube packed with granules by nitrogen carrier gas (1 l min^{-1}) at 1 mg l^{-1} , 0% relative humidity, and 25°C and the exhaust concentration monitored with time by infrared spectrometry (Miran model 1Acvf).

2.11 Calculations

2.11.1 Calculation of a particles extra SSA

The specific surface area of smooth non-porous spheres of a known radius can be determined using the equation shown below.

$$S = \frac{6}{d_{vs} \times \rho} \quad \text{Equation 6}$$

Where d_{vs} is the mean volume to surface diameter, and ρ is the density of the particles. Assuming monodispersity, d_{vs} becomes the mean particle diameter. The particle mean diameter determined from TEM micrographs was used in the above equation to determine the theoretical SSA of the sample assuming smooth non-porous particles. This theoretical SSA was subtracted from the SSA measured by N_2 adsorption to find the extra SSA. Any extra SSA will have arisen from N_2 adsorption not on the external surface of the particles, but as a consequence of particle porosity.

2.11.2 Calculation of the number of pores in a porous film.

The number of pores in a porous latex film was calculated from the porosimetry data. During the porosimetry determination the volume of mercury intrusion into the sample is measured at pre-set pressure steps. Between two pressure values, a small size range of pores will be analysed and an average value taken for the purpose of creating the pore radius profile.

For example, at 100 bar, pores of 75 nm radius and larger are filled. The next pressure step up to 120 bar fills all pores from 75 down to 62.5 nm. Subtracting the volume of intruded mercury at 100 bar from the volume of

intruded mercury at 120 bar gives the volume of pores in the range 62.5 to 75 nm (averaged to 68.8 nm). Assuming all the pores are as deep as the diameter of the pore, the volume of one pore can be found using the equation for the volume of a cylinder. The total volume intruded for a given pressure step divided by the volume of the average pore for that step gave the number of pores for that pore range. Repeating this procedure for all the pressure steps gave the apparent total number of pores in the sample.

3 Results and discussion

3.1 Porous latex films

3.1.1 Specific surface area

Of all the methods tried (section 2.2) the most promising results were for the films obtained by leaching L30D, sucrose, PVP, glycerol and SDED from PBMA, and those obtained by exceeding the CPVF of NE30D with PS.

For L30D leaching experiments, PBMA films were cast with varying amounts of L30D based on the dry film weight with subsequent extraction of L30D by washing with 0.2M sodium hydroxide. For sucrose, PVP, and SDED leaching experiments, PBMA films were cast with varying amounts of each additive based on dry film weight with subsequent extraction by washing with DDW. All films were freeze dried after additive leaching and their specific surface areas evaluated and the results are shown in Chart 1. For the CPVF experiments, NE30D was cast with various loads of PS above its CPVF resulting in voids between PS particles. No further treatment was required after casting. The specific surface areas of these films are also shown in Chart 1.

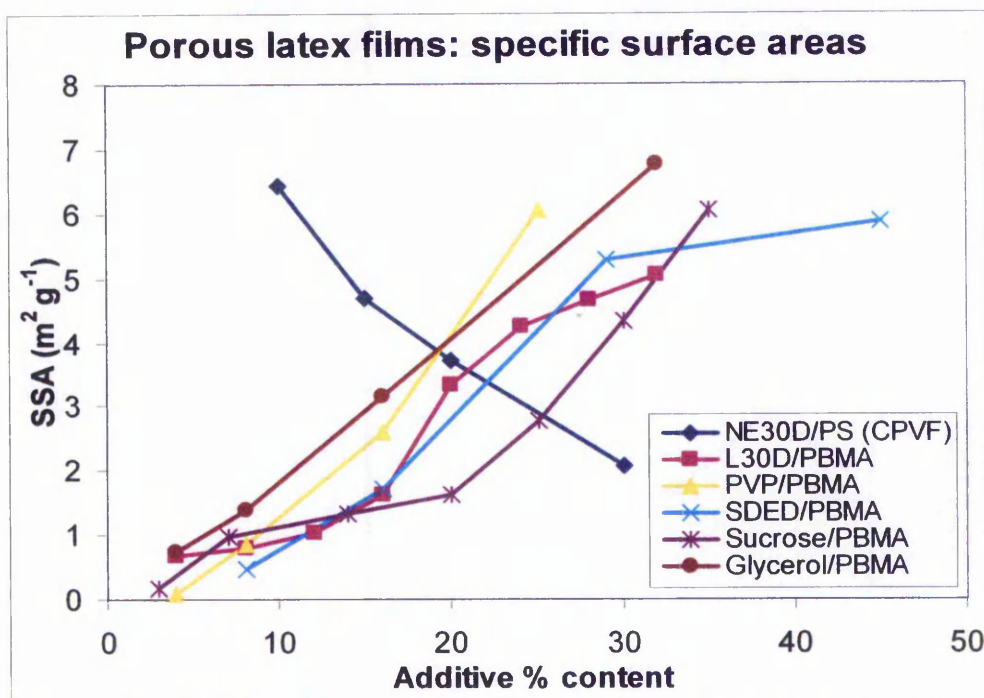


Chart 1: Plot of additive content vs specific surface area for porous latex films.

Study of the results reveals that L30D leached films show an increase in specific surface area with increasing L30D loading. Films leached of sucrose, PVP, and SDED all show higher specific surface areas with increasing additive loading, in the same way as L30D. For sucrose films containing loadings greater than 35% no films were attainable, due to the washing step redispersing the polymer particles. This suggests that larger amounts of sucrose hinders particle-particle contact restricting coalescence of the film. PBMA films with PVP and SDED loadings greater than 25 and 45% respectively, also suffer from redispersion during the washing step. In CPVF experiments, a gradual decrease in specific surface area is seen with increasing NE30D loading. This is in accord with the assumption that larger

NE30D loadings cover more of the poly(styrene) spheres and will begin to block interstices completely.

3.1.2 Porosimetry

The porous nature of all films was determined by mercury porosimetry for each pore generating process. The trends in total pore volume for all films are shown in Chart 2. Pore size profiles for all successful films are shown in Charts 3 - 8.

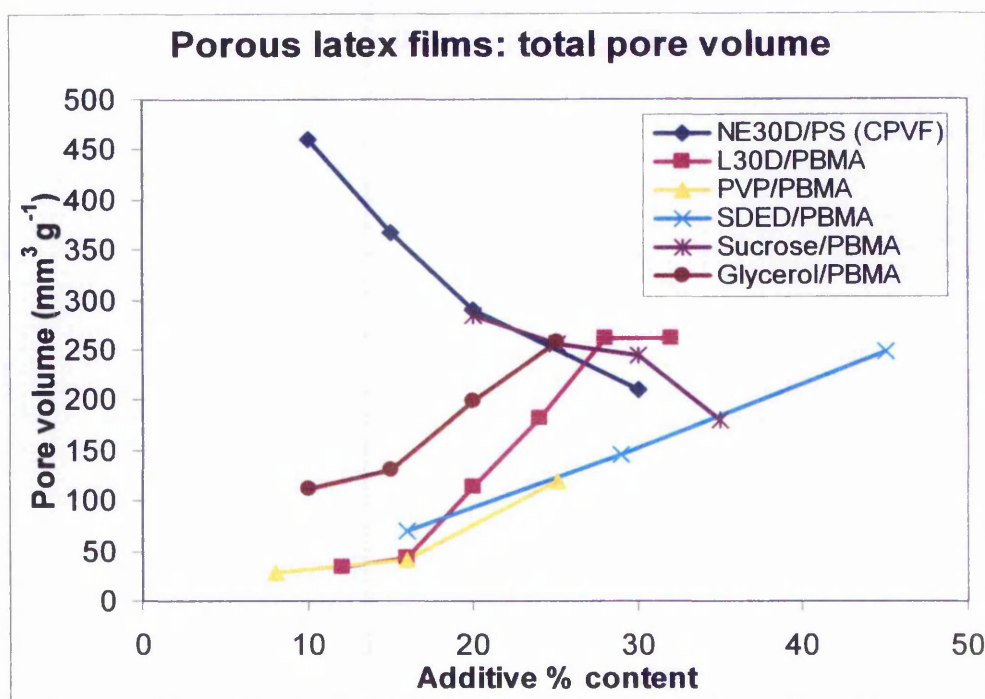


Chart 2: Plot of additive content vs total pore volume for porous latex films.

PBMA films leached of L30D show a general increase in pore radius and cumulative pore volume with increasing amount of L30D added then leached (Chart 2 & 3). All films contain relatively the same amount of small pores, but with increasingly larger pores being added with increasing amounts of L30D.

This indicates that with more L30D spheres present, larger agglomerates of L30D can be formed in the cast film which will produce larger pores once leached out.

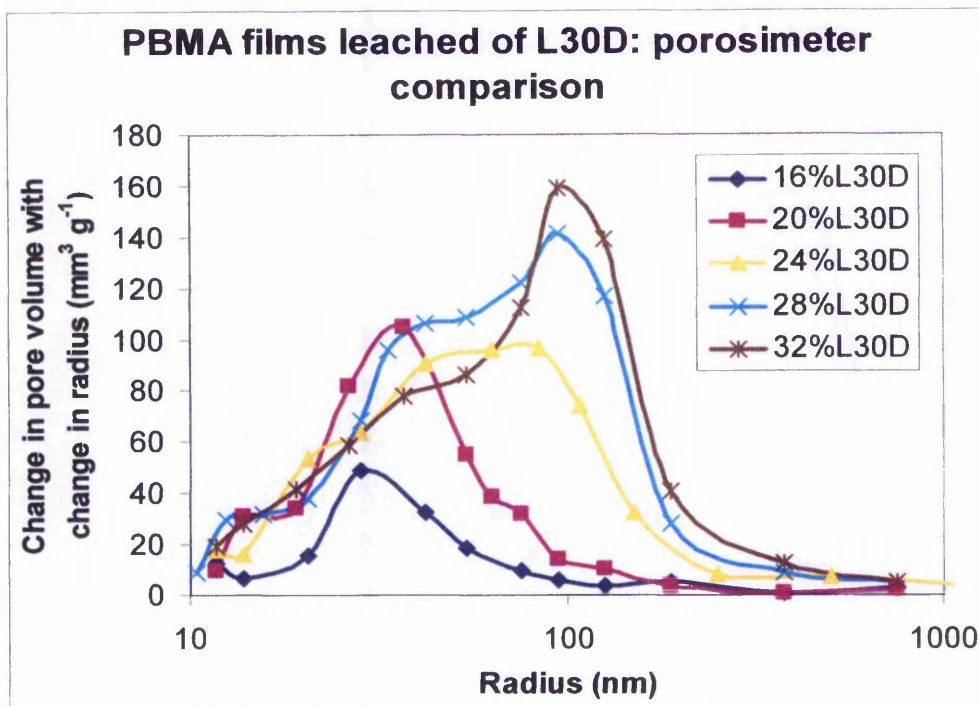


Chart 3: Pore radius profiles for films prepared using L30D.

PBMA films leached of sucrose show a decrease in pore radius and total pore volume with increasing amount of sucrose added then leached (Chart 2 & 4). This suggests that with higher sucrose loadings sugar is more easily expelled from the film possibly due to more complete migration channels to the surface formed during drying. This results in more sucrose exuded to the surface and less sucrose inside the dry film.

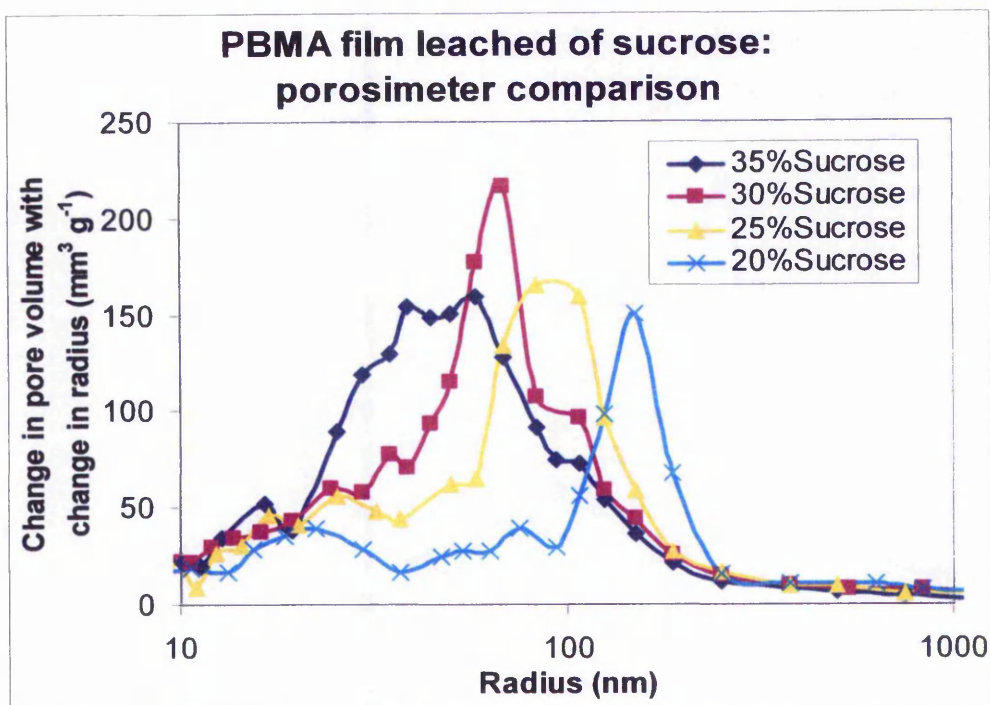


Chart 4: Pore radius profiles for films prepared using sucrose.

PBMA films leached of glycerol show an increase in pore radius and total pore volume with increasing amount of glycerol added then leached (Chart 2 & 5). This indicates that with addition of more glycerol, more and larger pores are formed.

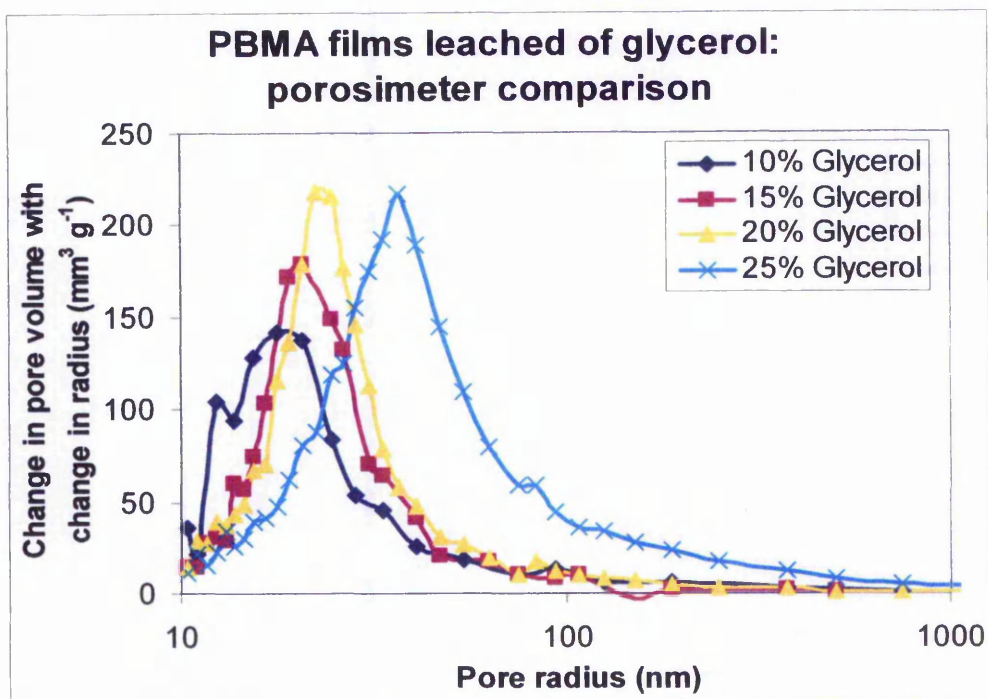


Chart 5: Pore radius profiles for films prepared using glycerol.

PBMA films leached of PVP added at different levels, show an increase in total pore volume with increasing amount of PVP leached, while the average pore radius stays relatively unchanged (Chart 2 & 6). This suggests that PVP separates out into domains of a single size. Addition of more PVP increases the number of pores while the pore radius stays constant.

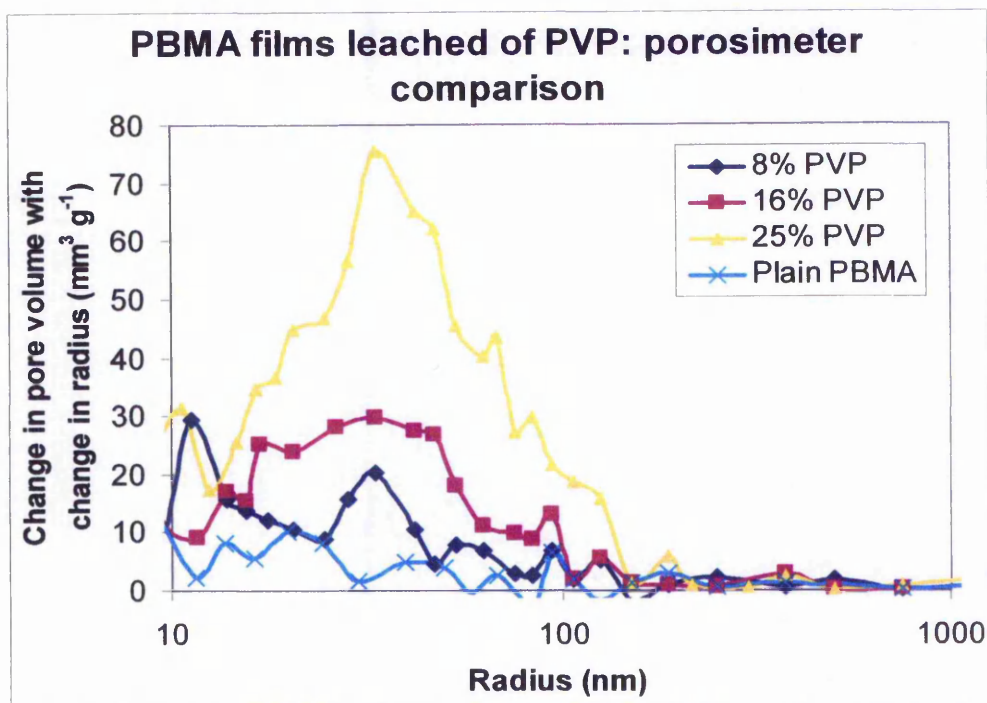


Chart 6: Pore radius profiles for films prepared using PVP.

PBMA films leached of SDED show increasing total pore volume with increased loadings, while the average pore radius stays relatively unchanged (Chart 2 & 7). This indicates, like PVP, that SDED forms domains of a similar size and on addition of more additive increases the number of pores.

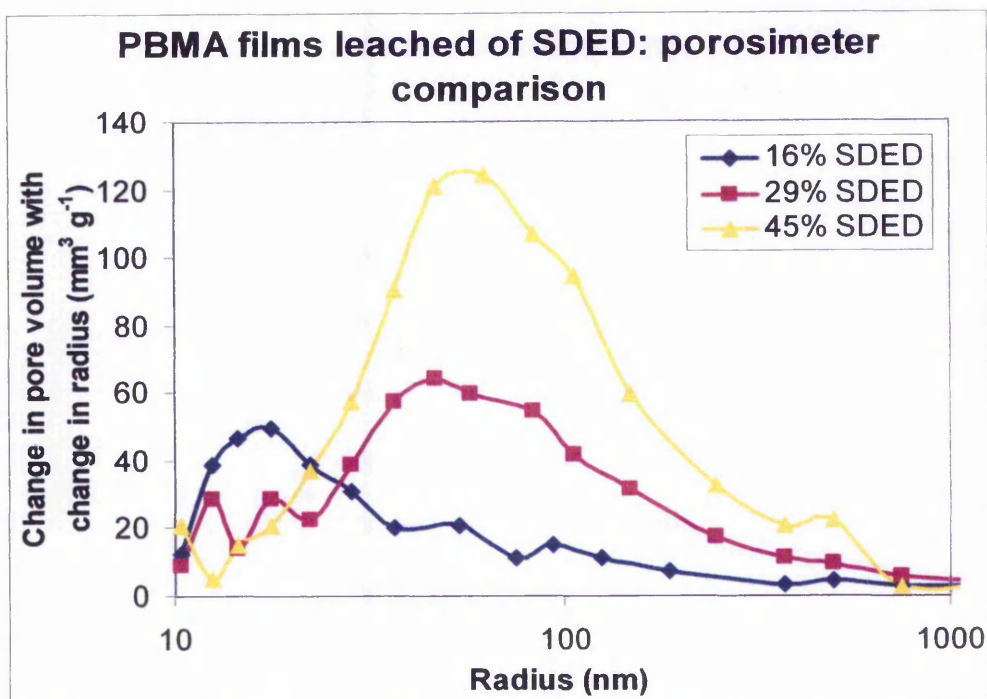


Chart 7: Pore radius profiles for films prepared using SDED.

Films prepared by exceeding the CPVF of NE30D with PS have a relatively narrow pore size distribution and high total pore volumes (Chart 2 & 8). At low amounts of NE30D there are two apparent pore size distributions close together. As NE30D loading is increased firstly the larger pore distribution is reduced leaving only the smaller, and then secondly the smaller distribution is reduced until no pores are present. The narrow pore radius distribution is due to the uniform interstices formed from the monodisperse PS latex. The reduction in total pore volume with increasing NE30D content is due to the filling of the interstices with polymer, which is also apparent in the specific surface area loss (Chart 1). The presence of two peaks in the pore size distribution could be due to the presence of completely empty and partially empty interstices. Some interstices will be void of any binder and will contribute to the larger peak in the profile. The smaller peak will arise from

interstices, which are partly filled with binder, and are therefore smaller compared to the empty interstices. It would be expected that with increasing binder that less interstices will remain empty and that the larger peak will decrease in size. The initial reduction of the large peak is, indeed, seen in the porosimetry results (Chart 8).

Porous Latex Films: Exceeding CPVF of NE30D with PS

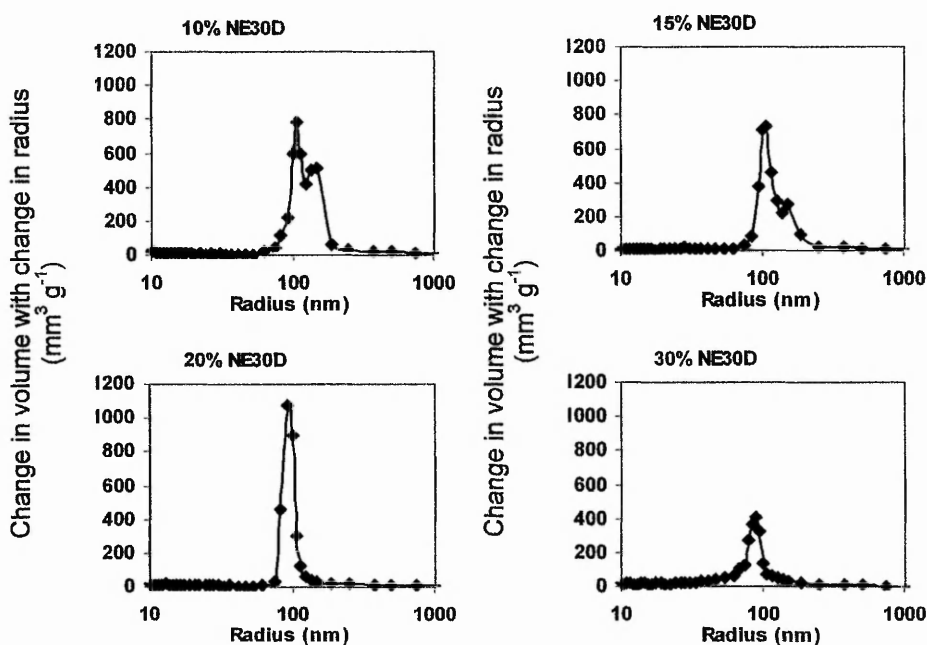


Chart 8: Pore radius profiles for films by exceeding the CPVF of NE30D with a PS latex.

Leaching HPMC, SDS, and low and high concentrations of NaCl were ineffective in producing films with detectable specific surface areas under the casting conditions used. Limited solubility of HPMC in water, prevented films being formed with high enough quantities to form a porous film. After leaching

only the surface of the film was opaque while the interior was still transparent. The degree of opacity is a good indication of porosity due to light scattering by a large number of small pores (unless the pores are significantly smaller than the wavelength of light). Only small amounts of sodium chloride could be added to the latex without affecting stability. These small quantities were not effective for pore generation.

NaCl was added to the latex in quantities so that some films were prepared from initially flocculated latex. Other films were cast from stable latex, but flocculation occurred at various stages of casting as the serum ionic strength increased during water evaporation. All films prepared by this method were very opaque and, in the case of higher sodium chloride contents, rough textured. The opacity will be due to the NaCl being finely dispersed throughout the polymer and the differing refractive indices of NaCl and PBMA. No visible change occurred during the leaching process and the SSA of the film was too small to be determined by the Quantachrome method. This suggests that the NaCl is dispersed throughout the film in the form of small islets completely surrounded by polymer and not in the form of a continuous phase. This prevents the removal of NaCl by leaching in water.

Films prepared by leaching SDS showed only surface opacity with a transparent interior. Du Chesne¹⁸² *et al* showed that incompatible stabilisers migrate to the film surfaces and to islets within the polymer film. These islets may not be accessible to leaching so only the surface surfactant will be removed resulting in very little porosity. The successful pore generation by SDED compared to SDS correlates with the findings of Zhao *et al*¹²⁰ who studied the distribution of these two anionic surfactants and found SDED to be

more compatible. The findings illustrates the importance of partial additive-polymer compatibility for porous film production.

3.1.3 Electron microscopy.

Freeze-fractured scanning electron microscopy (FFSEM) micrographs of the cross-section for films prepared via the CPVF method, using glycerol and using NaCl are shown in Figures 27-29 respectively.

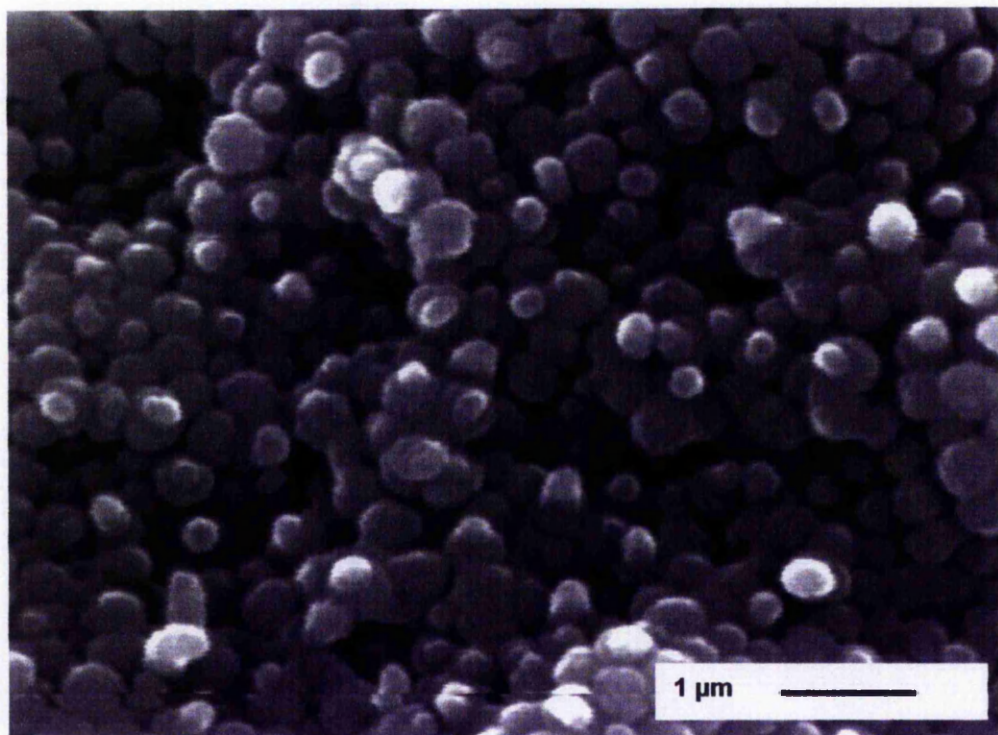


Figure 27: FFSEM micrographs of a film prepared via the CPVF method.

Study of the micrograph of the PS film prepared via the CPVF method shows NE30D mixed in with the larger PS spheres. The NE30D particles appear to be bigger than the original 160 nm diameter spheres. Although not clear in this micrograph it may be due to the NE30D particles being 'pancaked' between the PS particles. The CPVF films have significant mechanical

strength and can be easily handled without breakage. Preparation of the same film without the presence of NE30D resulted in a powder residue.

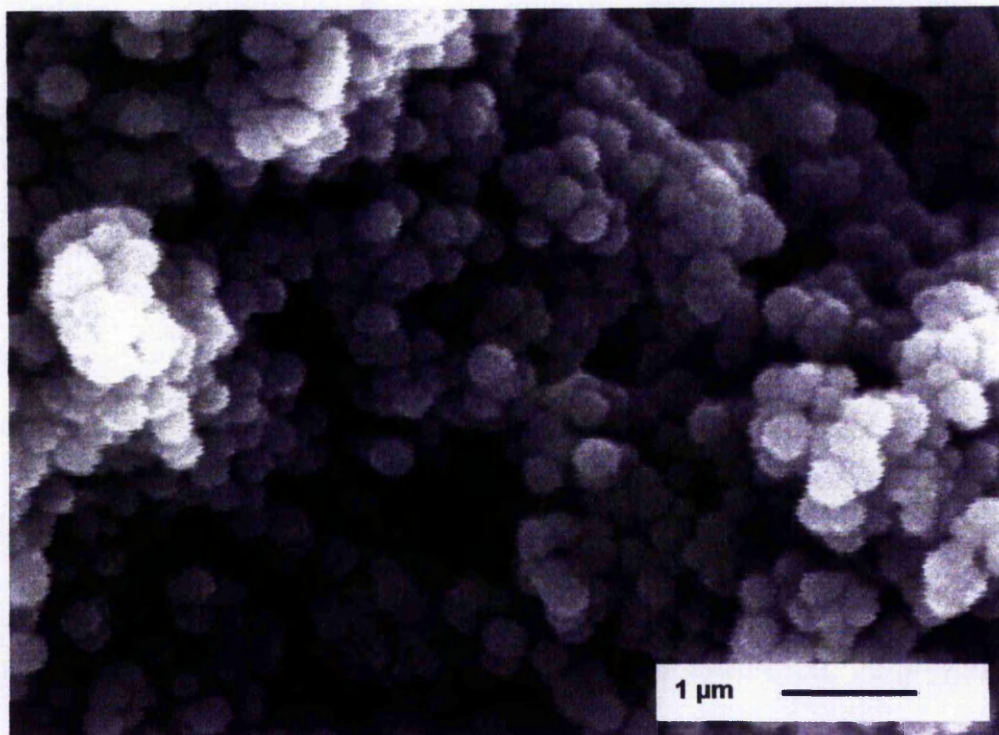


Figure 28: FFSEM micrographs of a film prepared using glycerol.

Study of the micrograph of the PBMA film prepared using glycerol shows a dense packing of particles with each particle maintaining its own identity. The mechanical strength of the film will result from limited polymer diffusion at the points of contact between particles. The presence of glycerol during the casting process has the effect of limiting particle-particle contact preventing the particles from fully coalescing

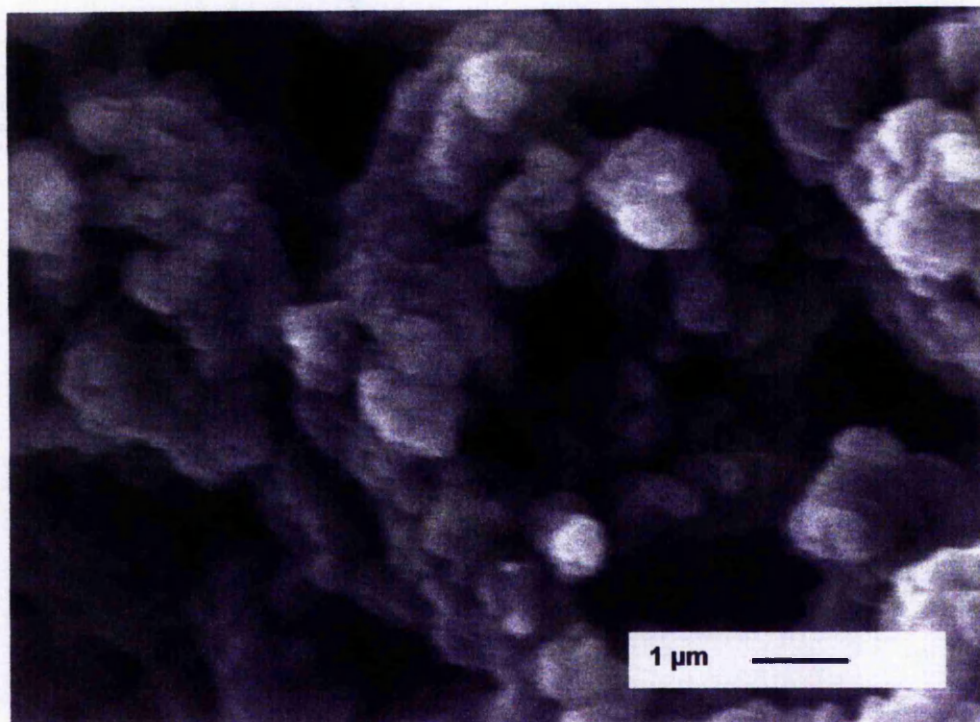


Figure 29: FFSEM micrographs of a film prepared using NaCl.

Study of the micrograph of the PBMA film prepared using NaCl shows that the identity of each particle is diminished. NaCl does not have the ability to prevent the particles from completely deforming resulting in closure of the interstices. This is shown in the SSA of the film which is too low to measure by the Quantachrome method.

For successful production of porous films, leachable additives must neither be too compatible nor too incompatible. If too compatible with the polymer then the additive may dissolve into the particles producing a homogenous film, whereas an incompatible additive may be completely exuded from the film during coalescence. Work by Zhao¹⁸³ *et al* measured surface concentrations of SDS and SDED in coalesced acrylic latex films. It was found that SDS

readily migrated to the films surfaces (film-air and film-casting substrate) and continued to be exuded to the surface during film maturation. However, SDED had a much less pronounced surface enrichment that did not change during film ageing, indicating better polymer compatibility.

3.1.4 Pore closure

The effect of capillary forces, on coalescence of porous films, arising from the curvature of the water surface within the interstitial voids were investigated. Capillary forces were originally postulated by Brown¹⁸⁴ to be the main driving force behind latex particle coalescence during water evaporation. This was later discounted by workers^{185,186} who showed that capillary forces alone were insufficient to cause particle coalescence. In this study where porosity has been created by leaching additives the films are effectively at film formation stage two with pores water filled. When they are dried there is the potential for completion of film formation and the 'healing' of the pores. Comparison of the properties of naturally dried films and freeze dried films, evaluated by specific surface area and mercury porosimetry, will show the effect that water evaporation has on particle coalescence.

Films prepared for this study from PBMA with various loadings of leachable L30D show a different range of pore sizes between each film. The lower loadings form relatively small pores while higher loadings add larger pores to the profile (Chart 3). After casting and leaching of L30D from the film a porous PBMA film is left with all pores filled with water. These films are effectively at film formation stage two as the particles are already ordered and partly coalesced. These films were divided into two halves, which were dried

differently. One half was dried in a nitrogen gas stream at room temperature and the other half freeze dried so that water sublimed rather than evaporated from pores within the film. After freeze drying was complete the film was kept at room temperature for an equal time as for the nitrogen dried sample, before both halves were stored at 4°C ready for analysis. Each film was evaluated for their SSA and pore radius profile.

The SSA results for freeze dried and nitrogen dried films are shown in Chart 9.

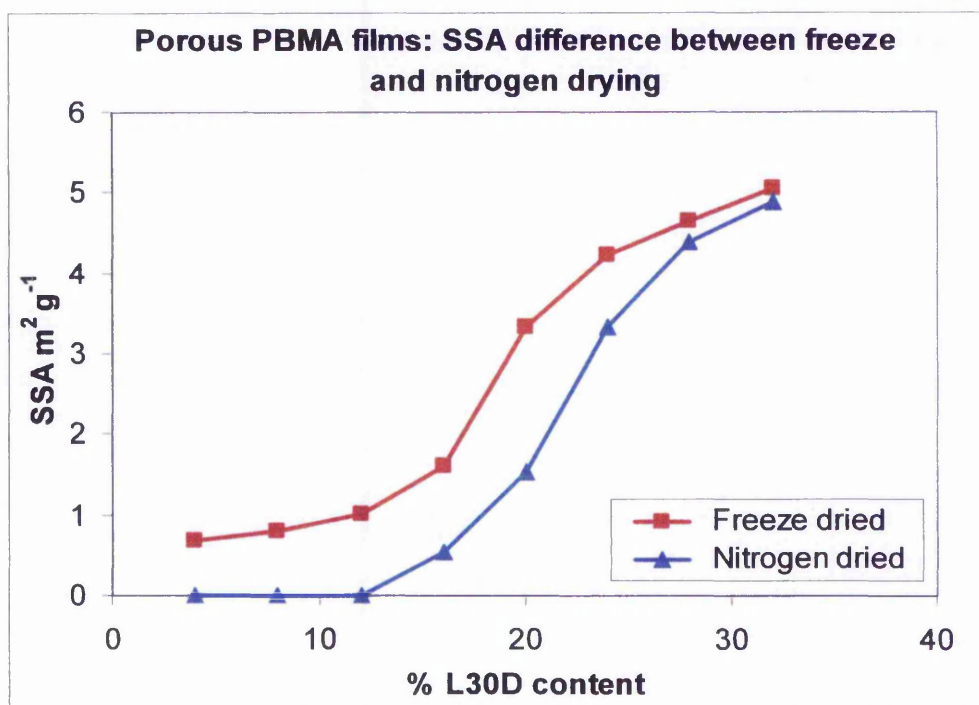


Chart 9: Plot of % L30D content vs SSA for films freeze dried and nitrogen dried.

Comparison of the pore radius profile for films leached of 10% and 30% L30D both freeze and nitrogen dried are shown in Chart 10.

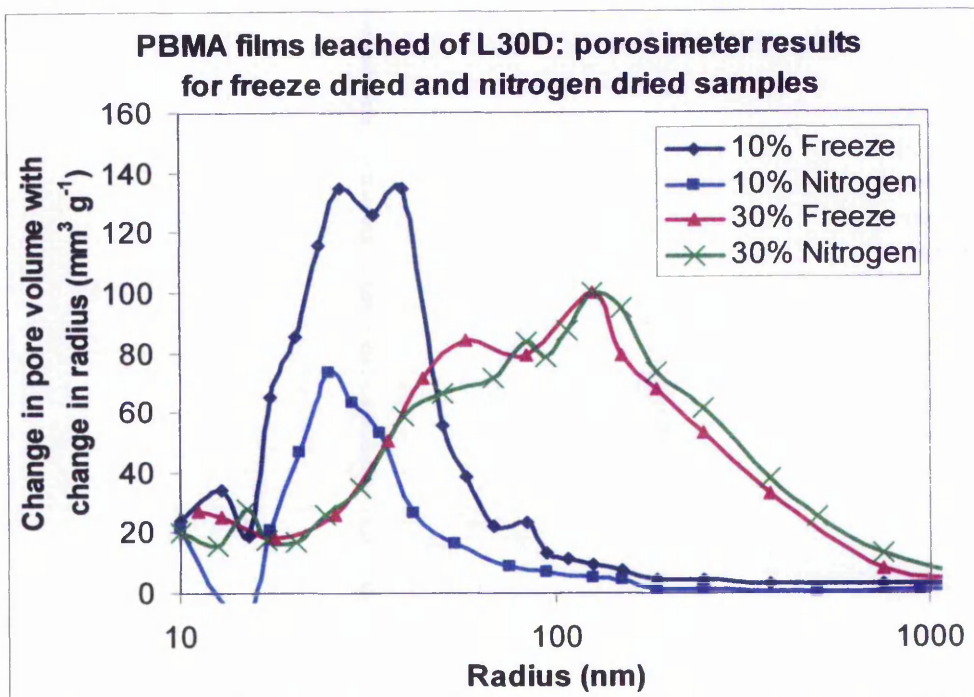


Chart 10: Pore radius profiles for films prepared using 10% and 30% L30D freeze dried and nitrogen dried.

Nitrogen dried samples with low additive contents show complete loss of surface area compared to their freeze dried counterparts (Chart 9). As additive content increases the difference in surface area between nitrogen dried and freeze dried samples decreases until little difference is noted.

Films prepared from 10% L30D show similar pore radii by both methods of drying, but the nitrogen dried sample shows a reduced number of pores suggesting pore closure (Chart 10). This pore closure is responsible for the differing SSAs seen for these two films.

Films prepared from 30% L30D by both drying regimes have similar pore radius profiles at similar heights indicating little difference in pore characteristics between the two (Chart 10). This is evident in the similar specific surface areas obtained for both these samples. This indicates that

films with only small pores further coalesce during nitrogen drying, but if larger pores are present less coalescence is seen. Pore closure can arise through viscoelastic deformation caused either by polymer-water interfacial tension (wet sintering)¹⁸⁷, polymer-air interfacial tension (dry sintering)¹⁸⁸ or from the water-air interfacial tension (capillarity)¹⁸⁴. Both film halves experienced a similar period of leaching, so that wet sintering is unlikely to lead to a difference and both films experienced a similar period in a dry state at room temperature, so that dry sintering is also an unlikely cause. It is thus tentatively suggested, since it is a matter of much debate¹⁸⁵ whether water has a direct role to play in the mechanism of film formation from hydrophobic latex particles, that pore closure is driven by capillary forces as water evaporates from fine pores. These forces being proportional to pore radius, have the greatest effect on the population of small pores. Lin & Meier¹⁸⁶ have also claimed a role for water and capillary forces in film formation from hydrophobic latex particles.

3.2 Reactive latex films

3.2.1 Sulphonated latex characterisation.

The latex surface as characterised by conductometric titration was found to be dominated by strong acid groups with no discernible weak acid contribution giving a total charge of $15.9 \mu\text{mole g}^{-1}$. The average particle diameter measured by electron microscopy was found to be 501 nm (3% coefficient of variance), and the specific surface area was $12.7 \text{ m}^2 \text{ g}^{-1}$. The conductometric titration is shown in Chart 11.

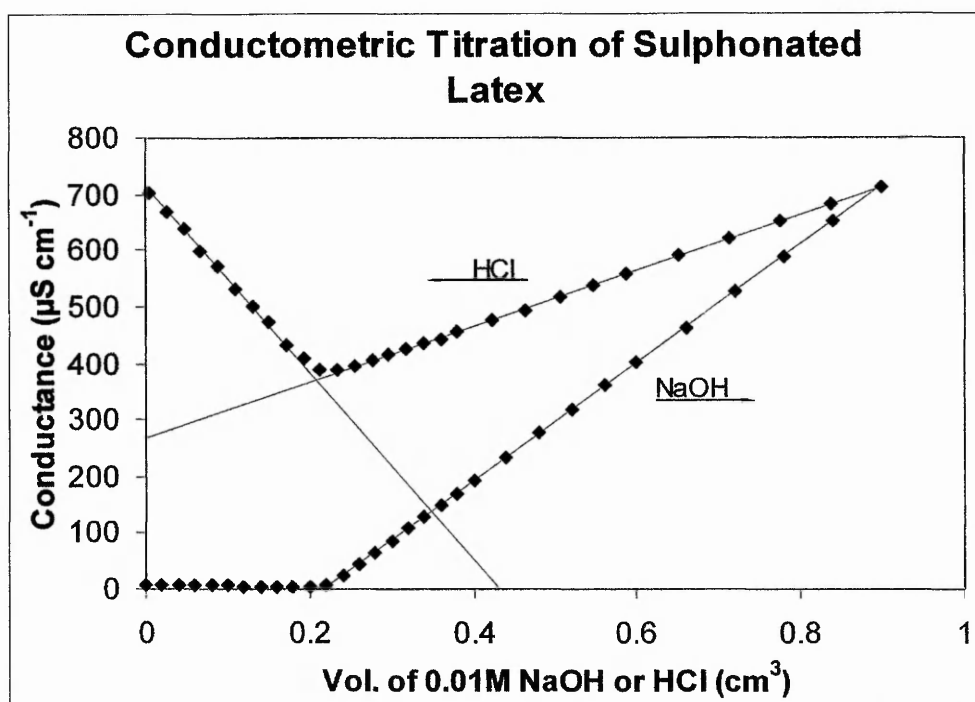


Chart 11: Conductometric titration curve of the sulphonated latex, SLATEX.

3.2.2 Film characterisation

3.2.2.1 Specific surface area.

Films were prepared as shown in Table 1 with percentage of additive based on post-cast dry film weight. Film NOADD was prepared additive free. Films prepared using glycerol and sucrose additives, following leaching, show

similar trends in SSA with increasing additive content (Table 1). Films prepared using L30D, following leaching, also show increasing SSA with additive content, but to a lesser extent. The films have less total surface area than the particles due to loss of surface from fusing of particles during casting. The SSA for film NOADD was too low for accurate determination using the Quantachrome apparatus.

Sample	Glycerol	Sucrose	L30D	SSA (m ² /g)
GLY10	10%	-	-	5.14
GLY15	15%	-	-	6.52
GLY20	20%	-	-	8.04
GLY25	25%	-	-	9.02
SUC10	-	10%	-	3.49
SUC15	-	15%	-	6.75
SUC20	-	20%	-	8.52
SUC30	-	30%	-	10.1
L30D15	-	-	15%	5.90
L30D20	-	-	20%	6.67
L30D30	-	-	30%	7.38
L30D40	-	-	40%	8.71
NOADD	-	-	-	<0.5

Table 1: Additives used and their amounts added based on percentage weight of post-cast film.

3.2.2.2 Porosimetry

Pore radius profiles for SLATEX films prepared using glycerol, sucrose and L30D are shown in Charts 12-14.

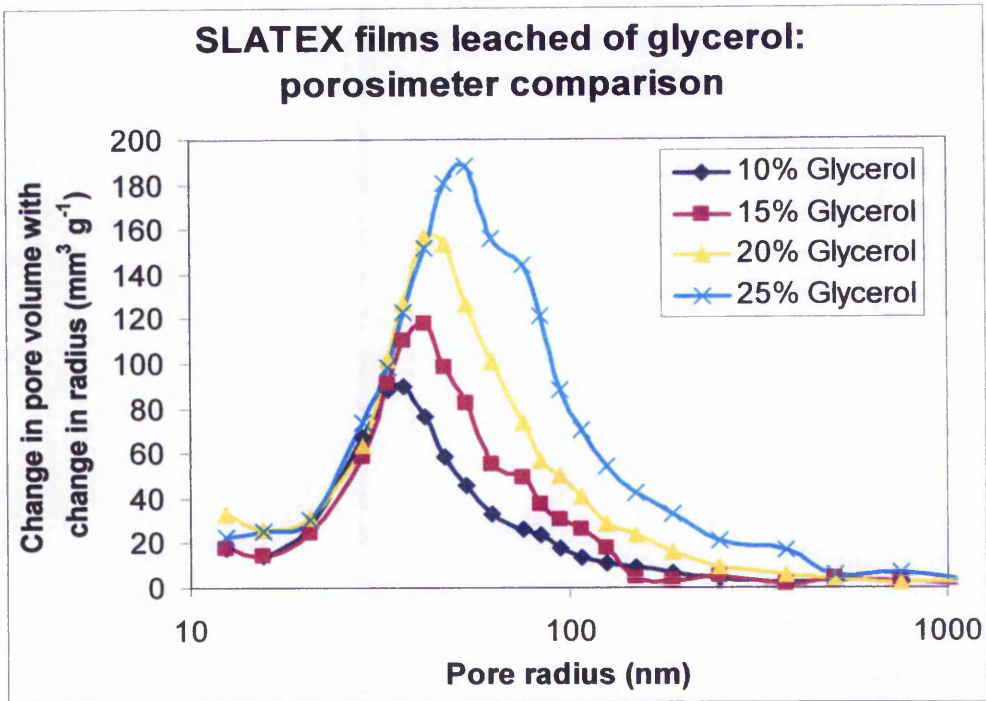


Chart 12: Pore radius profiles for films prepared using glycerol.

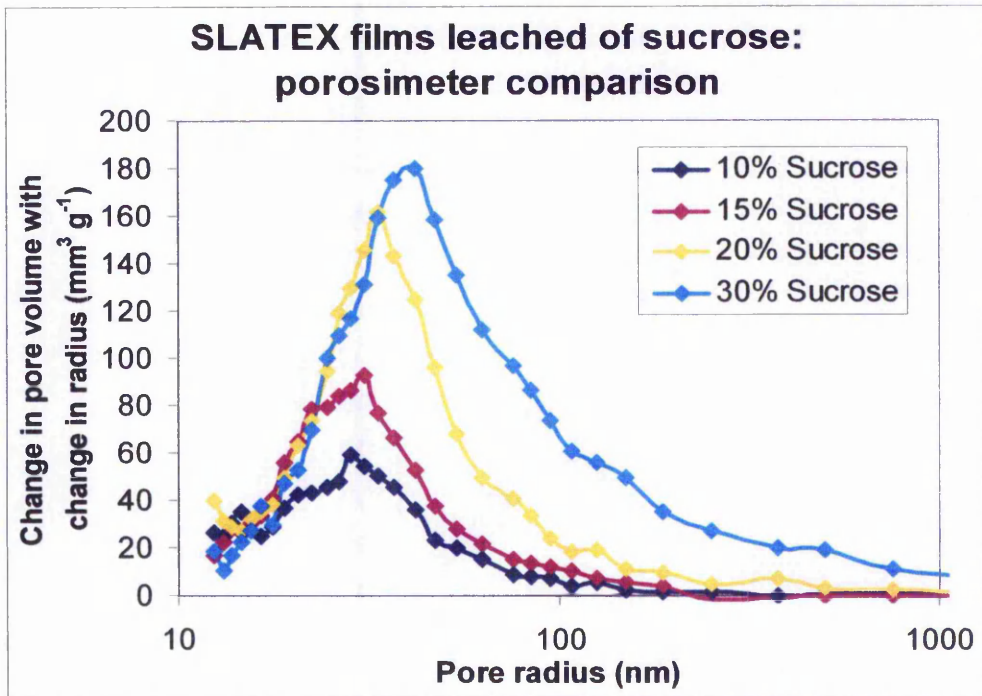


Chart 13: Pore radius profiles for films prepared using sucrose.

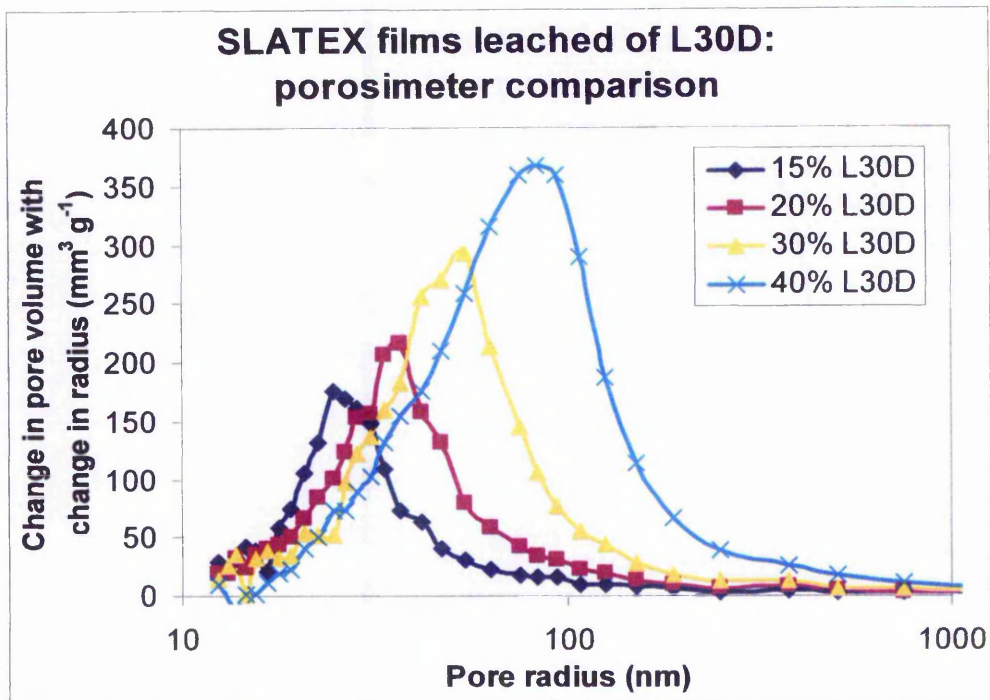


Chart 14: Pore radius profiles for films prepared using L30D.

The profile trends for all three additives show that with increasing additive content the total pore volume and average pore radius increased. The number average pore radius increased with additive content in all films. For SLATEX films prepared using glycerol and sucrose the number of pores per gram increased with additive content, whilst films prepared using L30D showed a decrease in number of pores per gram with increasing additive (Chart 15).

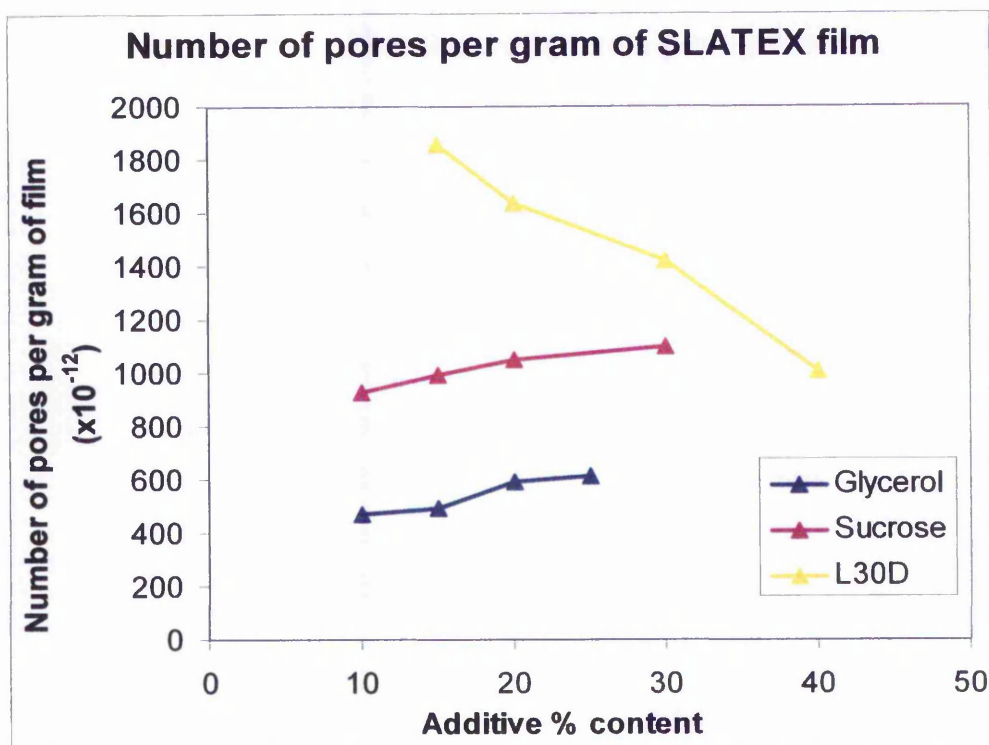


Chart 15: Number of pores per gram of SLATEX film.

The pore radius profiles for the SLATEX films prepared from glycerol and from L30D show the same trends as the films prepared using the same additives with the plain PBMA latex (see Charts 3 and 5). There are slight differences which can be accounted for by the different polymer/additive interactions due to the more hydrophilic surface of the sulphonated latex. However, a striking difference is seen between porous films prepared from the sulphonated latex and the plain PBMA latex using sucrose as the pore forming additive. When a porous film is made from the plain PBMA latex, unexpected characteristics result i.e. a decrease in pore radius and total pore volume with increasing amount of sucrose used to prepare the film (Chart 2 & 4). This suggests that with higher sucrose loadings sugar is more easily expelled from the film possibly due to more complete migration channels to the surface

formed during drying. This results in more sucrose exuded to the surface and less sucrose inside the dry film. The films prepared from the sulphonated latex using sucrose show more expected pore characteristics with changes in the amount of sucrose used to prepare the film. With increasing sucrose content the total pore volume and average pore radius increased. The higher hydrophilicity of the sulphonated latex, compared to the plain PBMA latex, will result in more favourable polymer/sucrose interaction. This will result in an increased compatibility and there will be less interfacial energy trying to exude sucrose out of the film.

3.2.3 Electron microscopy.

FFSEM micrographs for films prepared from SLATEX using 20% glycerol, 20% sucrose, 20% L30D and no additive are shown in Figures 30-33 respectively.

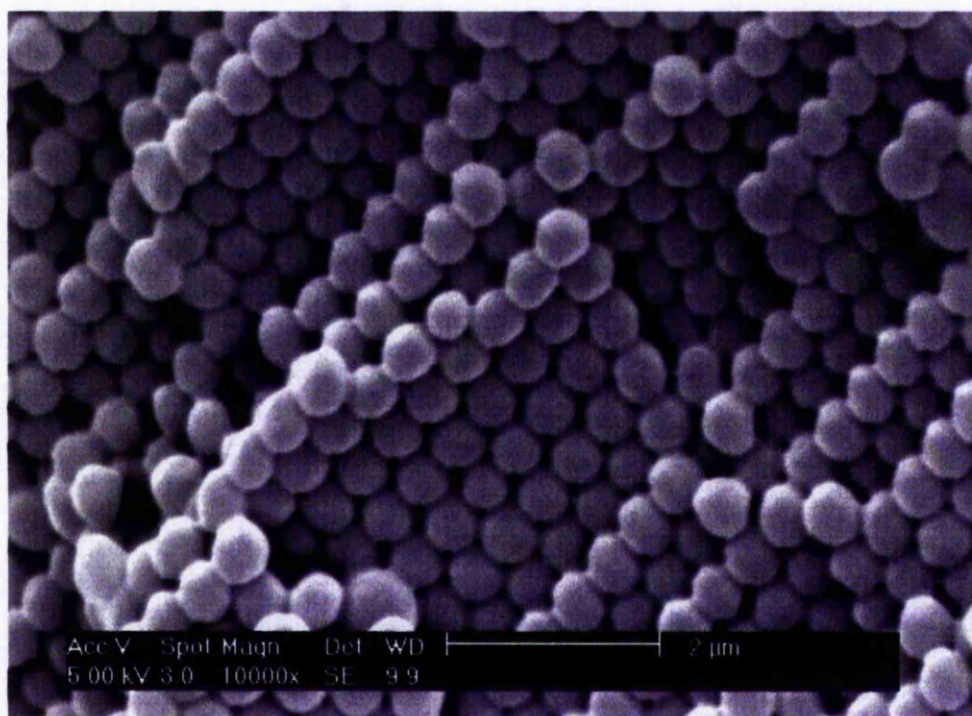


Figure 30: FFSEM micrographs of film GLY20.

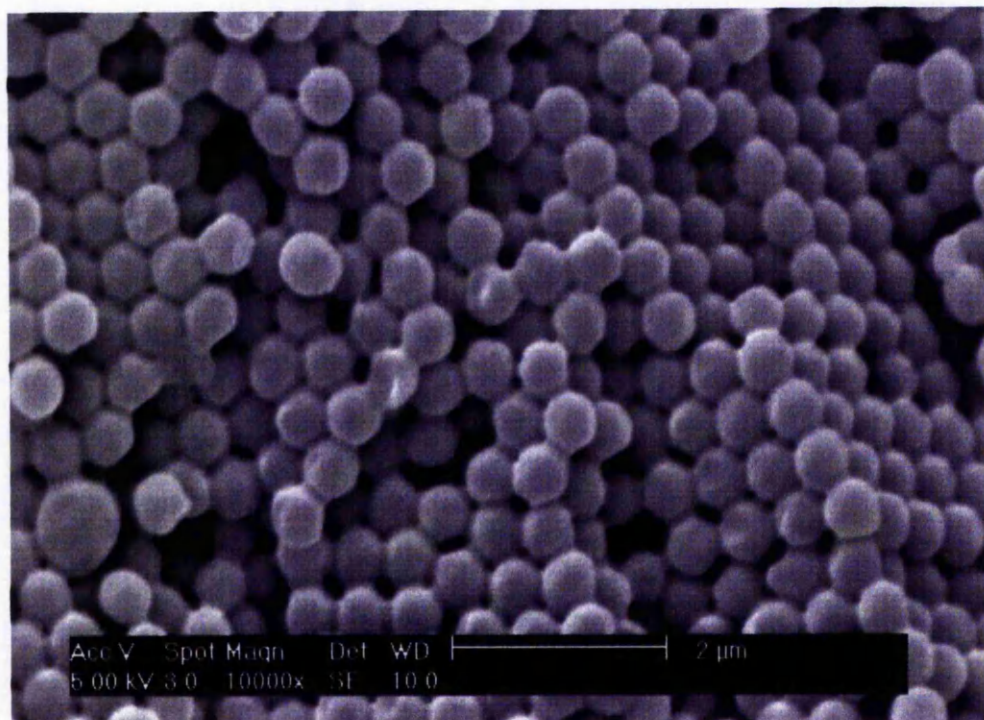


Figure 31: FFSEM micrographs of film SUC20.

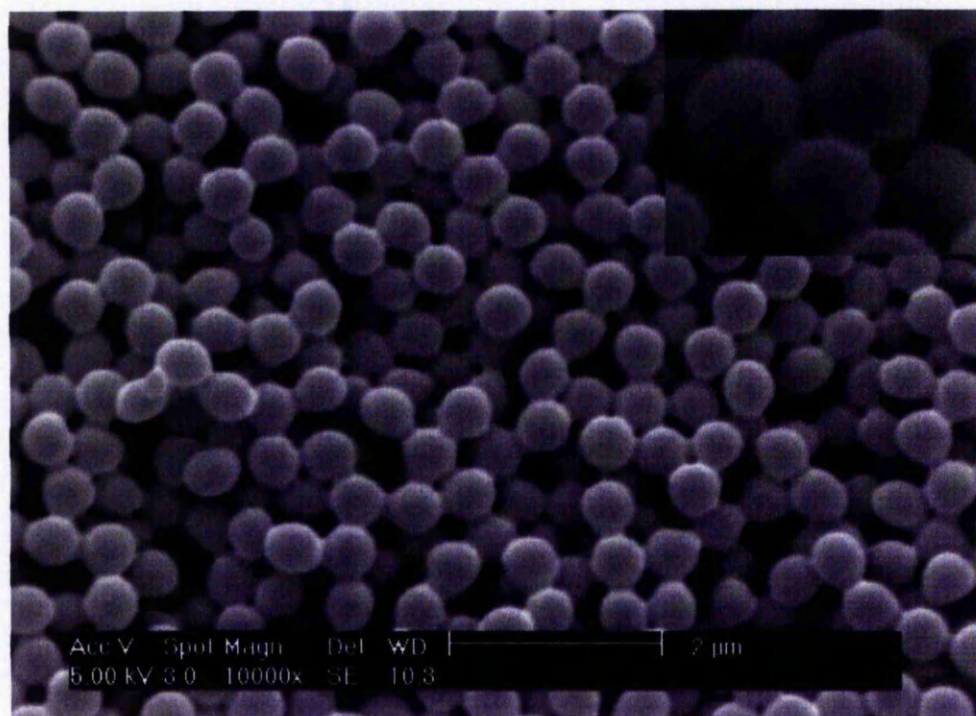


Figure 32: FFSEM micrographs of film L30D20. Insert: film at higher magnification.

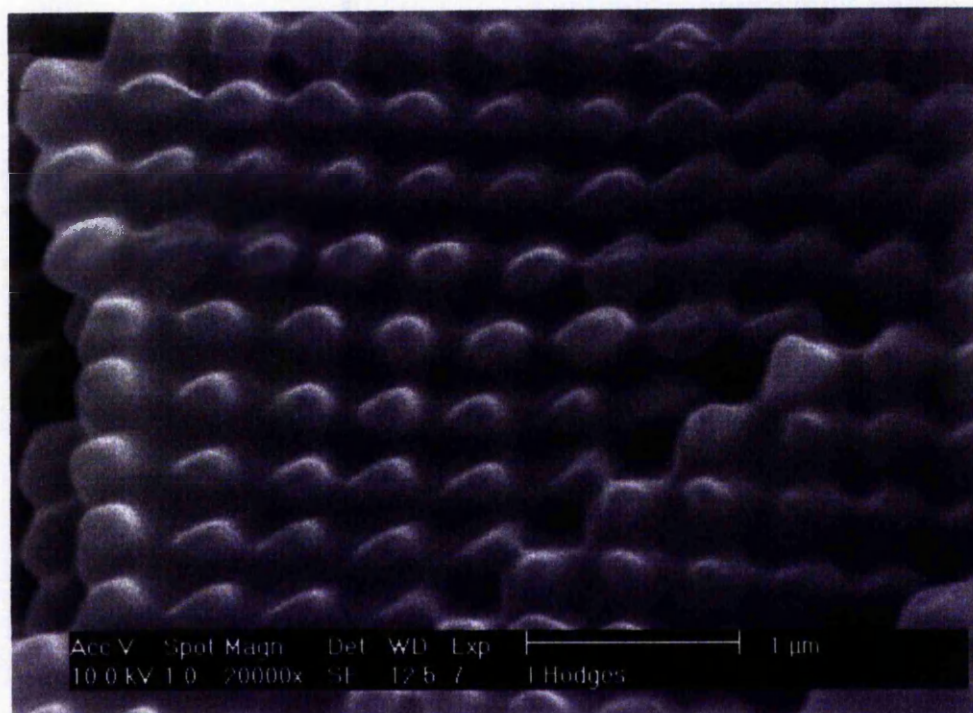


Figure 33: FFSEM micrographs of film prepared with no additive.

Films prepared using glycerol (Figure 30) and sucrose (Figure 31) show similar structural characteristics with particles close packed. The film prepared using glycerol has a higher degree of ordering than the sucrose film. A possible reason for this could be increasing viscosity of the sucrose solution as water leaves during film formation, hindering particle movement into the close packed arrangement. The film prepared using L30D (Figure 32) shows a disordered structure. This is due to the relatively large size of L30D, which cannot be pushed into interstices or exuded from the film, therefore stopping the development of the close packed structure during drying. This results in the relatively open, random order seen in the micrograph. Films prepared using additives are held together by partial particle fusion with neighbouring

particles (Figure 32, insert). If no additive is used then no pores are formed in the SLATEX film (Figure 33).

3.2.4 Suggested pore generation mechanisms

3.2.4.1 Small molecule leachable additives

The physical properties and micrographs of films prepared using glycerol and sucrose are compatible with the idea that the additive becomes trapped in the interstices during film formation preventing full particle deformation. This produces a network of additive throughout the film, which is present in the final cast film. Leaching the additive leaves interconnecting pores spread throughout the whole film. At low amounts of additive not all interstices between the spherical particles form pores. Increasing the amount of additive in the film increases the number of interstices which are retained as pores and increases the average pore size because there is more trapped material. This process is shown schematically in Figure 34.

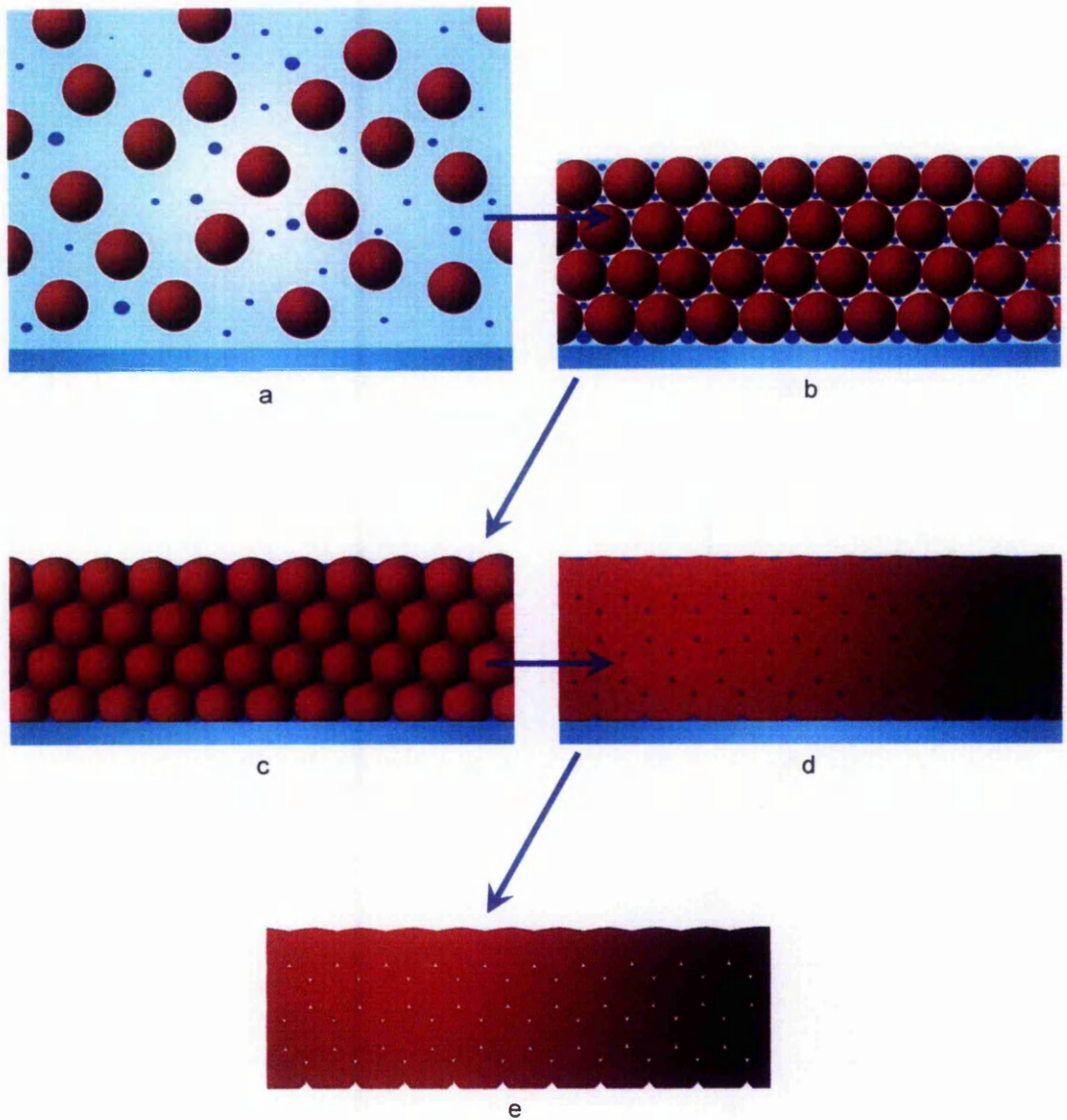


Figure 34: Schematic representation of pore formation using small molecule leachable additives. a) Latex particles and additive (small blue spheres) suspended in water. b) Close packed latex particles with water and additive filled interstices. c) Deformed latex particles with additive filled interstices. d) Coalesced latex particles with continuous additive domains. e) Coalesced latex particles with continuous porous domains

3.2.4.2 Large particulate leachable additives

A different pore generation process is in operation for films prepared using L30D. L30D forms domains of particles within the film. Upon addition of more L30D these domains grow and join together forming larger and fewer domains, which in turn produce larger and fewer pores once L30D is removed from the film. This process is shown schematically in Figure 35.

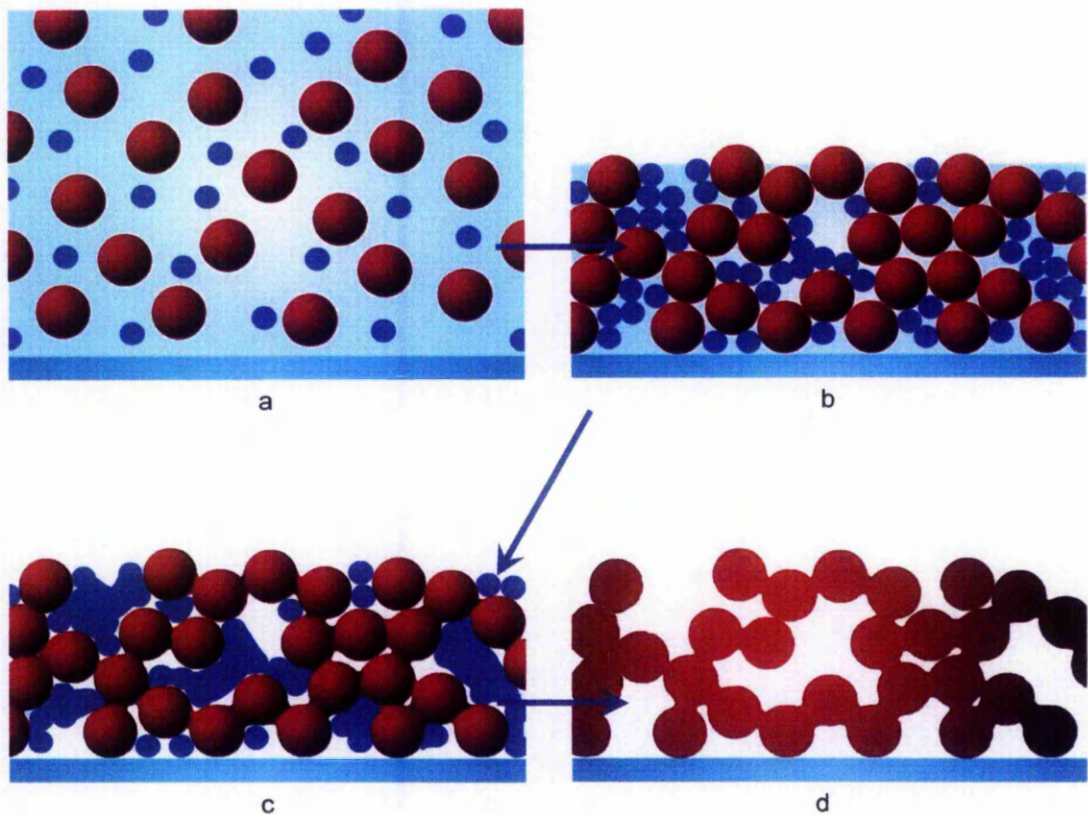


Figure 35: Schematic representation of pore formation using large particulate leachable additives. a) Latex particles and L30D (small blue spheres) suspended in water. b) Disorderedly packed latex particles and L30D with water filled interstices. c) Deformed latex particles with domains of deformed L30D. d) Coalesced latex particles with continuous porous domains

It has been shown previously that a successful pore forming additive needs partial compatibility with the polymer¹⁷⁸. If the additive is too compatible it will dissolve into the polymer; if too incompatible it will be fully exuded to the surfaces and to islets within the film during the casting process¹⁸⁹. L30D behaves differently due to its large size in comparison to molecular additives, it will not get exuded out the film or dissolve into the film. This property makes L30D potentially more compatible for a wider range of latices as compared to the small molecular additives.

3.2.4.3 Critical pigment volume fraction

This method will work for all latices with a minimum film formation temperature higher than the casting/application temperature acting as pigments. As water evaporates a mixture of small binder latex particles dispersed throughout the larger non film-forming latex will result. The small binder latex particles will deform and stick the larger particles together forming a strong whole film. As long as the larger particles do not deform then porosity will result from the interstices formed by the large particles. A disadvantage of this method is that a proportion of the functionality of the large latex particles will be covered where the binder latex has fused with the larger latex.

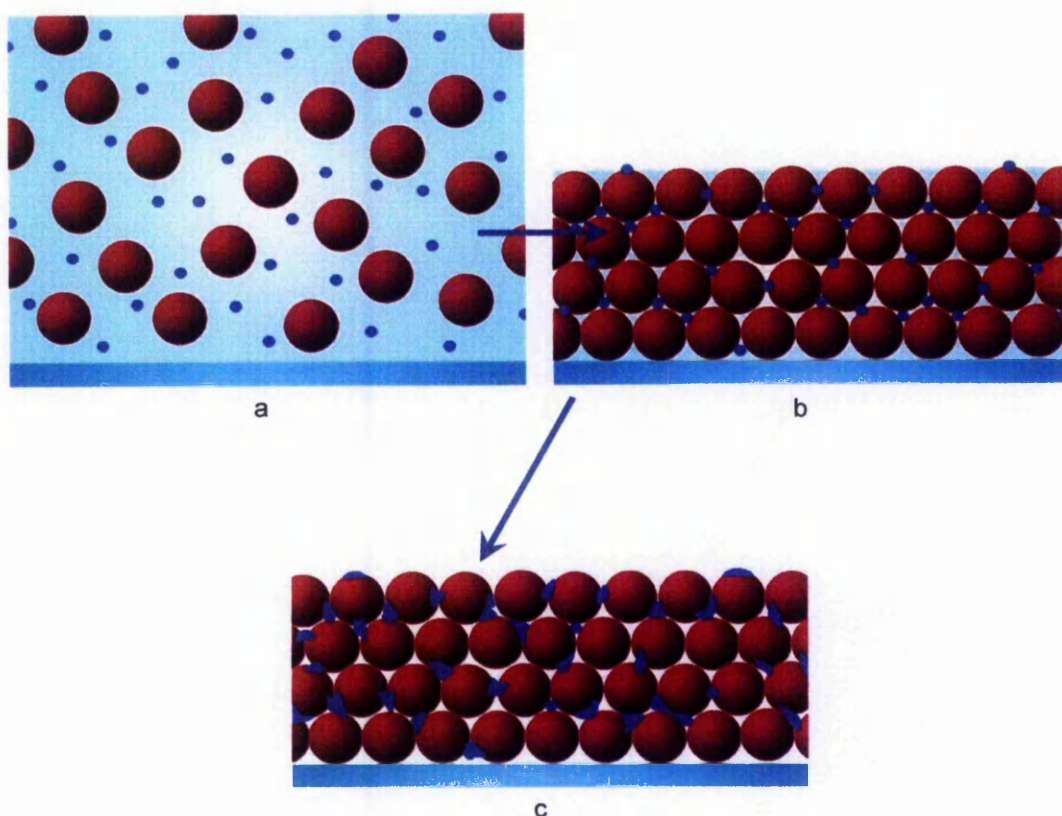


Figure 36: Schematic representation of pore formation by exceeding a binders CPVF. a) Latex particles and NE30D suspended in water. b) close packed latex particles with NE30D trapped between particles and water filled interstices. c) Latex particles "glued" together with porous domains.

3.2.5 Temperature study

PBMA films were prepared identically, but over a temperature range between 60°C and 90°C for 24 hours, using 15% glycerol. FFSEM of the films are shown in Figure 37.

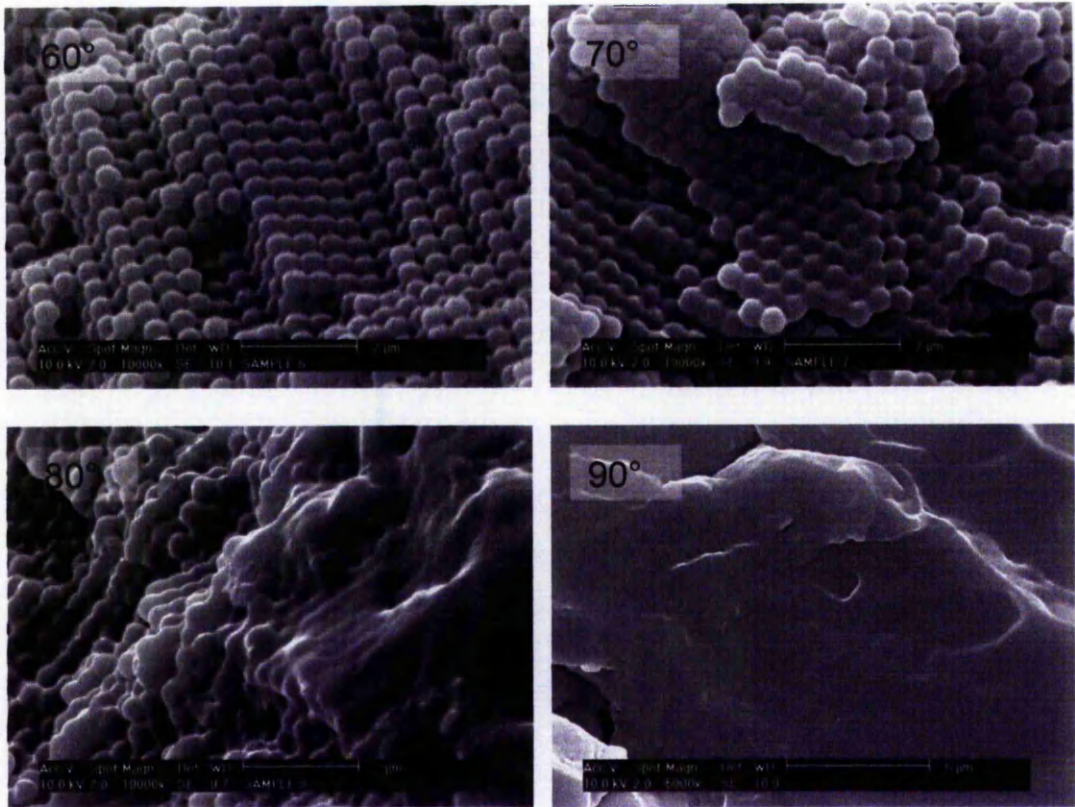


Figure 37: FFSEM micrographs photographs of PBMA films cast at various temperatures using 15% glycerol.

Study of the micrographs shows the disappearance of the pores as the casting temperature is increased. The film cast at 60°C has minimal particle deformation and a relative high degree of porosity. Casting at 70°C increases particle deformation closing interstices resulting in less porosity. Casting at 80°C appears to be a transitional stage showing areas where particle definition can still be seen and areas where coalescence has occurred to a degree where particle definitions are no longer visible. Casting at 90°C results in a film similar in appearance to a film prepared with no additive, where no particle definition can be seen. The pore closure and subsequent loss of surface area can be seen in the SSAs of the films, shown in Chart 16.

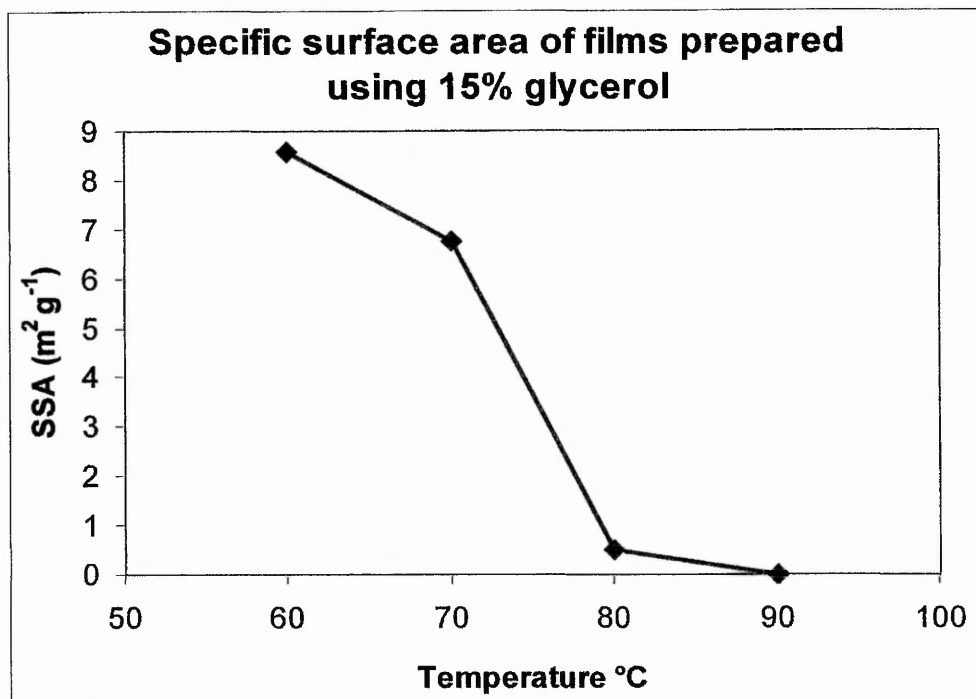


Chart 16: Plot of casting temperature vs specific surface area of films prepared using 15% glycerol.

The loss of porosity at higher temperatures is due to the reduced viscosity of the polymer and the additive. Coalescence of polymer spheres occurs faster at higher temperatures due to a reduction in the polymer viscosity. The increase in the rate of polymer coalescence coupled with the reduced viscosity of glycerol will increase the rate of additive exudation from interstices until at a certain temperature all additive is exuded and full coalescence of the particles can occur.

3.2.6 Surface characterisation

The charge density of the films is close to that of the original latex (SLATEX) across the additive range for all films (Chart 17) except for film

NOADD that had a charge density too low for determination by titration under the conditions used.

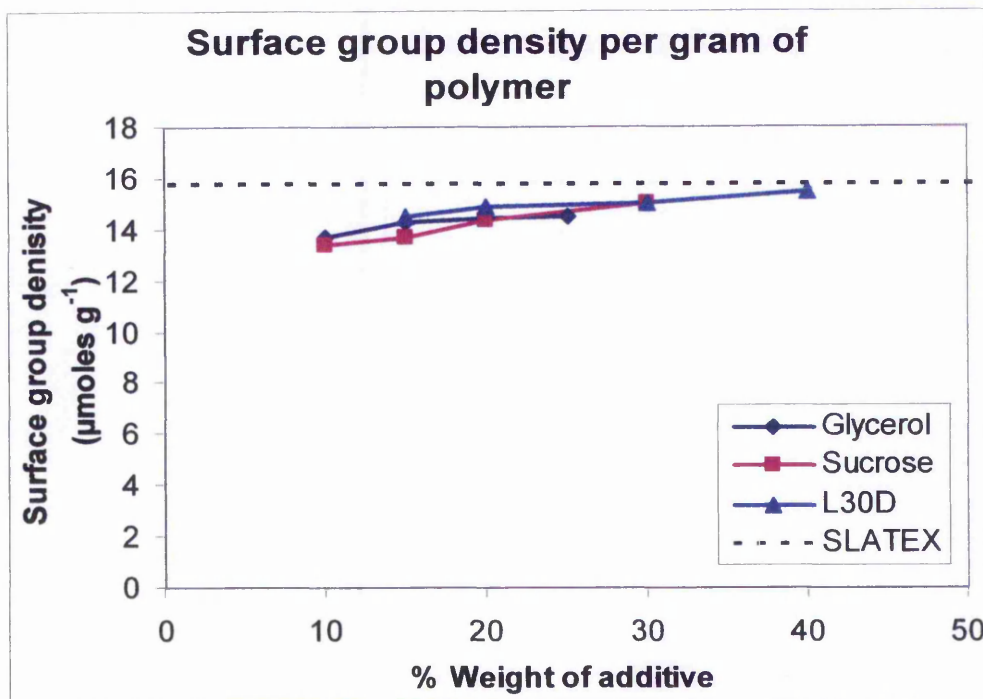


Chart 17: Plot of % weight of additive vs surface group density per gram for porous latex film.

At lower additive levels despite lower SSA the charge density is still high suggesting that during coalescence the polar groups tend to stay at the surface. This will enable the use of low amounts of additive, which would be favourable to film strength, while still retaining the majority of the functional groups. The fact that most of the functional groups are accessible is beneficial for improving reaction rates and would be helpful if the catalytic groups used were expensive or difficult to synthesise.

3.2.7 Reactions with porous latex films

3.2.7.1 Catalytic activity.

All films, prepared using an additive, give a rate of hydrolysis in the range 60%-90% of the rate shown by the discrete latex particles (Chart 18). See section 2.5.1 Reactive latex films - acid catalysis, for experimental details.

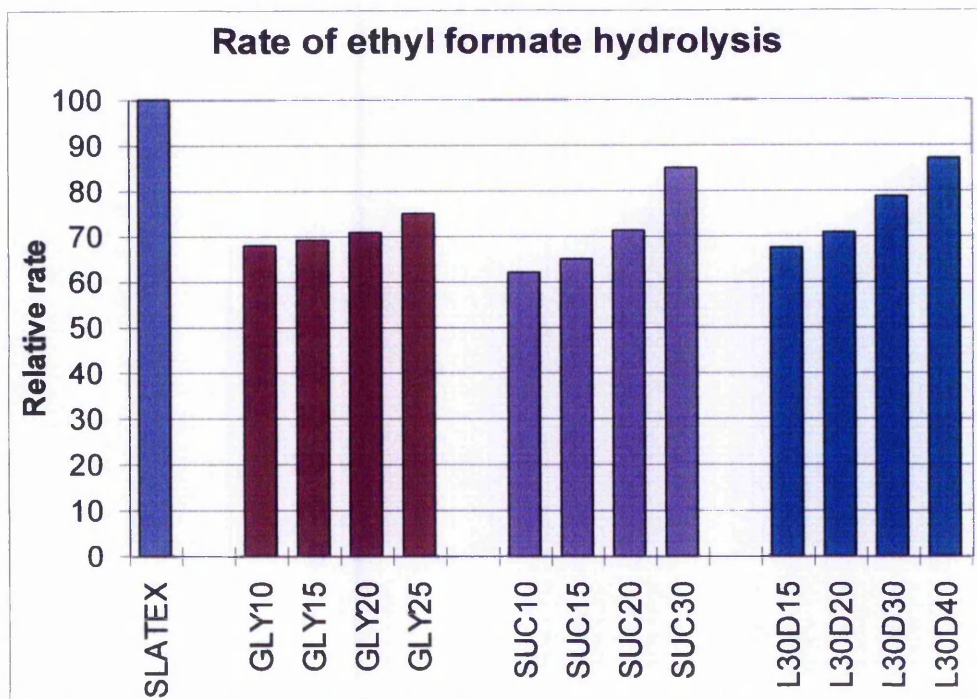


Chart 18: Relative rate of ethyl formate hydrolysis for sulphonated films and particles.

With increasing additive content for all films an increase in rate is seen and this can be attributed to the higher sulphonate group density available, and to bigger pores reducing mass transfer restrictions.

It was noted that the surface charge density of the films (Chart 17) was close to that of the latex and varies little across the additive content range. This is in contrast to the SSA, which varies significantly across the additive

content range with some films having less than half the SSA of the latex (Chart 19).

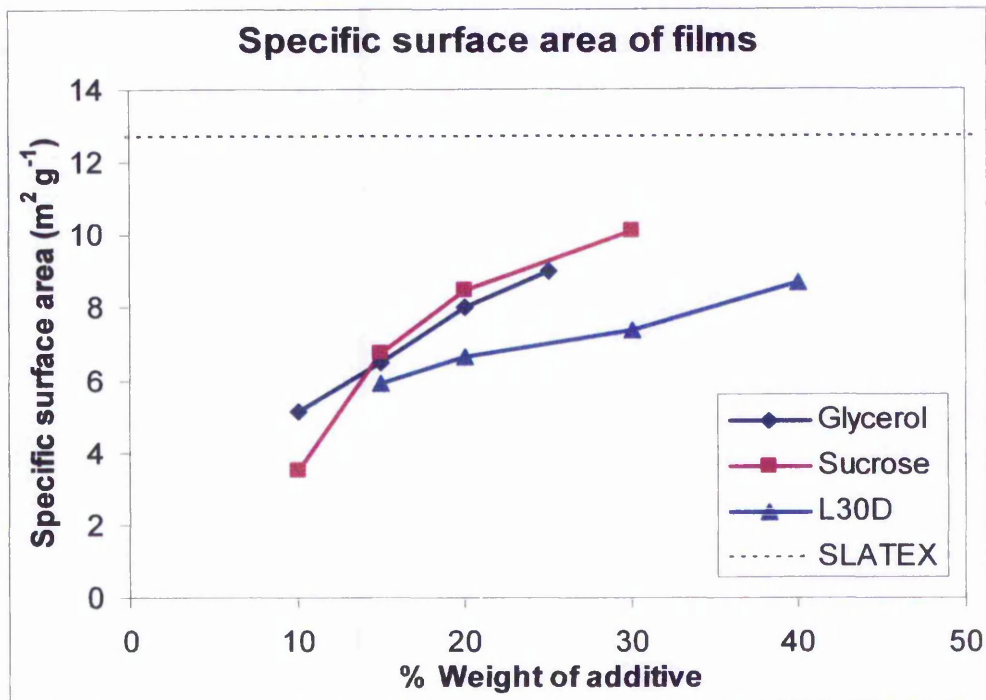


Chart 19: The SSA of the films prepared using glycerol, sucrose and L30D compared to the SSA of SLATEX.

It would be expected that when two particles fuse together the functional groups on the surface that is lost during fusion would also be lost within the polymer bulk. This is illustrated in Figure 38. If this were true then a direct correlation between SSA and surface charge density would be expected.

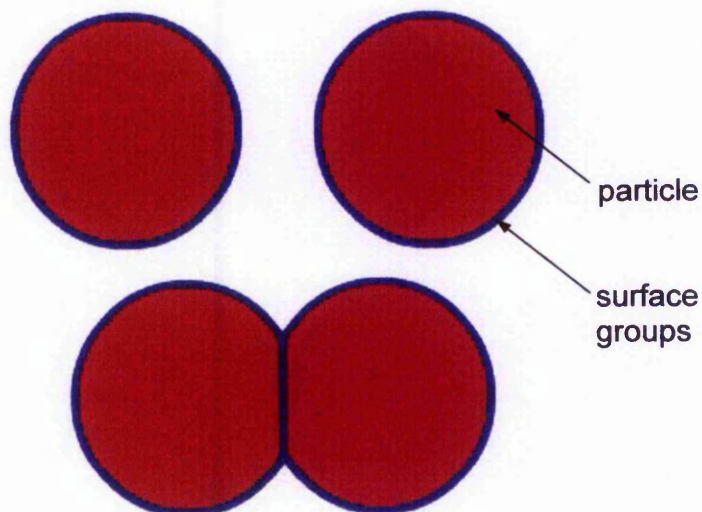


Figure 38: Schematic representation of surface groups potentially lost between the polymer bulk during particle deformation.

However, taking film GLY10 as an example, there is a 60% drop in surface area, but only a 15% drop in surface charge density. A chart of functional groups per square metre of film surface (Chart 20) shows that all the films have a higher surface group density per m^2 of film surface than SLATEX. See section 2.4.1 Conductometric titration, for experimental details.

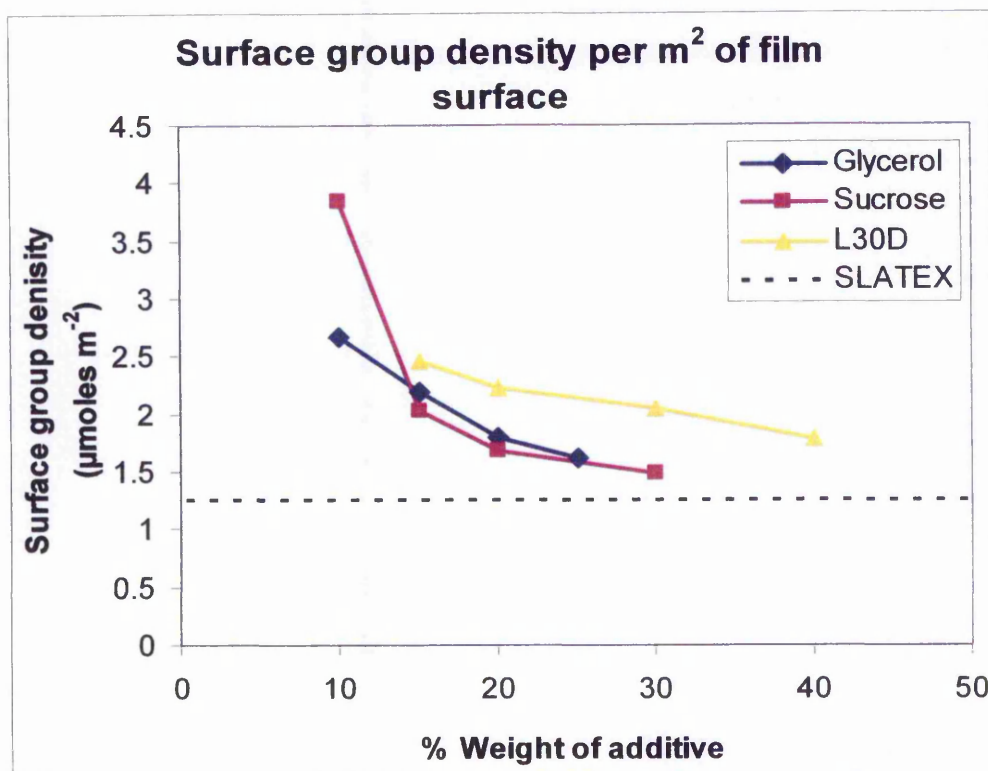


Chart 20: Plot of % weight of additive vs surface group density per m² of surface area for porous latex films.

Films prepared from small amounts of each additive have the largest charge density showing a decreasing charge density with increasing additive content. This suggests that during fusion the majority of functional groups at risk of being lost, are able to migrate and escape being trapped within the polymer. This will result in a local increase in surface charge density on the film, around the points where particles have fused as illustrated in Figure 39.

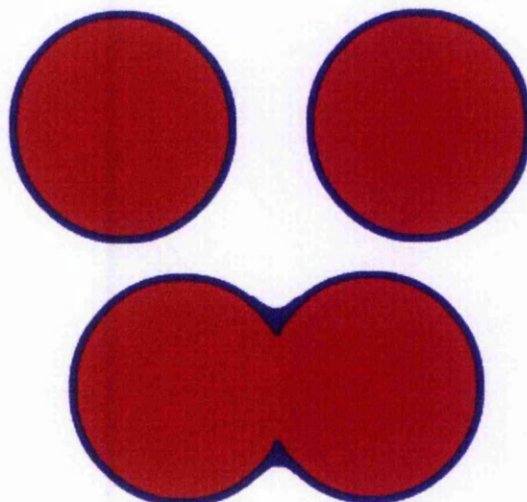


Figure 39: Schematic representation of surface groups retained at the polymer surface during particle coalescence.

This is likely to arise due to the difference in hydrophilicity of the core polymer compared to the polymer at the particle surface. As the hydrophobic core coalesces it pushes the hydrophilic material to the side, concentrating the hydrophilic polymer segments at the surface.

3.2.7.2 Copper chelation

The uptake of copper ions by chitosan coated polymer films is shown in Chart 21. The films evaluated originate from the same sample, the only difference between runs is the amount of film used and therefore the total amount of chitosan in each system. It would be expected that an increase in ion uptake with increasing chitosan content would be seen, and indeed occurs.

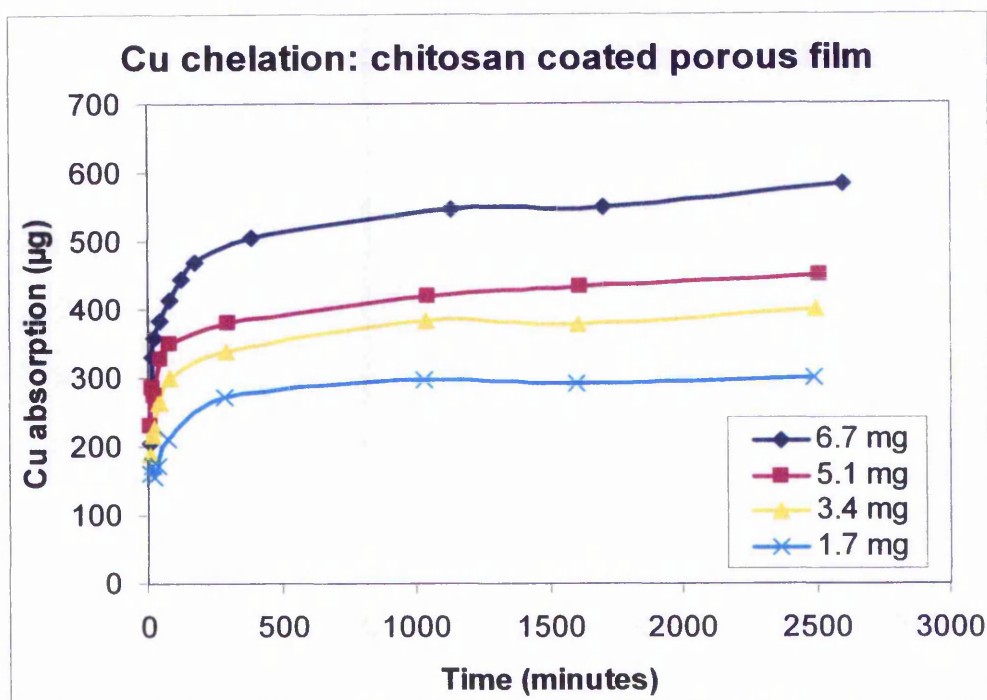


Chart 21: Plot of copper absorption with time for chitosan coated porous latex films.

The uptake of copper ions by chitosan flakes is shown in Chart 22. Again it would be expected that increased ion uptake with increasing chitosan content would be seen, and indeed occurs. Comparison of Charts 21 and 22 shows that chitosan flakes absorb less ions over the same time scale compared to the same weight of chitosan coated on a porous film.

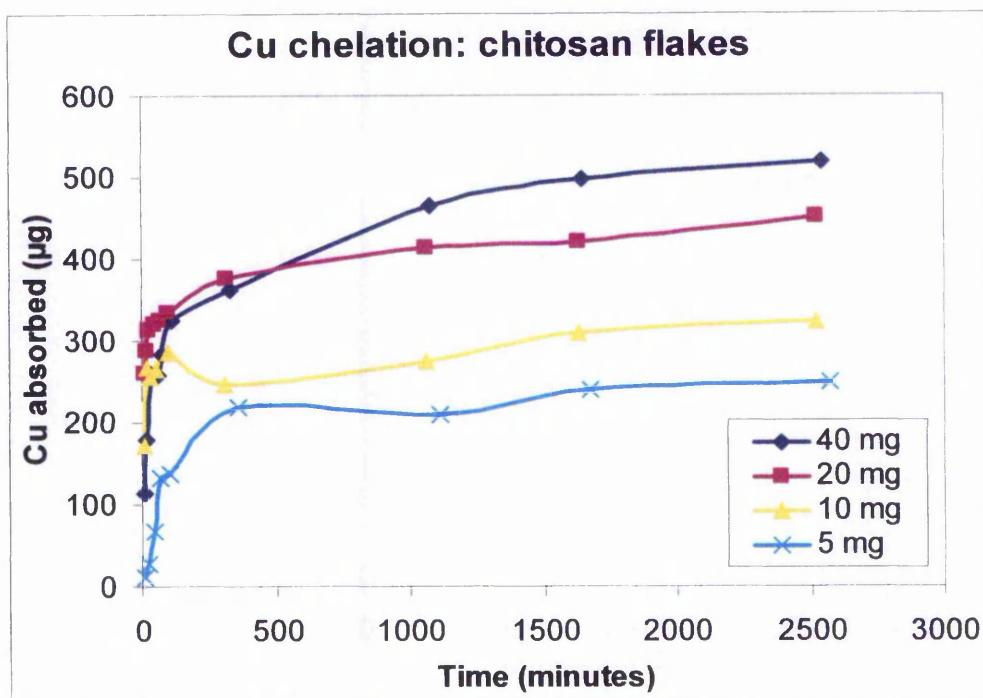


Chart 22: Plot of copper absorption with time for chitosan flakes.

Chart 23 compares the copper ion uptake of 5 mg of chitosan flakes against 5.1 mg of chitosan coated on a porous film. It can be seen that the chitosan on the film adsorbs ions at a faster rate and overall absorbs more than the chitosan flakes.

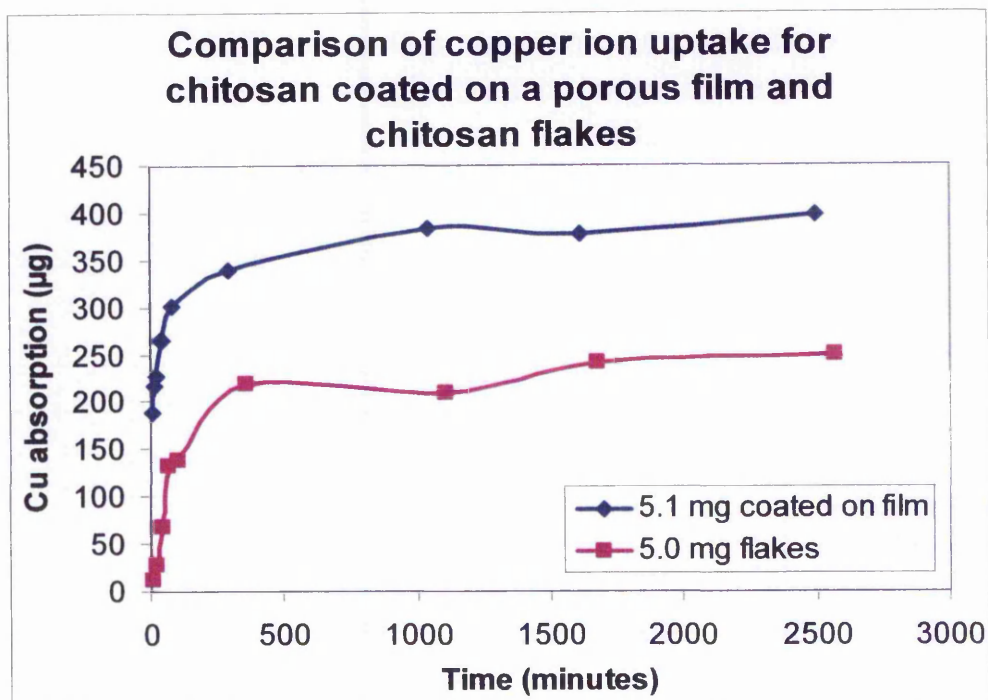


Chart 23: Comparison of copper absorption with time for chitosan coated film and chitosan flakes.

The differing performance can be explained by the much larger surface-to-volume ratio. The chitosan flakes are approximately 500 μm thick so the majority of the reactive sites are within the film. This limits the rate at which copper ions can be taken up due to relatively small surface initially available for adsorption and diffusion limitation of the ions into the interior of the flake. Studies of copper ion up take by chitosan films ($\sim 100 \mu\text{m}$) have shown that even after contact times of up to 200 hours no copper ions had reached the centre of the film¹⁹⁰. Coating chitosan onto the surface of the porous film results in a chitosan film thickness of only 1 or 2 nm, significantly increasing the initial surface area available, reducing diffusion limitations and increasing the degree of available sites of the chitosan sample.

3.3 Porous latex particles

The effect each component of the ECCP had on the properties of the final particles was evaluated by systematic variation of the components. This would help build a picture of what occurs during an ECCP. A polymerisation run would be carried out containing up to 9 samples at one time. For each run a single component's concentration would be varied across the samples. Runs were carried out in 'shaken reactors' as described in the experimental section.

Once the effect of each component on the polymerisation was determined, selected polymerisations were carried out in a stirred 4 neck Pyrex round bottom flask allowing sampling of the reaction mixture for rate measurements. The effect of each of the organic components and the DVB/styrene ratio on the properties of the particles and the rate of reaction were evaluated.

3.3.1 Systematic variation of the polymerisation components

Table 2 shows the components that were varied for each run of the shaken polymerisations.

Components	A	B	C	D	E
Styrene (cm ³)	2	2	varied	2	2
DVB (cm ³)	2	2	varied	2	2
Toluene (cm ³)	2	2	2	varied	2
Octane (cm ³)	-	-	-	-	varied
KPS (g)	0.125	varied	0.125	0.125	0.125
SDS (g)	varied	0.5	0.1	0.1	0.1
DDW (cm ³)	50	50	50	50	50

Table 2: Component variations for the porous latex particle preparations.

Table Summary:

Sample A's:	Surfactant SDS varied.
Sample B's:	Initiator KPS varied.
Sample C's:	Ratio of styrene to DVB varied with the total amount always equal to 4 cm ³ .
Sample D's:	Toluene varied.
Sample E's:	Octane varied.

The use of polymeric porogen was not studied for two reasons. Firstly the use of polymeric porogen produces macroreticular particles with a relatively small SSA. Secondly the polymeric porogen requires extraction from the particles by soxhlet extraction, which is not possible due to the small size of the particles produced under emulsion polymerisation conditions.

All of these reactions were carried out in glass jars as described in the experimental section. The identification of each individual sample is found from the degree of displacement from the left of the chart i.e. the first sample on the left of Chart 24 corresponds to sample A1, the third sample along corresponds to sample A3 etc.

3.3.1.1 Variation of surfactant concentration

The effects on particle size and extra SSA (extra SSA is defined in section 2.11.1 Calculation of a particles extra SSA) by varying the amount of surfactants SDS used in the preparations are shown in Chart 24.

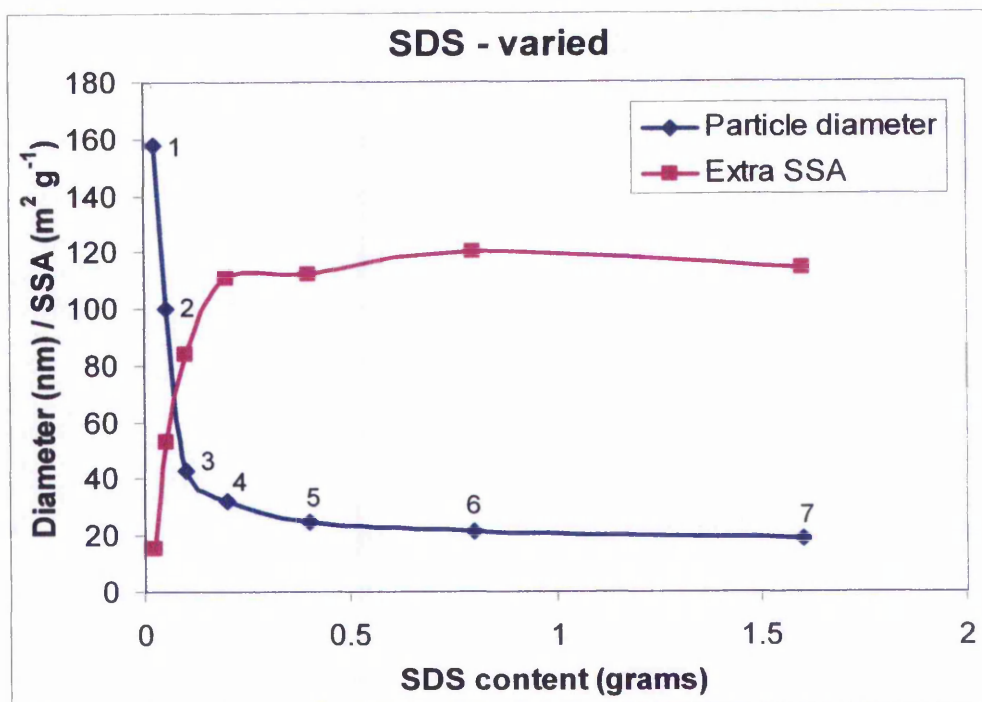


Chart 24: Porous latex samples A1-A7: various SDS surfactant weights.

From the plot of surfactant content against particle diameter it can be seen that increasing the amount of surfactant in the system decreases the diameter of the particles. This is due to the increased number of monomer filled micelles at the beginning of reaction, which result in more nucleated particles. With more growing particles competing for available monomer the reaction proceeds at a faster rate and less monomer is available per particle resulting, finally, in more and smaller particles. All samples show an extra SSA above the surface area expected for plain spheres of equal diameter, which increases with increasing amount of surfactant.

3.3.1.2 Variation of initiator concentration

The effects on particle size and extra SSA by varying the initiator content with fixed amounts of SDS are shown in Charts 25.

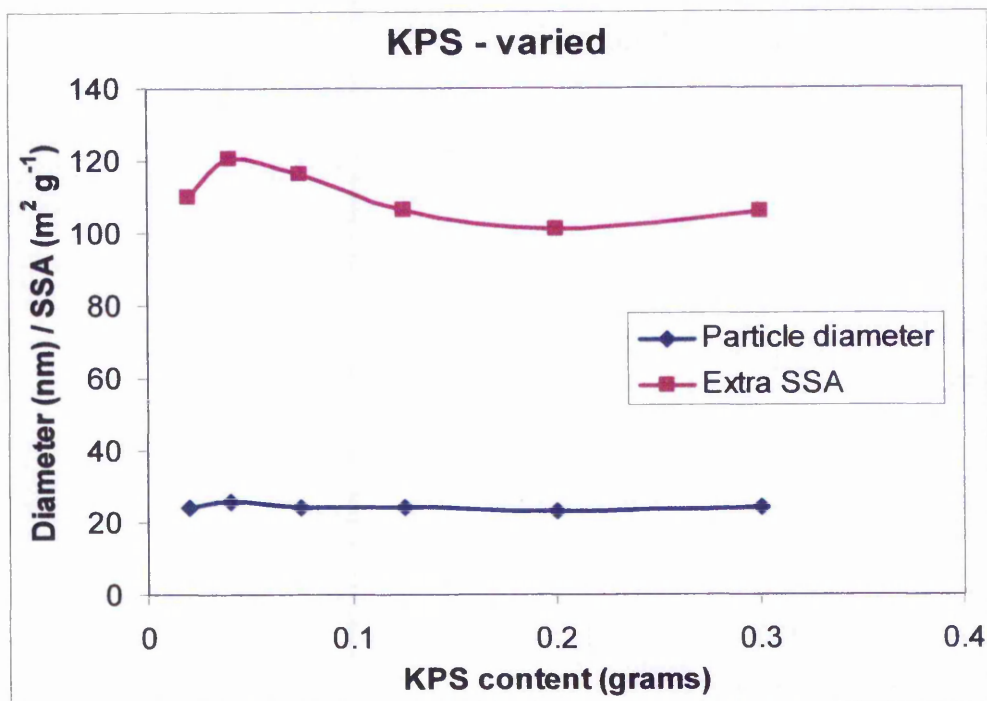


Chart 25: Porous latex samples B1-B6: various KPS initiator weights.

Varying the initiator concentration had virtually no effect on the particle diameter and had very little effect on the extra SSA across the range of KPS amounts used.

3.3.1.3 Variation of DVB/styrene ratio

The effects on particle size and extra SSA by increasing the DVB/styrene ratio using fixed amounts of SDS are shown in Charts 26.

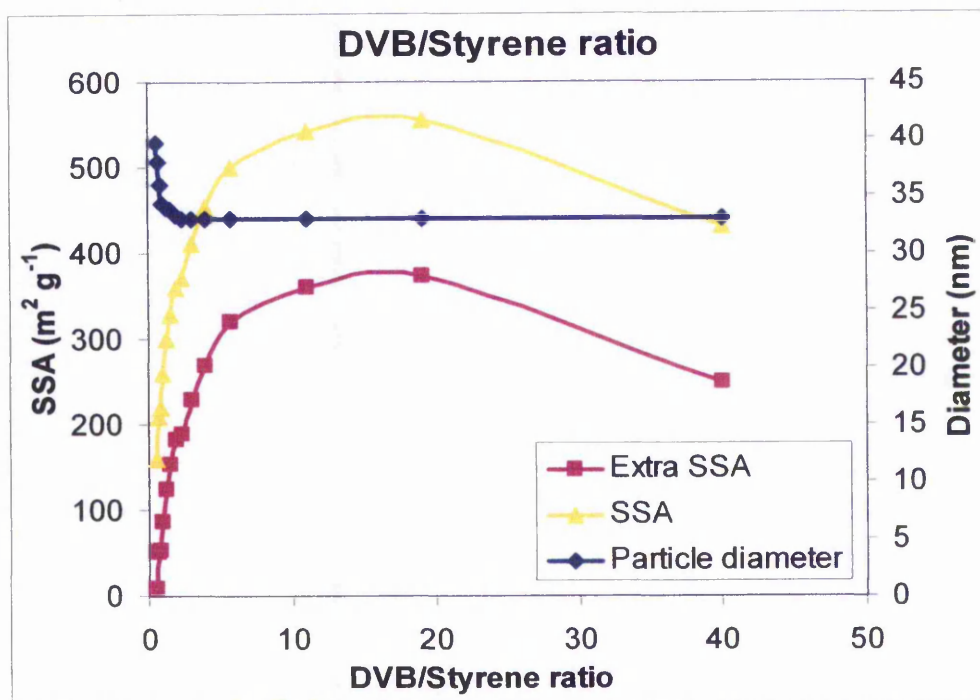


Chart 26: Porous latex samples C1-C14: ratio of DVB to styrene varied with the total amount always equal to 4 cm^3 .

Increasing the DVB/styrene ratio has the small effect of decreasing the particle diameter. Increasing the DVB/styrene ratio shows a large increase in extra SSA. The increase slows down with increasing DVB/Styrene ratio until at the very highest amount of DVB where the extra SSA decreases. The decrease in particle size with increasing DVB content is due to the increased crosslinking density, which lowers the monomer concentration within the growing polymer particle by restricting monomer absorption into the particle. This results in more particles being formed, which compete for the available monomer so that smaller particles are formed. The increasing extra surface area with increasing DVB content may result from the more rigid structure formed. This will restrict the tendency of the structure to collapse once the porogen is removed, maintaining the porous network. Chart 26 also shows

the overall SSA of the particles. It can be seen that the SSA follows the same profile as the extra surface area, with a maximum SSA of $554.9 \text{ m}^2 \text{ g}^{-1}$.

3.3.1.4 Variation of porogen concentration

The effect on particle size and extra SSA by increasing the amount of porogen toluene in the system is shown in Chart 27.

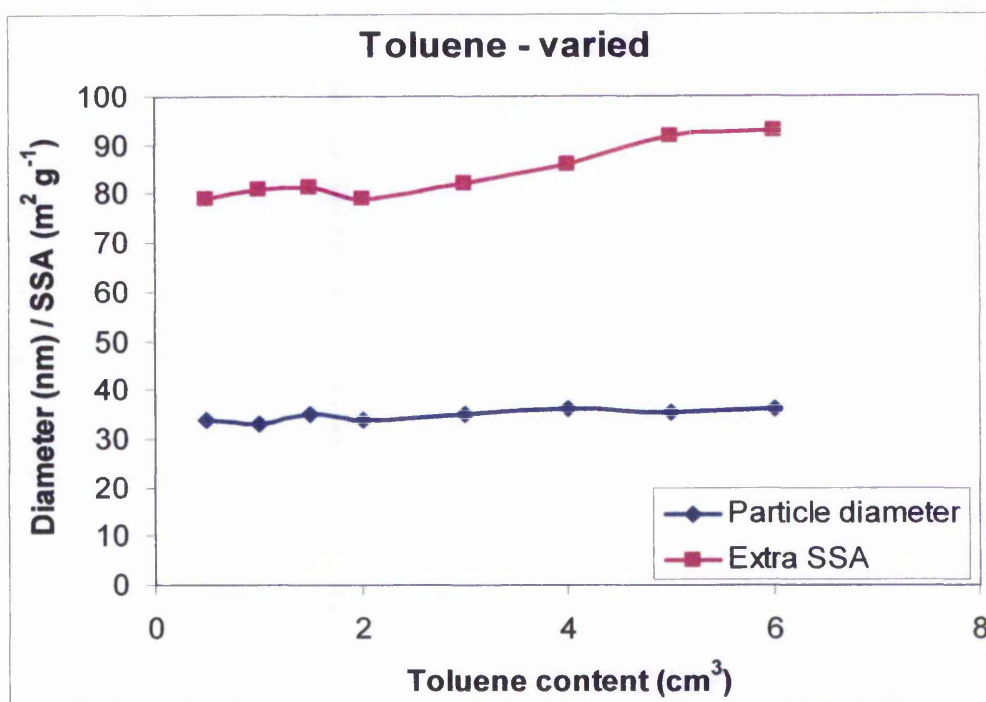


Chart 27: Porous latex samples D1-D8: various toluene porogen volumes.

Varying the amount of toluene has no significant effect on the particle diameter of the samples. There is a small general increase in extra SSA with increasing toluene content. It might be expected from macroreticular resin synthesis that increasing the amount of toluene would have a larger effect on the extra SSA, by creating a more expanded network. However this is not seen, suggesting that at the DVB/styrene level used i.e. 1:1 ratio, there is a limit to how much the network can be expanded by toluene. This could be

explained by the higher polymer concentration within the growing particle when compared to suspension polymerisation. The initial crosslinked polymer nuclei grows and will be fully solvated with toluene and monomers, the amount being dependent on the crosslinking density. Adding more toluene will not effect the swelling of the growing polymer particle.

The effect on particle size and extra SSA by increasing the amount of octane in the system is shown in Chart 28.

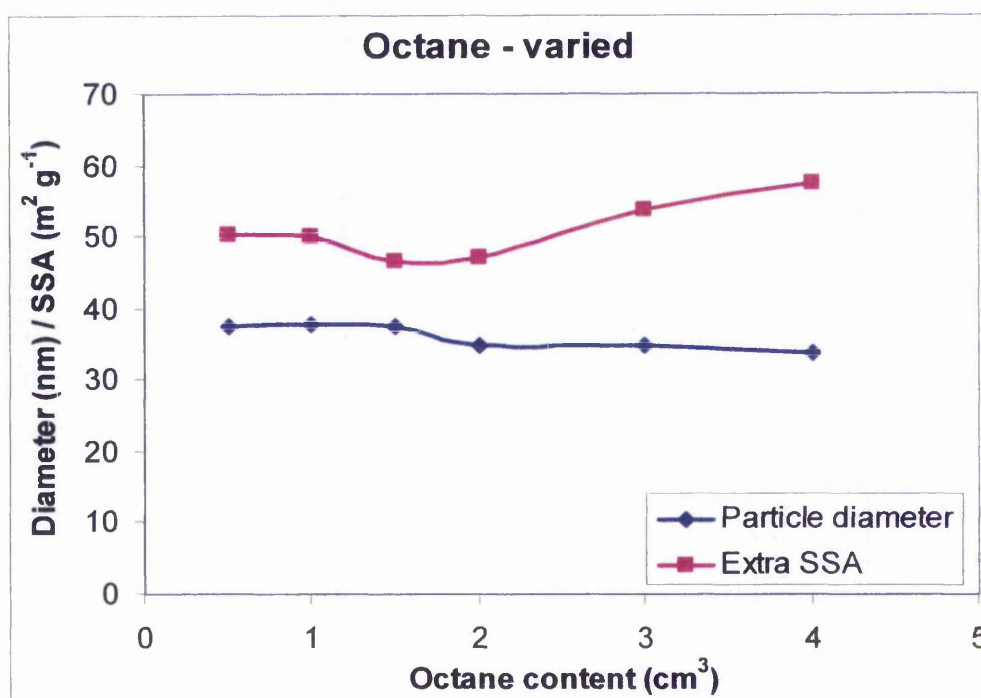


Chart 28: Porous latex samples E1-E6: various octane porogen volumes.

Varying the octane levels has no significant effect on the particle diameter of the samples. Increasing the amount of octane initially reduces the extra SSA slightly then produces a slight increase in extra SSA. The extra SSAs produced using octane are smaller than for the samples prepared using toluene.

3.3.1.5 Variation of oil soluble initiator concentration

Oil soluble initiators benzoyl peroxide and 2,2'-azo-*bis*-isobutronitrile were not successful in the preparation of stable latices. All attempts resulted in complete coagulation of the polymer.

3.3.1.6 Maximising extra surface area

The components KPS and both porogens do not make a significant impact on the extra SSA of the particles compared to the effect made on the particles by the surfactant SDS and the DVB/styrene ratio.

The extra surface area reaches a plateau after the CMC of SDS is reached suggesting that the presence of micelles is important for the formation of extra SSA. The reason for the importance of micelles maybe due to the compartmentalisation of the reaction loci and the separation of the main bulk of the monomer in the monomer droplets preventing all the DVB from reacting too early leaving a styrene rich monomer phase to block the pores. The increase in DVB/styrene ratio is the only other component to effect the extra SSA of the particles. At low DVB/styrene ratios the extra SSA will be low due to the low crosslinking density, which will result in collapse of the pore structure once the porogen has been removed. Increasing the DVB/styrene ratio results in a higher crosslinking density and a more rigid structure that does not collapse on removal of the porogen retaining the porosity of the particle.

3.3.2 Repeatability of shaken polymerisations

Due to the process of changing the variables between each set of runs, some of the samples were prepared more than once. These can be used to evaluate the repeatability of the polymerisation. Three such equivalent samples are A3, C4 and D4, which all used the same amounts of each component. The average particle diameter, SSA and extra SSA are shown in Table 3.

Average diameter	SSA	Extra SSA
42.9 ± 6.9 nm	225.6 ± 27.8 m ² g ⁻¹	82.2 ± 4.3 m ² g ⁻¹

Table 3: Repeatability of shaken polymerisations.

3.3.3 Effect of initiator and surfactant concentration on particle number.

Using the results from polymerisation runs A and B the dependence of the particle number on the initiator and surfactant concentrations were found. The dependence was determined from the gradient of a log-log plot of particle number versus the component concentration. It was found that the particle number is proportional to [SDS]^{1.7} and [KPS]^{0.0}. This is a substantial deviation from the results gained by Smith and Ewart²¹ for the polymerisation of styrene alone, which was [SDS]^{0.6} and [KPS]^{0.4}.

The constant number of particles irrespective of the amount initiator used suggests that, at the surfactant level used, all micelles capture a radical and are converted to polymer particles. Because all micelles are converted to particles, increasing the surfactant concentration will result in more micelles and therefore more particles. Due to all the extra micelles being converted

this will lead to a higher exponent compared to emulsion polymerisation of styrene.

To confirm this the number of micelles present in the reaction mixture, prior to polymerisation, was compared to the resulting number of particles after polymerisation, for run A. The CMC of SDS was taken as $0.0086 \text{ mol dm}^{-3}$ ¹⁹¹ and the number of SDS molecules forming a micelle was taken as 54 ¹⁹².

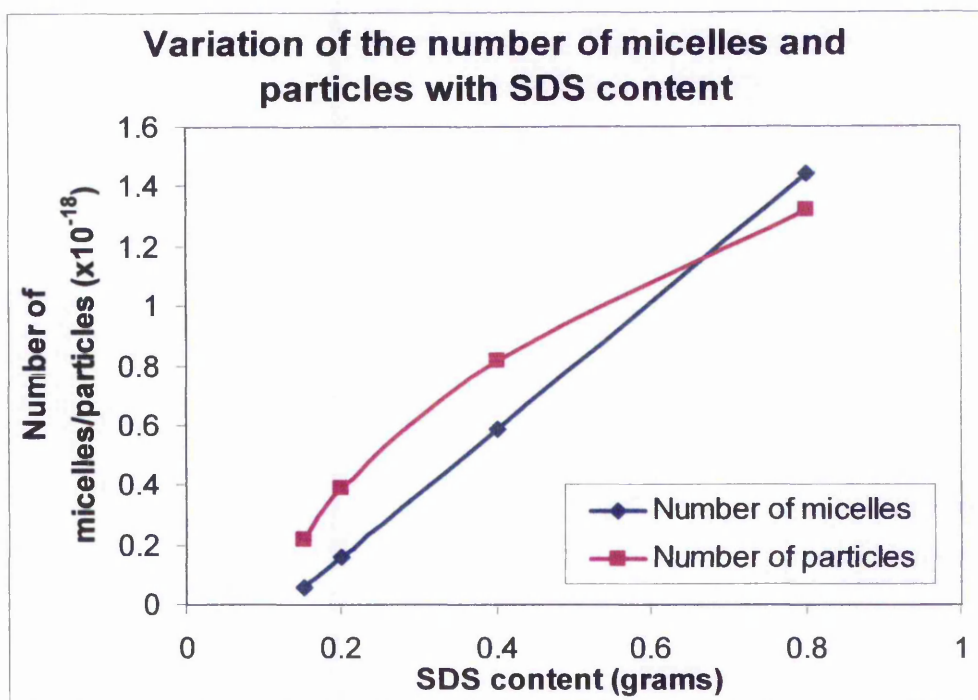


Chart 29: Variation of the number of micelles and particles with SDS content.

Study of Chart 29 shows that at these surfactant levels the number of micelles and particles follow the same trend with increasing surfactant content.

The increased fraction of micelles converting to polymer particles will be related to the slower growth of the polymer particles compared to styrene emulsion polymerisation. The slower growing polymer particles will draw surfactant from the uninitiated micelles at a slower rate so micelles will be

present in the system for longer. The longer a micelle is present the greater the chance of being initiated. Chart 29 shows that at all the surfactant levels the initiator is able to initiate all the micelles before being sacrificed to stabilise the growing polymer particles.

3.3.4 Varying organic phase components in a stirred reactor

These polymerisations were carried out in a stirred 4 neck Pyrex round bottomed flask allowing sampling of the reaction mixture for rate measurements. The effect of each of the organic components and the DVB/styrene ratio on the properties of the particles and the rate of reaction were evaluated.

Table 4 shows the recipes for each run.

Components	Org1	Org2	Org3	Org4	Org5	Org6	Org7	Org8
Styrene (cm ³)	10.4	8	5.6	-	16	12	-	24
DVB (cm ³)	5.6	8	10.4	16	-	12	24	-
Toluene (cm ³)	8	8	8	8	8	-	-	-
KPS (g)	0.5	0.5	0.5	0.5	0.5	0.5	0.5	0.5
SDS (g)	0.4	0.4	0.4	0.4	0.4	0.4	0.4	0.4
DDW (cm ³)	200	200	200	200	200	200	200	200

Table 4: Organic component variations for the porous latex particle preparations.

Table summary:

Org1: Low DVB/styrene ratio

Org2: Equal amounts of DVB and styrene

Org3: High DVB/styrene ratio

Org4: DVB and toluene only, no styrene

Org5: Styrene and toluene only, no DVB

Org6: Styrene and DVB only, no toluene

Org7: DVB only

Org8: Styrene only

The total amount of the organic phase was kept constant in all preparations.

The physical properties of the resulting particles are shown in Table 5.

Components	Org1	Org2	Org3	Org4	Org5	Org6	Org7	Org8
SSA (m ² g ⁻¹)	212.9	276.5	312.3	255.9	121.8	156.8	191.4	105.6
Diameter (nm)	34.9	33.8	40.2	40.0	56.0	47.4	39.4	68.6
Extra SSA (m ² g ⁻¹)	41.0	99.0	162.3	84.5	14.7	30.2	39.2	18.1
Reaction rate (%conversion min ⁻¹)	0.071	0.041	0.026	0.030	0.124	0.099	0.034	0.524

Table 5: Physical properties of porous latex particles.

There is an increase in extra surface area going from sample Org1 to Org3 (Chart 30) consistent with the results found earlier where increasing the DVB/styrene ratio (increasing DVB content) resulted in an increase in extra surface area (Chart 25). Sample Org4, prepared using DVB and toluene only, also has a significant extra surface area indicating that styrene does not need to be present for pore formation, although comparison with sample Org3 shows that styrene has the effect of increasing the amount of extra surface. Sample Org5, prepared from styrene and toluene only, shows an insignificant extra SSA as expected from an uncrosslinked polymer bead. The small extra SSA is indicative of the error in the evaluation process. Sample Org6, prepared from styrene and DVB only, shows a relatively small extra SSA, suggesting that either a porogen is not essential (although the use of one

greatly enhances the amount of extra SSA) or the unpolymerised monomer itself acts as a porogen during polymerisation. Sample Org7, prepared from DVB only, has a similar extra SSA as sample Org6 for the same reasons. Sample Org8, like Org5 has a very small extra SSA. This is as expected for an uncrosslinked polystyrene latex.

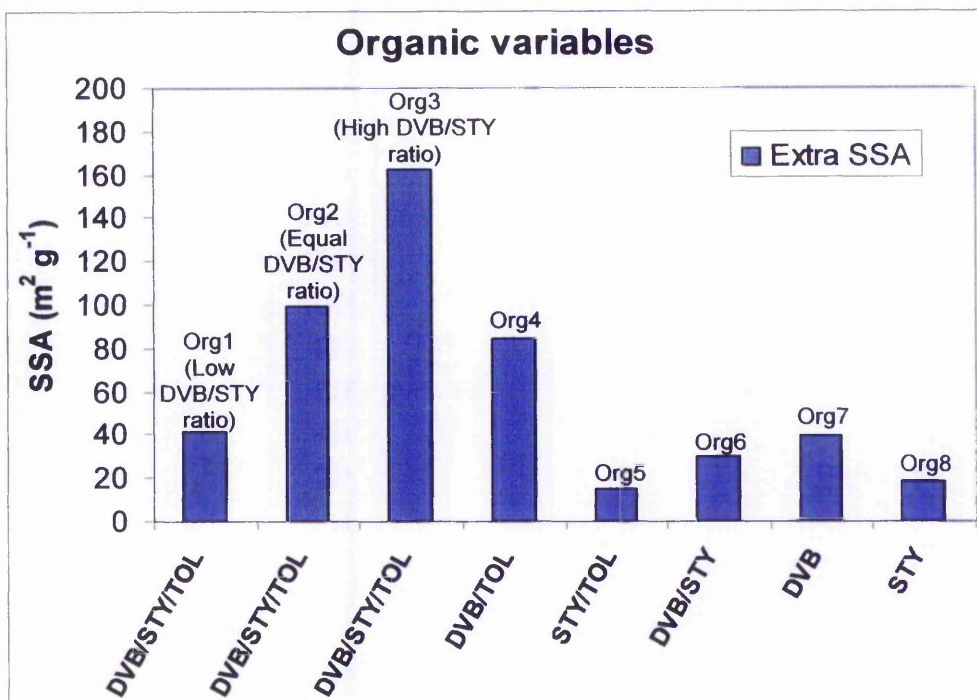


Chart 30: Varying organic phase components of porous latex particles.

The polymer conversion with time curves for Org2 and Org4-Org8 are shown in Chart 31 and those for Org1, 2 and 3 are shown in Chart 32.

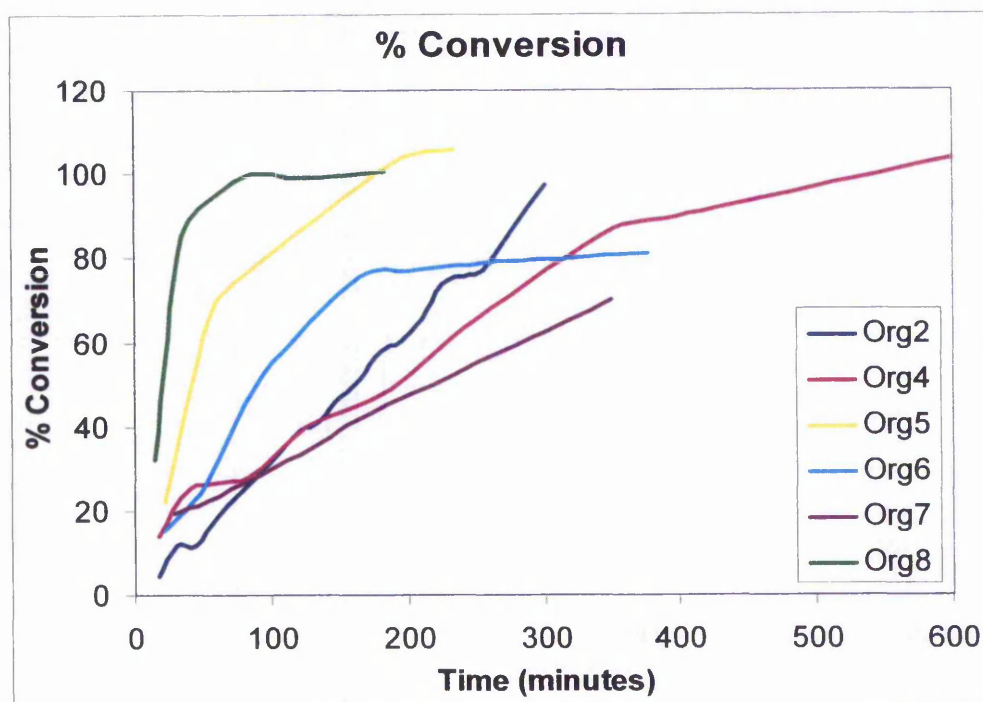


Chart 31: Polymer conversion with time curves for porous latex particle polymerisations.

Sample Org4 has a slower rate compared to the standard Org2 due to the increased crosslinking density, which lowers the monomer concentration within the growing polymer particle by restricting monomer adsorption into the particle.

Sample Org5 has a high polymerisation rate, because there is no crosslinking restricting the adsorption of monomer into the polymer particle. However, the rate is not as fast as sample Org8 due to the toluene effectively diluting the monomer within the growing polymer particle.

Sample Org6 has a rate in between samples Org2 and Org5. It has a faster rate than sample Org2 due to the fact that there is no toluene diluting the available monomer within the growing particle. It has a slower rate than sample Org5 due to the presence of DVB which introduces crosslinking which

reduces the amount of monomer in the growing particle. It can be concluded that with the amounts of toluene and DVB used in the study, the crosslinking density has a greater effect on reducing the polymerisation rate than the presence of toluene in a typical polymerisation recipe (i.e. styrene, DVB and toluene present).

Sample Org7 has the slowest rate of all the samples investigated. In the cases where styrene is present the presence of toluene has a reducing effect on the polymerisation rate due to monomer dilution within the growing particle. However, comparing samples Org4 and Org7 prepared using only DVB monomer, the presence of toluene has the effect of increasing the polymerisation rate. This shows that toluene has two effects. It can decrease the rate by diluting the monomer within the growing particle or it can increase the rate by providing a route for the monomer to enter the highly crosslinked growing particle. Which effect dominates depends on the crosslinking density of the growing particles. In the samples prepared with styrene the swelling of the particle with monomer is not such a problem so the toluene dilution effect is the rate determining factor. In the samples prepared with only DVB monomer the swelling of the particle with monomer is the rate limiting factor so the advantage toluene gives to monomer absorption into the particle outweighs the dilution effect.

Sample Org8 has the fastest rate of all the samples. It neither has crosslinking reducing the monomer swelling of the particle nor the dilution effect of toluene.

Chart 32 shows the percent monomer conversion for samples Org1, Org2 and Org3. The difference between the samples is the DVB/styrene ratio, which becomes higher from Org1 through to Org3. It can be seen from the chart that with increasing DVB/styrene ratio that the reaction rate decreases. This is due to the increased DVB content which produces a tighter crosslinked network, which will reduce the swelling of the particles with monomer thereby reducing the monomer concentration within the particles and slowing the reaction down.

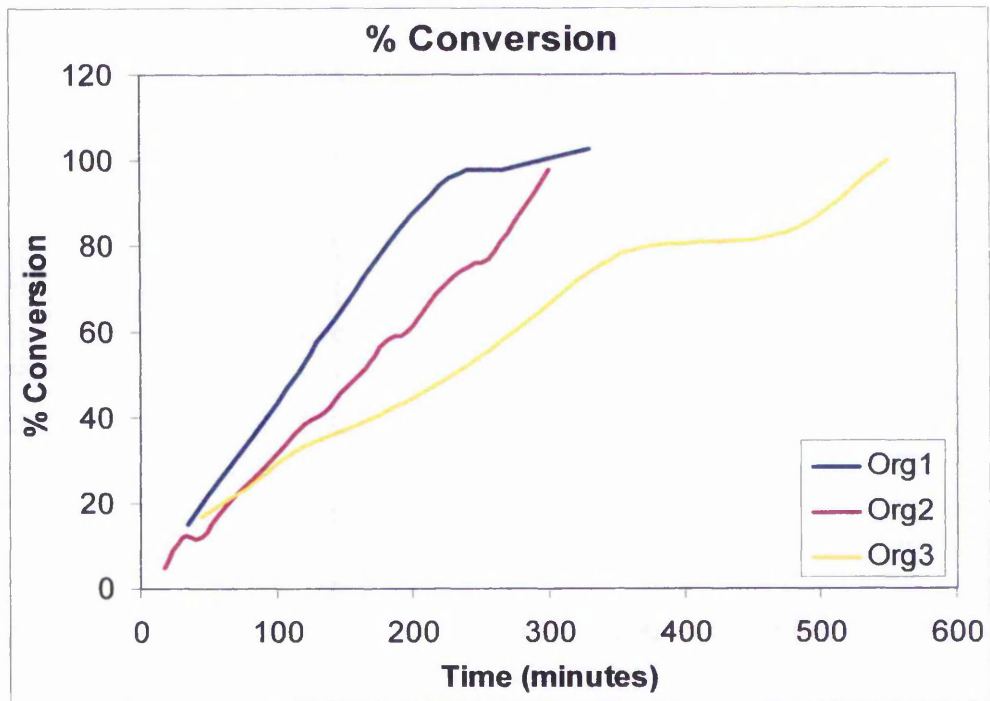


Chart 32: Polymer conversion with time curves for porous latex particle polymerisations.

3.3.4.1 Comparison of shaken and stirred reactors.

Three recipes polymerised in the shaken vessel were also repeated in the stirred reaction vessel. Table 6 summarises which samples were compared. Comparison of the properties between the recipes, which were both reacted in

shaken and stirred reaction vessels are shown in Chart 33. It can be seen that the diameter of the particles produced and extra SSA of the sample were largely unaffected by which method of agitation is used. The only significant difference occurs between the extra SSA of the low DVB/styrene ratio samples.

Shaken sample	Stirred equivalent
D1	Org1
D4	Org2
D7	Org3

Table 6: Porous latex particle preparations with the same component make-up carried out in both shaken and stirred polymerisations.

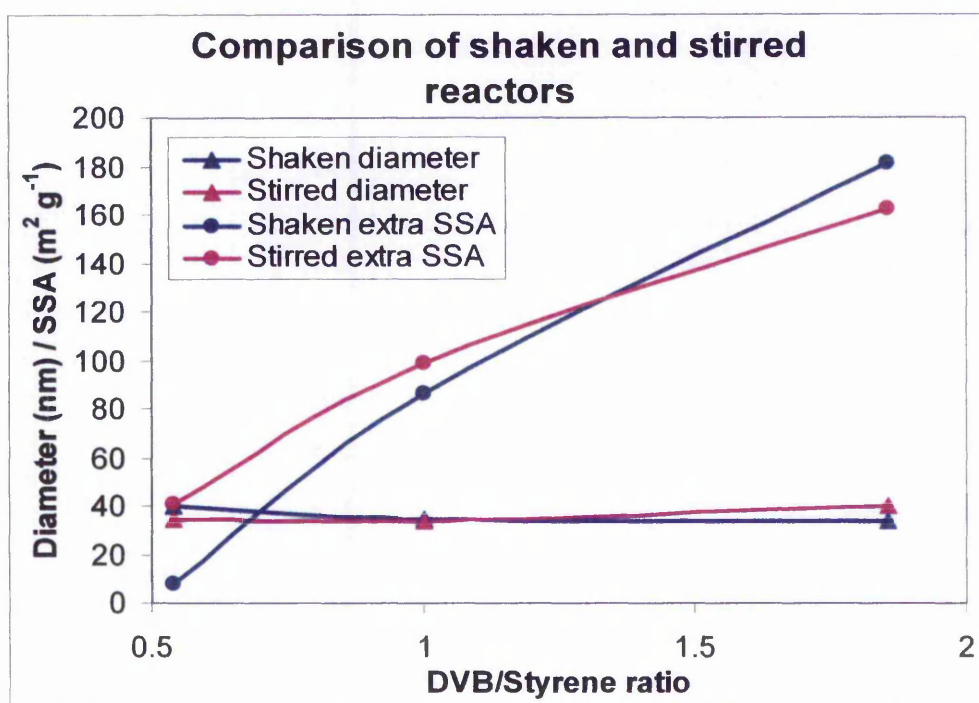


Chart 33: Repeatability of shaken polymerisations compared with stirred polymerisations.

3.3.5 Nonane pre-adsorption

Nitrogen isotherms were carried out on a sample of untreated Org2 and a sample of nonane pre-adsorbed Org2 (nonane pre-adsorption is described in section 1.8.1.3 Nonane pre-adsorption). The two adsorption and desorption isotherms are shown in Charts 34 and 35.

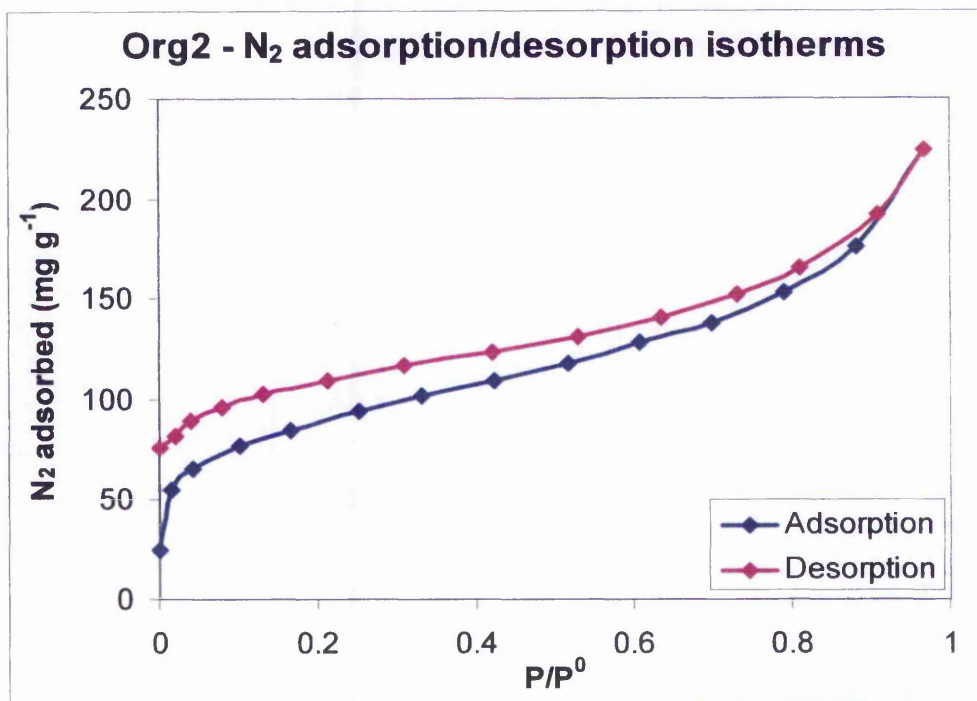


Chart 34: Adsorption/desorption isotherm of sample Org2.

The hysteresis seen in the desorption isotherm is not indicative of the presence of mesopores. The hysteresis in a nitrogen isotherm caused by the different pore filling and pore emptying processes of mesopores always closes before a P/P^0 value of 0.42. The hysteresis goes all the way to the very low pressure end of the isotherm with no shoulder, indicating no contribution to the hysteresis by mesopores¹⁷².

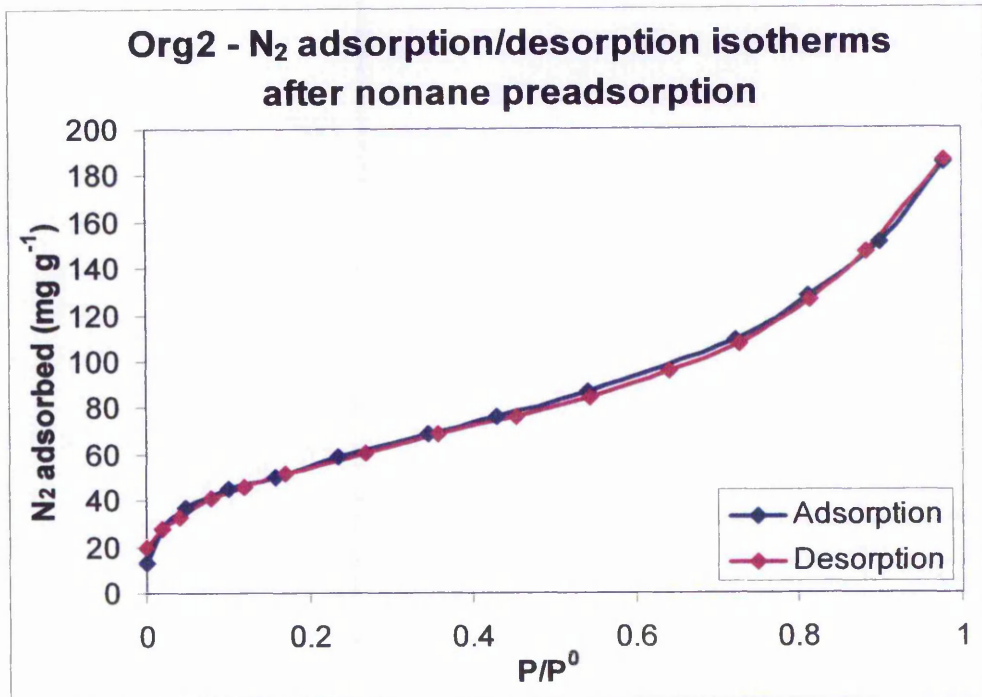


Chart 35: Adsorption/desorption isotherm of sample Org2 after nonane preadsorption.

The study of Chart 35 shows that the nonane preadsorbed sample of Org2 has a typical type 2 adsorption/desorption isotherm with no hysteresis. This shows that the preadsorbed nonane is eliminating the hysteresis found in the untreated sample.

Chart 36 is the adsorption/desorption isotherm for sample Org8. It is expected that polystyrene spheres will produce a pure type 2 isotherm and indeed Org8 produces a type 2 profile with no hysteresis.

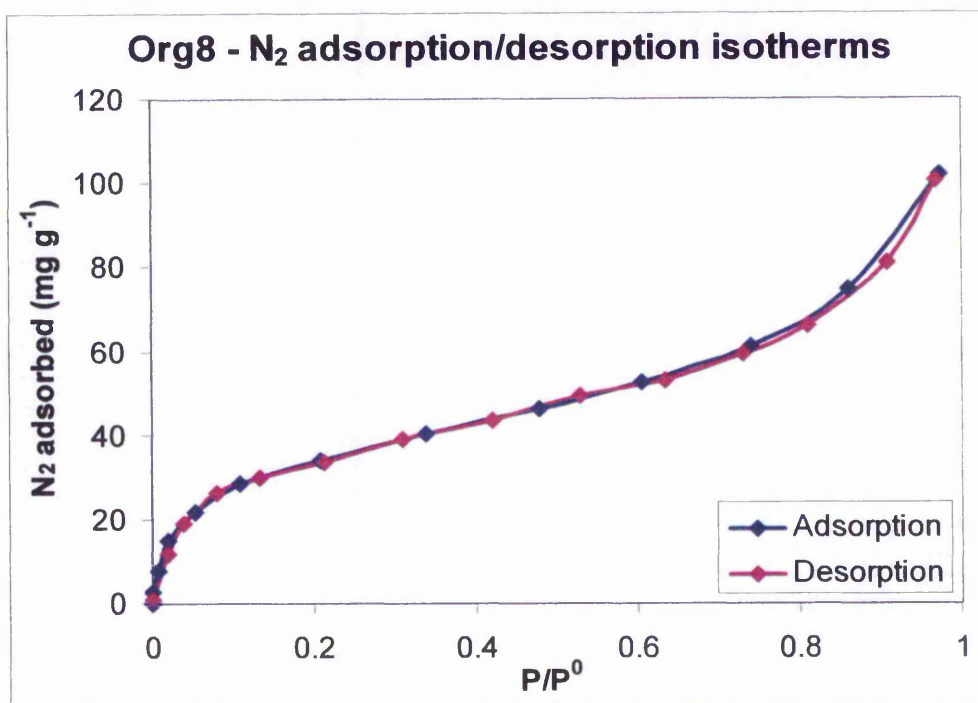


Chart 36: Adsorption/desorption isotherm of sample Org8.

Chart 37 shows all the adsorption isotherms together. Comparison of Org2 and Org2 nonane shows that the preadsorbed sample has the same profile, but shifted down to lower nitrogen uptakes. This suggests that the nonane has filled in micropores eliminating the initial strong uptake at low pressures. Org8 has the lowest uptake, which is due to its larger particle size and resulting smaller SSA.

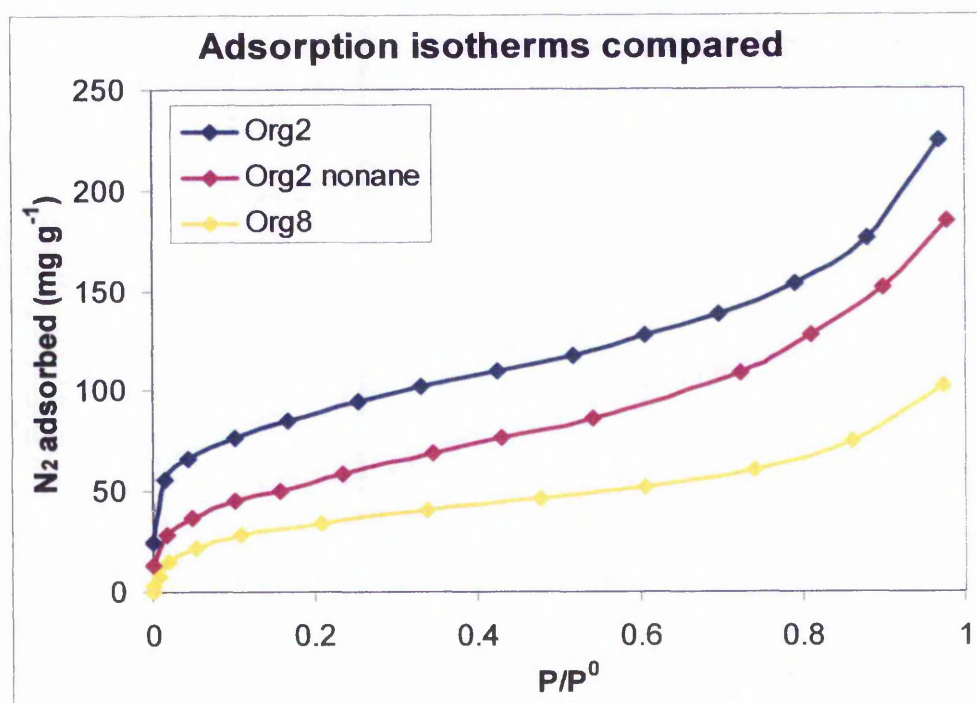


Chart 37: Adsorption isotherms of Org2, Org2 preadsorbed with nonane and Org8.

The nonane pre-adsorbed nitrogen isotherm shows significantly lower amounts of nitrogen adsorption over the whole pressure range of the isotherm. Subtraction of the nonane pre-adsorbed nitrogen isotherm from the original isotherm leaves a type 1 isotherm typical of microporous solids.

The SSA obtained from the isotherm of the nonane pre-adsorbed sample will be expected to be the same as the SSA of the spheres external surface area only, without the contribution from any pores. Therefore the SSA obtained from the isotherm of the nonane pre-adsorbed sample should be the same as the SSA calculated from the TEM micrographs, and indeed is close. The SSA calculated from the isotherm is $163.7 \text{ m}^2 \text{ g}^{-1}$ and the SSA calculated from the average particle diameter, found using TEM micrographs, is $177.3 \text{ m}^2 \text{ g}^{-1}$.

3.3.6 t-plot

The t-plots of samples Org2, Org2 preadsorbed with nonane and Org8 are shown in Chart 38.

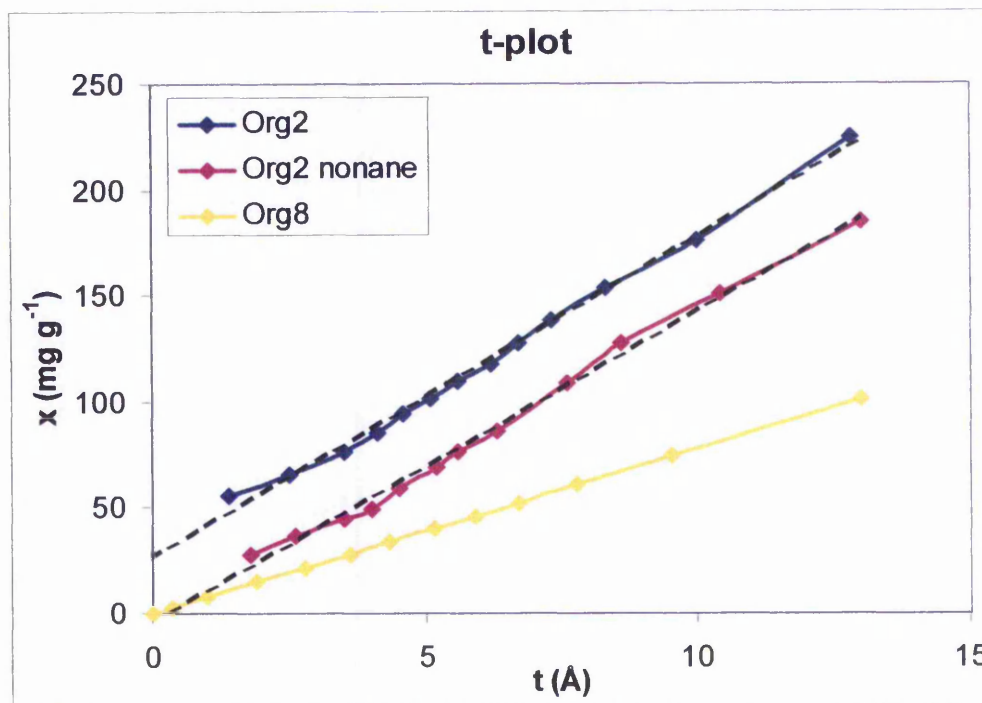


Chart 38: t-plot of Org2 and Org2 preadsorbed with nonane compared to the non-porous standard Org8.

The t-plot of the standard sample Org 8 is a straight line passing through the origin as expected. The t-plot of sample Org2 is a straight line with a positive intercept indicating the presence of microporosity in the sample. There is no indication of deviation from a straight line at the higher pressure end, again, indicating that there are no mesopores. The larger gradient compared to Org8 is due to the smaller particle size of Org2. The t-plot of sample Org2 preadsorbed with nonane is a straight line passing through the origin with the same slope as the t-plot of Org2. This shows that the nonane has blocked the microporosity of the sample.

3.4 Incorporation of porous latex particles into a porous latex film

Two porous films were prepared from a PBMA latex using glycerol as the pore forming agent. One film was prepared with the incorporation of 10 % weight of sample Org2 as detailed in the experimental section. Both films were evaluated for their SSA following leaching of the glycerol.

The SSAs of the films with and without Org2 are 25.3 and 2.4 m² g⁻¹ respectively. The initial incorporation of 10 % weight Org2 increases the SSA of the film 10 fold. Addition of 10% Org2 into the film would theoretically increase the SSA of the film by 27.7 m² g⁻¹ assuming that all the original surface area of Org2 is still available. The actual increase in specific area is 22.9 m² g⁻¹. The 17 % loss in SSA will result from some of the porous latex particles being washed away during the leaching/cleaning steps, particles being trapped between coalesced particles and surface loss due to particle-particle fusion.

The high retention of the porous latex particles within the porous latex film may arise from the surface active and hydrophobic properties of latex particles. These are exploited in stabilizing 'Pickering' emulsions^{193,194}. The porous latex particles (~35 nm diameter) will tend to gather at the SLATEX (501 nm diameter) particle/water interface during casting and thus reduce the amount of dispersed porous latex lost throughout the leaching/cleaning process.

3.5 Barrier characteristics of porous latex films

Dynamic adsorption profiles for plain BPL carbon, non-porous latex coated carbon, and porous latex coated carbon are shown in Chart 39.

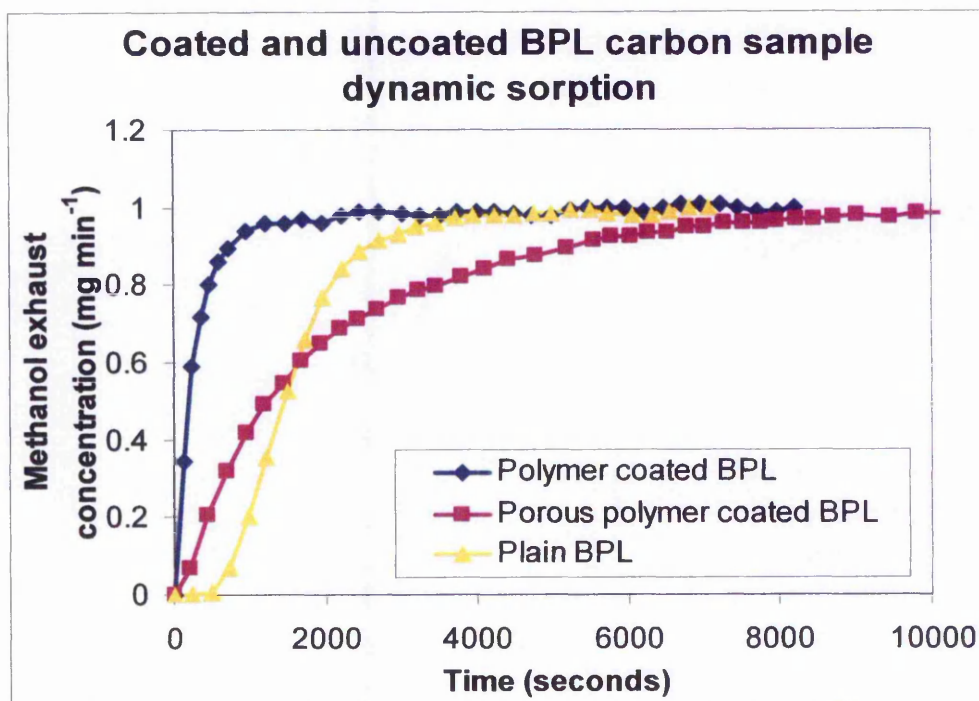


Chart 39: Coated and uncoated BPL carbon sample dynamic sorption.

The latex coat consisted of PBMA and L30D at 50% loading. The non-porous coat involved no leaching and the porous coat required removal of L30D via washing. Plain BPL carbon shows a typical profile¹⁰ with an initial period (~10 minutes) where no vapour passes completely through the bed. The non-porous latex coated sample shows an immediate and rapid increase in methanol exhaust concentration indicating severe loss of performance. The porous latex coated sample has an initial period with no methanol in the exhaust stream (~3 minutes) and a slower rate of adsorption compared to the plain carbon sample. Integration of the area above the curves gives the total amount of methanol adsorbed per sample and shows that the plain and

porous coated carbons have adsorbed approximately the same quantity of vapour. Although the porous coated sample showed poorer dynamic performance than the plain sample the results indicate that the adsorbent sites are still accessible, but at a slower rate.

4 Conclusion

Porous polymer films can be prepared from a functionalised latex by leaching of additives. The films retain 60-90% of the catalytic activity of the original latex particles, depending on the film preparation conditions. Coating chitosan onto a porous latex film enhanced the rate and amount of metal ion uptake from solution compared to chitosan flakes.

The advantages of a catalytic polymer film compared with individual latex particles is the ease of removal from the reaction medium (literally lifted out) and subsequent cleaning, which can be achieved by repeated washing/decanting steps. In contrast removal and cleaning of latex particles requires microfiltration or centrifugation, which are both time consuming and potentially wasteful processes. Cleaning of the porous polymer films is a far simpler and quicker process.

Initial studies on the transport properties of these porous latex films have been evaluated via dynamic adsorption. Carbon adsorbents coated in porous latex show their complete adsorption capacity for a vapour, but at a slower adsorption rate compared to plain carbon performance, whereas with a non porous film the capacity is lost completely.

Porous latex particles with extra specific surface area were successfully prepared via emulsion crosslinking copolymerisation of divinylbenzene, styrene using an inert diluent. Latex samples were made with total specific surface areas of $554 \text{ m}^2 \text{ g}^{-1}$, which were $373 \text{ m}^2 \text{ g}^{-1}$ higher than predicted by electron microscopy for non porous particles of the same diameter. Clear trends were seen with the ratio of styrene to divinyl benzene having the most effect on the creation of pores. Evaluation, by t-plots, of particles with more

specific surface area than theoretically predicted showed that the pores were all in the microporous range.

Porous latex particles were successfully incorporated into a porous latex film increasing the surface area of the film from $2.4 \text{ m}^2 \text{ g}^{-1}$ to $25.3 \text{ m}^2 \text{ g}^{-1}$. Only 17% of the surface area of the porous particles was lost after incorporation into the film.

5 Further work

5.1 Super water-repellent surfaces

Wettability of surfaces with a liquid is governed by two factors. First the chemical factor, which is modified by using different surface groups to alter the surface free energy. Second the geometric factor or roughness of the surface. The roughness of the surface alters the wettability of a solid with a liquid by increasing the solid-liquid interfacial area, which alters the balance between the three interfacial tensions (solid-liquid, liquid-vapour and solid-vapour). Super water-repellent surfaces, with a contact angle with water of 174° , can be formed using a wax which spontaneously forms a fractal surface¹⁹⁵.

Porous latex films have surface roughness resulting from the latex particles at the surface. The roughness can be controlled by the particle size of the latex used to make the film i.e. smaller particles will produce a rougher surface with a higher surface area. The controllability of the surface roughness makes porous latex films a potentially good media for the study of liquid wetting.

5.2 Controlled release

Inclusion of organic solvents as porogens in latex particles offers the prospect of introducing oil soluble active ingredients into the particles for subsequent sustained release from the particles themselves or from films. In further work oil soluble/sparingly water soluble chemicals, including dyes, could be added during latex particle preparation and subsequently their sustained release into aqueous media investigated. Any tendency for the particles to become imprinted can also be examined by adsorption from solution.

5.3 Further understanding

Colloidal size porous latex particles have been prepared, for the first time, by emulsion polymerisation. Porogens similar to those used in macroreticular resin synthesis were employed. Further work to increase the understanding of the mechanism of reaction involved should include the effects of surfactant type (mono- or bi- functional, anionic and non-ionic) and concentration and initiator type (water soluble, oil soluble or redox). The feasibility of surfactant-free emulsion polymerisation could also be studied.

Although latex film formation can be depicted as a simple 3 stage process (water evaporation, close particle packing and deformation/chain inter-diffusion) in practice coalescence processes are quite complex^{65,196}. Each of the individual components may influence the extent of coalescence and hence the film properties. Further studies are needed to increase understanding of particle coalescence.

The effects of thermal aging upon the porous film morphology requires investigation in relation to the polymer type (T_g), degree of cross-linking and the components used in film formation. The retention of porosity at ambient and possibly at elevated temperatures is important for practical applications, in relation to shelf-life, as well as giving an increased understanding of the mechanism of particle coalescence.

6 Appendix

6.1 Abbreviations

AIBN	2,2'-azo- <i>bis</i> -isobutronitrile
BET	Brunauer, Emmett and Teller
BMA	Butyl methacrylate
CPVF	Critical pigment volume fraction
DDW	Double distilled water
DVB	Divinylbenzene
ECCP	Emulsion crosslinking copolymerisation
EHP	Emulsion homopolymerisation
FCC	Face centred cubic
FFSEM	Freeze-fracture transmission electron microscopy
FFTEM	Freeze-fracture transmission electron microscopy
FTIR	Fourier transform infrared spectroscopy
HPMC	Hydroxypropyl methyl cellulose
KHCO ₃	Potassium hydrogen carbonate
KPS	Potassium persulphate
L30D	Ethyl acrylate/methacrylic acid latex, 131 nm diameter latex
MFFT	Minimum film formation temperature
MW	Molecular weight
MWD	Molecular weight distribution
NaCl	Sodium chloride
NaSS	Sodium styrene sulphonate
NET	Nonradiative energy transfer
NE30D	Ethyl acrylate/methylmethacrylate latex, 160 nm diameter latex

PBMA	Poly(butyl methacrylate)
PS	Poly(styrene)
PTFE	Poly(tetrafluoroethylene)
PVAc	Poly(vinyl acetate)
PVP	Poly(vinyl pyrrolidone)
RT	Room temperature
S-DVB	Styrene-divinylbenzene
SANS	Small angle neutron scattering
SAXS	Small angle x-ray scattering
SDED	Sodium diphenyl ether disulphonate
SDS	Sodium dodecyl sulphate
SEM	Scanning electron microscopy
SLATEX	Sulphonate poly(butyl methacrylate), 501 nm diameter latex
SSA	Specific surface area
TEM	Transmission electron microscopy
T _g	Glass transition temperature

7 Index

7.1 Index of figures

- Figure 1:** Particle formation in the presence of surfactant above its cmc.
- Figure 2:** Monomer conversion vs. time plot for emulsion polymerisation in the presence of surfactant above its cmc.
- Figure 3:** Particle formation in the absence/presence of surfactant below its cmc.
- Figure 4:** Film formation from a latex dispersion.
- Figure 5:** Freeze-fractured SEM photograph of a PBMA film cast at 50°C.
- Figure 6:** % water loss vs. time plot for a drying latex dispersion.
- Figure 7:** Schematic diagram of a drying front normal to the surface.
- Figure 8:** Schematic diagram of a drying front lateral to the surface.
- Figure 9:** Freeze-fractured TEM photograph of a PBMA film dried at room temperature.
- Figure 10:** Capillary force of interstitial water acting on three neighbouring particles.
- Figure 11:** Polymer/air interfacial tension forces acting on two particles.
- Figure 12:** Limiting conditions for film formation from a latex dispersion.
- Figure 13:** Schematic drawing of a packed bed of adsorbent in a VA (volume/activity) tube.
- Figure 14:** A functional polymer support from a functional monomer.
- Figure 15:** functionalising an initially inert polymer support.
- Figure 16:** Molecular structure of chitin and chitosan.
- Figure 17:** Schematic diagram of a nitrogen adsorption/desorption cycle.
- Figure 18:** Schematic representation of all six types of adsorption isotherm.

- Figure 19:** Schematic profile of a type 4 isotherm. The corresponding type 2 isotherm is shown as a broken line.
- Figure 20:** Schematic representation of the effect microporosity has on the adsorption isotherm. The profiles shown as broken lines are the adsorption isotherms in the absence of microporosity.
- Figure 21:** (A) effect on microporosity on the isotherm and t-plot of a sample. (1) is the standard sample (2) is the same sample with micropores. (B) effect of mesoporosity on the isotherm and t-plot of a sample. (1) is the standard sample (2) is the same sample with mesopores.
- Figure 22:** Schematic diagram of a mercury porosimetry run.
- Figure 23:** Section through the ring and plate used for latex film casting.
- Figure 24:** Diagram of "shaken" reaction vessel.
- Figure 25:** Diagram of "stirred" reaction vessel.
- Figure 26:** Schematic diagram of a vacuum frame.
- Figure 27:** Freeze-fracture SEM of a film prepared via the CPVF method.
- Figure 28:** Freeze-fracture SEM of a film prepared using glycerol.
- Figure 29:** Freeze-fracture SEM of a film prepared using NaCl.
- Figure 30:** Freeze-fracture SEM of film GLY20.
- Figure 31:** Freeze-fractured SEM of film SUC20.
- Figure 32:** Freeze-fractured SEM of film L30D20. Insert: film at higher magnification.
- Figure 33:** Freeze-fractured SEM of film prepared with no additive.
- Figure 34:** Schematic representation of pore formation using small molecule leachable additives.

- Figure 35:** Schematic representation of pore formation large particulate leachable additives.
- Figure 36:** Schematic representation of pore formation by exceeding a binders CPVF.
- Figure 37:** Freeze-fracture SEM photographs of PBMA films cast at various temperatures using 15% glycerol.
- Figure 38:** Schematic representation of surface groups potentially lost between the polymer bulk during particle deformation.
- Figure 39:** Schematic representation of surface groups retained at the polymer surface during particle coalescence.

7.2 Index of charts

- Chart 1:** Plot of Additive content vs specific surface area for porous latex films.
- Chart 2:** Plot of Additive content vs total pore volume for porous latex films.
- Chart 3:** Pore radius profiles for films prepared using L30D.
- Chart 4:** Pore radius profiles for films prepared using sucrose.
- Chart 5:** Pore radius profiles for films prepared using glycerol.
- Chart 6:** Pore radius profiles for films prepared using poly(vinyl pyrrolidone).
- Chart 7:** Pore radius profiles for films prepared using SDS.
- Chart 8:** Pore radius profiles for films by exceeding the CPVF of NE30D with a poly(styrene) latex.
- Chart 9:** Plot of % L30D content vs specific surface area for films freeze dried and nitrogen dried.
- Chart 10:** Pore radius profiles for films prepared using 10% and 30% L30D freeze dried and nitrogen dried.
- Chart 11:** Conductometric titration curve of the sulphonated latex, SLATEX.
- Chart 12:** Pore radius profiles for films prepared using glycerol.
- Chart 13:** Pore radius profiles for films prepared using sucrose.
- Chart 14:** Pore radius profiles for films prepared using L30D.
- Chart 15:** Number of pores per gram of film.
- Chart 16:** Plot of casting temperature vs specific surface area films prepared using 15% glycerol.

- Chart 17:** Plot of % weight of additive vs surface group density per gram for porous latex films.
- Chart 18:** Relative rate of ethyl formate hydrolysis for sulphonated films and particles.
- Chart 19:** The SSA of the films prepared using glycerol, sucrose and L30D compared to the SSA of SLATEX.
- Chart 20:** Plot of % weight of additive vs surface group density per m² of surface area for porous latex films.
- Chart 21:** Plot of copper absorption with time for chitosan coated porous latex films.
- Chart 22:** Plot of copper absorption with time for chitosan flakes.
- Chart 23:** Comparison of copper absorption with time for chitosan coated film and chitosan flakes.
- Chart 24:** Porous latex sample A's: Surfactant SDS varied.
- Chart 25:** Porous latex sample B's: Initiator KPS varied.
- Chart 26:** Porous latex sample C's: Ratio of styrene to DVB varied with the total amount always equal to 4 cm³.
- Chart 27:** Porous latex sample D's: Toluene varied.
- Chart 28:** Porous latex sample E's: Octane varied.
- Chart 29:** Variation of the number of micelles and particles with SDS content.
- Chart 30:** Varying organic phase components of porous latex particles.
- Chart 31:** Polymer conversion with time curves for porous latex particle polymerisations.

- Chart 32:** Polymer conversion with time curves for porous latex particle polymerisations.
- Chart 33:** Repeatability of shaken polymerisations compared with stirred polymerisations.
- Chart 34:** Adsorption/desorption isotherm of sample Org2.
- Chart 35:** Adsorption/desorption isotherm of sample Org2 after nonane preadsorption.
- Chart 36:** Adsorption/desorption isotherm of sample Org7.
- Chart 37:** Adsorption isotherms of Org2, Org2 preadsorbed with nonane and Org8.
- Chart 38:** t-plot of Org2 and Org2 preadsorbed with nonane compared to the non-porous standard Org8.
- Chart 39:** Coated BPL carbon sample dynamic sorption.

7.3 Index of tables

- Table 1:** Additives used and their levels of addition based on percentage weight of post-cast film.
- Table 2:** Component variations for the porous latex particle preparations.
- Table 3:** Repeatability of shaken polymerisations.
- Table 4:** Organic component variations for the porous latex particle preparations.
- Table 5:** Physical properties of porous latex particles.
- Table 6:** Porous latex particle preparations with the same component make-up carried out in both shaken and stirred polymerisations.

8 References

- 1 Sherrington, D.C. *Chemistry & Industry* **1991**, 7th Jan. 15-19.
- 2 Hassanein, M.; Aly, El-S. A.; Abbas, Y.A.; El-Signey, S.M. *Makromol.Chem.* **1993**, 194, 1817.
- 3 Ford, W.T.; El-Hamshary, H.; Stefanithis, I.; Spivy, H.O.; Hassanein, M.; Selim, A. *New J. Chem.* **1996**, 20(5), 549.
- 4 Hassanein, M.; Abdel-Hay, I.; El-Hefnawy El-Esawy, T. *Eur. Polym. J.* **1994**, 30(3), 335.
- 5 Lee, J-J.; Ford, W.T. *J. Org. Chem.* **1993**, 58, 4070.
- 6 Zhu, W.; Ford, W.T. *J. Polym. Sci.: Pt. A: Polym. Chem.* **1992**, 30, 1305.
- 7 Fitch, R.M. In *Macromolecules*; Benoit, H., Rempp, P. Eds.; Pergamon Press: Oxford, **1982**; p 39.
- 8 Arai, K.; Sugita, J.; Ogiwara, Y. *Makromol. Chem., Rapid Commun.* **1986**, 7, 427.
- 9 Hopkins, A.; Williams, A. *J.Chem. Soc., Perkin Trans.* **1983**, 2, 891.
- 10 Kinato, H.; Nakamura, K.; Ise, N. *J. Appl. Biochem.* **1982**, 4, 34.
- 11 Hassanein, M.; Ford, W.T. *Macromolecules* **1988**, 21, 525.
- 12 Turk, H.; Ford, W.T. *J. Org. Chem.* **1988**, 53, 460.
- 13 Ford, W.T.; Chandran, R.; Turk, H. *Pure Appl. Chem.* **1988**, 60, 395.
- 14 Chandran, R.S.; Srinivasan, S.; Ford, W.T. *Langmuir* **1989**, 5(4), 1061.
- 15 Ford, W.T.; Badley, R.D.; Chandran, R.S.; Babu, S.H.; Hassanein, M.; Srinivasan, S.; Turk, H.; Yu, H.; Zhu, W. *Am. Chem. Soc. Symp. Ser.* **492**., **1992**, Chapter 26.
- 16 Bernard, M.; Ford, W.T.; Taylor, T.W. *Macromolecules* **1984**, 17, 812.

-
- 17 Thiagarajan, V.S.; Huang, Z.; Scriven, L.E.; Schottel, J.L.; Flickinger, M.C.
J. Colloid Interf. Sci. **1999**, 215(2), 244.
- 18 Harkins, W.D. *J Polym. Sci.* **1950**, 5, 217.
- 19 Gilbert, R.G. *Emulsion Polymerisation; A Mechanistic Approach*; Academic Press, **1995**, p 175.
- 20 Smith, W.V. *J. Am. Chem. Soc.* **1948**, 70, 3695.
- 21 Smith, W.V.; Ewart, R.H. *J. Chem. Phys.* **1948**, 16, 592.
- 22 Smith, W.V. *J. Am. Chem. Soc.* **1949**, 71, 4077.
- 23 Gardon, J.L. *J. Polym. Sci.* **1971**, 9, 2763.
- 24 Harada, M.; Normura, M.; Kojima, H.; Eguchi, W.; Nagata, S. *J. Appl. Polym. Sci.* **1972**, 16, 811.
- 25 Fitch, R.M. *Br. Polym. J.* **1973**, 5, 467.
- 26 Min, K.W.; Ray, W.H. *J. Macromol. Sci., Rev. Macromol. Chem.* **1974**, C11, 177.
- 27 Priest, W.J. *J. Phys. Chem.* **1952**, 56, 1077.
- 28 Hanson, F.K.; Ugelstad, J. *Emulsion Polymerisation*; Piirma, I. Eds.; Academic Press: New York, **1992**.
- 29 Lichti, G.; Gilbert, R.G.; Napper D.H. *J. Polym. Sci. Polym. Chem.* **1983**, 21, 269.
- 30 Eliseeva, V.I. *Acta Polym.* **1981**, 32, 355.
- 31 Stockmayer, W.H. *J. Polym. Sci.* **1957**, 24, 314.
- 32 O'Toole, J.T. *J. Appl. Polym. Sci.* **1965**, 9, 1291.
- 33 Napper, D.H.; Parts, A.G. *J. Polym. Sci.* **1962**, 61, 113.
- 34 Gardon, J.L. *J. Polym. Sci., A-1* **1968**, 6, 665.
- 35 Katz, S.; Saidel, G.M. *J. Polym. Sci.* **1969**, 27, 149.

-
- 36 Katz, S.; Shinnar, R.; Saidel, G.M. *Addition and Condensation Polymerization Processes, Advances in Chemistry Series 91*; American Chemical Society: Washinton DC, **1969**; Chapter 8.
- 37 Kubota, H.; Omi, S. *J. Chem Eng Jap.* **1972**, *5*, 39.
- 38 Brodnyan, J.G. *J. Colloid Sci.* **1960**, *15*, 563.
- 39 Ewart, R.H.; Carr, C.I. *J. Phys. Chem.* **1954**, *58*, 640.
- 40 Watterson, J.G.; Parts A.G. *Makromol. Chem.* **1971**, *146*, 11.
- 41 Gardon, J.L. *J. Polym. Sci.* **1968**, *6*, 623.
- 42 Gardon, J.L. *J. Polym. Sci.* **1968**, *6*, 687.
- 43 Medvedev, S.S. *Proceedings of the International Symposium on Makromoleculuar Chemistry, Praque 1957*; Pergamon: New York **1958**, p 174.
- 44 Grancio, M.R.; Williams, D.J. *J. Polym. Sci.* **1970**, *8*, 2617.
- 45 Keusch, P.J.; Prince, J.; Williams, D.J. *Macromol. Sci.-Chem.* **1973**, *A7*, 623.
- 46 Keusch, P.J.; Williams, D.J. *J. Polym. Sci. Chem. Ed.* **1973**, *11*, 143.
- 47 Matsumoto, T.; Ochi, A. *Kobunshi Kagaku* **1965**, *22*, 481.
- 48 Arai, M.; Arai, K.; Saito, S. *J. Polym. Sci., Polym. Chem. Ed.* **1979**, *17*, 3655.
- 49 Fitch, R.M.; Prenosil, M.P.; Sprick, K.J. *J. Polym. Sci., Part C* **1969**, *27*, 95.
- 50 Goodall, A.R.; Wilkinson, M.C.; Hearn, J. *J. Polym. Sci., Polym. Chem. Ed.* **1977**, *15*, 2193.
- 51 Feeney, P.J.; Napper, D.H.; Gilbert R.G. *Macromolecules* **1987**, *20*, 2922.
- 52 Feeney, P.J.; Napper, D.H.; Gilbert R.G. *Macromolecules* **1984**, *17*, 2520.
- 53 Fitch, R.M.; Tsai, C.H. *Polymer Colloids*; Fitch, R.M., Eds.; Plenum Press: New York, **1971**.
- 54 Gilbert, R.G. *Emulsion Polymerisation; A Mechanistic Approach*; Academic Press **1995**, p 229.

-
- 55 Ottewill, R.H.; Shaw, J.N. *Kolloid Z.u.Z. Polymere* **1967**, *218*, 34.
- 56 Goodwin, J.W.; Ottewill, R.H.; Pelton, R.; Vianello, G.; Yates, P.E. *Brit. Polym. J.* **1978**, *10*, 173.
- 57 Goodwin, J.W.; Hearn, J.; Ho, C.C.; Ottewill, R.H. *Colloid Polym. Sci.* **1974**, *252*, 464.
- 58 Chainey, M.; Wilkinson, M.C.; Hearn, J. *Ind. Eng. Chem. Prod. Res. Dev.* **1982**, *21*, 171.
- 59 Hearn, J.; Wilkinson, M.C.; Goodall, A.R. *Adv. Colloid Interface Sci.* **1981**, *14*, 173.
- 60 Sunkara, H.; Jethmalani, J.; Ford, W. *J. Polym. Sci.: Part A: Polym. Chem.* **1994**, *32*, 1431.
- 61 Dobler, F.; Pith, T.; Lambla, M.; Holl, Y. *J. Colloid Interface Sci.* **1992**, *152*, 12.
- 62 Roulstone, B.J.; Wilkinson, M.C.; Hearn, J.; Wilson, A.J. *Polym. Int.* **1991**, *24*, 87.
- 63 Protzman, T.F.; Brown, G.L. *J. Appl. Polym. Sci.* **1960**, *10*, 81.
- 64 ASTM D 2354-68, *Standard Test Method for Minimum Film Formation Temperature (MFT) of Emulsion Vehicles*; American Society for Testing Materials: Philadelphia PA, **1993**.
- 65 Keddie, J.L. *Material Sci. Eng.* **1997**, *21*, 101.
- 66 Vanderhoff, J.W.; Bradford, E.B.; Carrington, W.K. *J. Polym. Sci.* **1973**, *41*, 155.
- 67 Croll, S.G. *J. Coatings Tech.* **1986**, *58*, 41.

-
- 68 Sutanto, E.; Ma, Y.; Davis, H.T.; Scriven, L.E. *Film Formation in Coatings. Mechanisms, Properties and Morphology. ACS Symposium Series 790.*; American Chemical Society: Washington DC **2001**, p 174.
- 69 Okuba, M.; Takeya, T.; Tsutsumi, Y.; Kabooka, T.; Matsumoto, T. *J. Polym. Sci., Polym. Chem. Ed.* **1981**, *19*, 1.
- 70 Wang, Y.; Kats, A.; Juhu , D.; Winnik, M.A. *Langmuir* **1992**, *8*, 1435.
- 71 Juhu , D.; Wang, Y.; Lang, J.; Leung, O.M.; Goh, M.C.; Winnik M.A. *J. Polym. Sci. B: Polym. Phys.* **1995**, *33*, 1123.
- 72 Isaacs, P.K. *J. Macromol. Chem.* **1966**, *1*, 163.
- 73 Chevalier, Y.; Pichot, C.; Graillat, C.; Joanicot, M.; Wong, K.; Maquet J.; Lindner, P.; Cabane, B. *Colloid Polym. Sci.* **1992**, *270*, 806.
- 74 Hwa, J.C.H. *J. Polym. Sci.* **1964**, *2*, 785.
- 75 Keddie, J.L.; Meredith, P.; Jones, R.A.L.; Donald, A.M. *Film Formation in Waterborne Coatings, ACS Symposium Series 648.*; American Chemical Society: Washington DC **1996**, p 332.
- 76 Ming, Y.; Takamura, K.; Davis, H.T.; Scriven, L.E. *Tappi J.* **1995**, *78(11)*, 151.
- 77 Pusey, P.N.; Van Megan, W.; Bartlett, P.; Ackerson, B.J.; Rarity, J.G.; Underwood, S.M. *Phys. Rev. Lett.* **1989**, *63*, 2753.
- 78 Dingenouts, N.; Ballauff, M. *Langmuir* **1999**, *15*, 3283.
- 79 Joanicot, M.; Wong, K.; Maquet, J.; Chevalier, Y.; Pichot, C.; Graillat, C.; Lindner, P.; Rios, L.; Cabane, B. *Progr. Colloid Polym. Sci.* **1990**, *81*, 175.
- 80 Sosnowski, S.; Li, L.; Winnik, M.A.; Clubb, B.; Shivers, R. *J. Polym. Sci.: Pt. B: Polym. Phys.* **1994**, *32*, 2499.
- 81 He, C.; Donald, A.M. *Langmuir* **1996**, *12*, 6250.

-
- 82 Sheehan, J.G.; Takamura, K.; Davis, H.T.; Scriven, L.E. *Tappi J.* **1993**, 76(12), 93.
- 83 Isaacs, P.K. *J. Macromol. Chem.* **1966**, 1, 163.
- 84 Roulstone, B.J.; Wilkinson, M.C.; Hearn, J. *Polym. Inter.* **1992**, 27, 43.
- 85 Brodnayan, J.G.; Konen, T. *J. Appl. Polym. Sci.* **1994**, 53, 1139.
- 86 Lissant, K.J.; Coll, J. *Interf. Sci.* **1966**, 22, 462.
- 87 Roulstone, B.J.; Wilkinson, M.C.; Hearn, J.; Wilson, A.J. *Polym. Inter.* **1991**, 24, 87.
- 88 Wang, Y.; Kats, A.; Juhué, D.; Winnik, M.A.; Shivers R.R.; Dinsdale C.J. *Langmuir* **1992**, 8, 1435.
- 89 Brown, G.L. *J. Polym. Sci.* **1956**, 22, 423.
- 90 Vanderhoff, J.W.; Tarkowski, H.L.; Jenkins M.C.; Bradford, E.B. *J. Macromol. Chem.* **1966**, 1(2), 361.
- 91 Sheetz, D.P. *J. Appl. Polym. Sci.* **1965**, 9, 3759.
- 92 Mason, G. *Br. Polym. J.* **1973**, 5, 101.
- 93 Eckersley, S.T.; Rudin, A. *J. Coatings Tech.* **1990**, 62, 89.
- 94 Eckersley, S.T.; Rudin, A. *J. Appl. Polym. Sci.* **1994**, 53, 1139.
- 95 Lin, F.; Meier, D.J. *Langmuir* **1995**, 11, 2726.
- 96 Sperry, P.R.; Snyder, B.S.; O'Dowd, M.L.; Lesko, P.M. *Langmuir* **1994**, 10, 2619.
- 97 Dobler, F.; Pith, T.; Lamba, M.; Holl, Y. *J. Colloid Interf. Sci.* **1992**, 152, 12.
- 98 Dillon, R.E.; Matheson, L.A.; Bradford, E.B. *J. Colloid Sci.* **1986**, 264, 1092.
- 99 Frenkel, J. *J. Phys. (Moscow)* **1945**, 9(5), 385.
- 100 Sperry, P.R.; Synder, B.S.; O'Dowd, M.L.; Lesko, P.M. *Langmuir* **1994**, 10, 2619.

-
- 101 Henson, W.A.; Taber, D.A.; Bradford, E.B. *Ind. Eng. Chem.* **1953**, *45*, 735.
- 102 Sheetz, P.D. *J. Appl. Polym. Sci.* **1965**, *9*, 3759.
- 103 Voyutskii, S.S. *J. Polym. Sci.* **1958**, *32*, 528.
- 104 Chevalier, Y. *Trends in Polym. Sci.* **1996**, *4(6)*, 197.
- 105 Hahn, K.; Ley, G.; Schuller, H.; Oberthur, R. *Colloid Polym. Sci.* **1986**, *264*, 1092.
- 106 Zhao, C.L.; Wang, Y.; Hruska, Z.; Winnik, M.A. *Macromolecules* **1990**, *23*, 4082.
- 107 Wang, Y.; Zhao, C.L.; Winnik, M.A. *J. Chem. Phys.* **1991**, *95*, 2143.
- 108 Boczar, E.M.; Dionne, B.C.; Fu, Z.; Kirk, A.B.; Lesko, P.M.; Koller, A.D. *Macromolecules* **1993**, *26*, 5772.
- 109 Pekcan, Ö.; Winnik, M.A.; Croucher, M.D. *Macromolecules* **1990**, *23*, 2673.
- 110 Wang, Y.; Winnik, M.A. *Macromolecules* **1993**, *26*, 3147.
- 111 de Gennes, P.G. *J. Chem. Phys.* **1971**, *55*, 572.
- 112 Zosel, A.; Ley, G. *Polym. Bull.* **1992**, *27*, 459.
- 113 Zosel, A.; Ley, G. *Macromolecules* **1993**, *26*, 2222.
- 114 Zosel, A. *Polym. Adv. Tech.* **1995**, *6*, 263.
- 115 Kientz, E.; Holl, Y. *Coll. Surf. A: Physicochem. Eng. Aspects* **1993**, *78*, 255.
- 116 Vijayendran, B.R.; Bone, T.; Sawyer, L.C. *J. Dispersion Sci. Tech.* **1982**, *3(1)*, 81.
- 117 Roulstone, B.J.; Wilkinson, M.C.; Hearn, J. *Polym. Int.* **1992**, *27*, 43.
- 118 Kawaguchi, S.; Odrobina, E.; Winnik, M.A. *Macromol. Rapid Commun.* **1995**, *16*, 861.

-
- 119 Bradford, E.B.; Vanderhoff, J.W. *J. Macromol. Chem.* **1966**, 1(2), 335.
- 120 Zhao, C.L.; Hol, Y.; Pith, T.; Lambla, M. *Colloid Polym. Sci.* **1987**, 265, 823.
- 121 Kast, H. *Makromol. Chem. Suppl.* **1985**, 10(11), 447.
- 122 Côté, W.A.; Day, A.C.; Wilkes, G.; Marchessault, R.H. *J. Colloid Interf. Sci.* **1968**, 27, 32.
- 123 Wilkes, G.; Marchessault, R.H. *J. Appl. Phys.* **1966**, 37, 3974.
- 124 Evanson, K.W.; Thorstenson, T.A.; Urban, M.W. *J. Appl. Polym. Sci.* **1991**, 42, 2297.
- 125 Staudinger, J.; Husemann, E. *Chem. Ber.* **1935**, 68, 1618.
- 126 D'Alelio, G.F. *US Patent* 2,366,007, **1945**.
- 127 Akelah, A.; Sherrington, D.C. *Chem. Rev.* **1981**, 81, 557.
- 128 Akelah, A.; Sherrington, D.C. *Polymer* **1983**, 24, 1369.
- 129 Kaneko, M.; Tsuchiida, E. *J. Polym. Sci., Macromol. Rev.* **1981**, 16, 397.
- 130 Bailey, D.C.; Langer, S.H. *Chem. Rev.* **1981**, 81, 109.
- 131 Klien, J.; Vorlop, K.D. *Foundations of Biochemical Engineering: Kinetics and Thermodynamics in Biological Systems. ACS Symposium Series 207*; Blanch, H.W., Papoutsaki, E.T., Stephanopoulos, G., Eds.; American Chemical Society: Washington DC, **1983**; Chapter 17.
- 132 Gribnau, T.C.J.; Visser, J.; Nivard, R.J.F. Eds. *Affinity Chromatography and Related Techniques*, Elsevier: Amsterdam, **1982**.
- 133 Brooks, B.W. *Macromol. Chem. Macromol. Symp.* **1990**, 35/36, 121.
- 134 Kun, K.A.; Kunin, R. *J. Polym. Sci.* **1967**, 16, 1457.
- 135 Kun, K.A.; Kunin, R. *J. Polym. Sci.* **1968**, 6, 2089.
- 136 Epton, R.; Holding, S.R.; McLaren, J.V. *Polymer* **1976**, 17, 843.

-
- 137 Milsson, H.; Mosbach, R.; Mosbach, K. *Biochem. Biophys. Acts* **1972**, 268, 253.
- 138 Bakhshae, M.; Pethrick, R.A.; Rashid, H.; Sherrington, D.C. *Polym. Commun.* **1985**, 26, 185.
- 139 Seidl, J.; Malinsky, J.; Dusek, K.; Heitz, W. *Adv. Polym. Sci.* **1967**, 5, 113.
- 140 Kun, K.A.; Kunin, R.J. *J. Polym. Sci. Part A* **1968**, 6, 2689.
- 141 Guyot, A.; Bartholin, M. *Prog. Polym. Sci.* **1982**, 8, 277.
- 142 Sederel, W.L.; DeJong, G.J. *J. Appl. Polym. Sci.* **1973**, 17, 2835.
- 143 Millar, J.R.; Smith, D.G.; Mar, W.E.; Kressman, T.R.E. *J. Chem. Soc.* **1963**, 218.
- 144 Bortel, E. *Przemy Chem.* **1965**, 44, 255.
- 145 Abrams, I.M. *Ind. Eng. Chem.* **1956**, 48, 1469.
- 146 Erbay, E.; Okay, O. *Polym. Bulletin* **1998**, 41, 379.
- 147 Haupke, K.; Pientka, V.J. *Chromatog.* **1974**, 102, 117.
- 148 Nyhus, A.K.; Hagen, S.; Berge, A. *J. Polym. Sci. Part A: Polym. Chem.* **1999**, 37, 3973.
- 149 Haupke, K.; Hoffman, H. *Z. Chem.* **1968**, 8, 463.
- 150 Guyot, A.; Bartholin, M. *Prog. Polym. Sci.* **1982**, 8, 277.
- 151 Chung, D.Y.; Bartholin, M.; Guyot, A. *Angew. Makromol. Chem.* **1982**, 103, 109.
- 152 Sederal, W.L.; De Jong, G.J. *J. Appl. Polym. Sci.* **1973**, 17, 2835.
- 153 Rabelo, D.; Coutinho, F.M.B. *Eur. Polym. J.* **1994**, 30, 675.
- 154 Poinescu, I. C.; Vlad, C. *Eur. Polym. J.* **1997**, 33, 1515.
- 155 Akelah, A.; Sherrington, D.C. *Polymer* **1983**, 24, 147.
- 156 Hall, L.D.; Yalpani, M.; *J. Chem. Soc. Chem. Comm.* **1980**, 1153.

-
- 157 Roberts, G.A.F. *Chitin Chemistry*; Macmillan Press Ltd: London, **1992**; p 6.
- 158 Muzzarelli, R.A.A. *Natural Chelating Polymers*; Pergamon: Oxford, **1973**.
- 159 Muzzarelli, R.A.A. *Chitin*; Pergamon: Oxford, **1977**.
- 160 Ishii, K. *Gel handbook* Osada, Y.; Kajiwara, K. editors Tokyo: NTS **1997**, 404.
- 161 Funke, W.; Okay, O.; Joos-Muller, B. *Adv. in Polym. Sci.* **1998**, 136, 139.
- 162 Nakamura, K.; Imoto, A.; Matsumoto, A. *Preprints for the 8th Polymeric Microsphere Symposium, November 9-11, Fukui, Japan, 1994*, 37.
- 163 Tobita, H.; Kumagai, M.; Aoyagi, N. *Polymer* **2000**, 41, 481.
- 164 Obrecht, W.; Seitz, U.; Funke, W. *ACS Symp. Ser. 24* **1976**, 92.
- 165 Nomura, M.; Fujita, K. *Polym. Int.* **1993**, 30, 483.
- 166 Lowell, S.; Shields, J.E. *Powder Surface Area & Porosity*; Chapman & Hall: London, **1984**.
- 167 Brunauer, S.; Deming, L.S.; Deming, W.E.; Teller, E. *J. Amer. Chem. Soc.* **1940**, 62, 1723.
- 168 Langmuir, I. *J. Amer. Chem. Soc.* **1916**, 38, 2221.
- 169 Langmuir, I. *J. Amer. Chem. Soc.* **1918**, 40, 1361.
- 170 Brunauer, S.; Emmet, P.H.; Teller, E. *J. Am. Chem. Soc.* **1938**, 60, 309.
- 171 Gregg, S.J.; Langford, J.F. *Trans. Faraday Soc.* **1969**, 65, 1394.
- 172 Lippens, B.C.; de Boer, J.H. *J. Catalysis* **1965**, 4, 319.
- 173 Lippens, B.C.; Linsen, B.G.; deBoer, J.H. *J. Catalysis* **1964**, 3, 32.
- 174 Steward, P.A.; Hearn, J.; Wilkinson, M.C.; Wilson, A.J.; Roulstone, B.J. *Film Formation in Waterborne Coatings, ACS Symposium Series 648*; American Chemical Society: Washington DC, **1996**; p 402.

-
- 175 Tobita, H.; Hamielec, A.E.; *Polym. Int.* **1993**, *30*, 195.
- 176 Chonde, Y.; Krieger, I.M. *J. Colloid Interface Sci.* **1980**, *77*, 138.
- 177 Chainey, M.; Wilkinson, M.C.; Hearn, J. *Ind. Eng. Chem. Prod. Res. Dev.* **1982**, *21*, 171.
- 178 Steward, P. Modification of the Permeability of Polymer Latex Films. Ph.D. Thesis, The Nottingham Trent University, Nottingham, **1995**
- 179 Chainey, M.; Hearn, J.; Wilkinson, M.C. *J. Colloid Interface Sci.* **1987**, *117*, 477.
- 180 Maghami, G.G.; Roberts, G.A.F. *Makromol. Chem.* **1988**, *189*, 2239.
- 181 Karpowicz, F.; Hearn, J.; Wilkinson, M.C.; *Carbon* **1995**, *33 (11)*, 1573.
- 182 Du Chesne, A.; Gerharz, B.; Lieser, G. *Polym. Int.* **1997**, *43*, 187.
- 183 Zhao, C.L.; Dobler, F.; Pith, T.; Holl, Y.; Lambla, M. *J. Colloid Interf. Sci.* **1988**, *128*, 437.
- 184 Brown, G.L. *J. Polym. Sci.* **1956**, *22*, 423.
- 185 Sperry, P.R.; Synder, B.S.; O'Dowd, M.L.; Lesko, P.M. *Langmuir* **1994**, *10*, 2619.
- 186 Lin, F.; Meier, D.J. *Langmuir* **1995**, *11*, 2726.
- 187 Vanderhoff, J.W.; Tarkowski, H.L.; Jenkins, M.C.; Bradford, E.B.; *J. Macromol. Chem.* **1966**, *1(2)*, 361.
- 188 Dillon, R.E.; Matheson, L.A.; Bradford, E.B.; *J. Colloid Sci.* **1951**, *6*, 108.
- 189 Zhao, C.L.; Dobler, F.; Pith, T.; Holl, Y.; Lambla, M. *J. Colloid Interface Sci.* **1988**, *128*, 437.
- 190 Averbach, B.L. *Chitin and Chitosan*, The Japanese Society of Chitin and Chitosan: Tottori, **1982**; p 248.
- 191 Flockhart, B.D. *J. Colloid Sci.* **1961**, *16*, 484.

-
- 192 Tartar, H.V.; Lelong, A. *J. Phys. Chem.* **1955**, *59*, 1185.
- 193 Pickering, S.U. *J. Chem. Soc.* **1907**, *91*, 2001.
- 194 Binks, B.P.; Lumsdon, S.O. *Phys. Chem. Chem. Phys.* **2000**, *2*, 2959.
- 195 Shibuichi, S.; Onda, T.; Satoh, N.; Tsujii, K. *J. Phys. Chem.* **1996**, *100*, 19512.
- 196 Steward, P.A.; Hearn, J.; Wilkinson, M.C. *Adv. Colloid & Interf. Sci.* **2000**, *86*, 195.

Published Papers

1. Hodges, I.C.; and Hearn, J. *Langmuir*, **2001**, *17*(11), 3419.
2. Hodges, I.C.; Hearn, J.; Wilkinson, M.C. *ACS Symposium Series 790*; American Chemical Society: Washington DC, **2001**; p233.

Reactive Latex Films

Ian C. Hodges and John Hearn*

Nottingham Trent University, Clifton Lane, Nottingham, NG11 8NS, United Kingdom

Received January 11, 2001. In Final Form: March 19, 2001

Porous polymer films have been prepared from poly(butyl methacrylate) latex particles with surface sulfonate groups and been shown to retain up to 90% of the catalytic capacity of the original latex particles. Advantages of latex films over latex particles as reactive surfaces include easier removal from the reaction medium and easier cleaning/rejuvenation of the polymer films. The films have been characterised by specific surface area, mercury porosimetry, and conductometric titration. Reactivity was evaluated for the acid-catalyzed hydrolysis of ethyl methanoate.

Introduction

Chemical reagents and catalysts attached to polymeric supports offer the prospect of cleaner, more environmentally friendly, chemistry. Corrosive, noxious and toxic species can be rendered safe, and expensively synthesised molecules and precious metal complexes can be more effectively recovered and reused when immobilised to a polymeric support.¹ Activity in the commonly used coarse macroporous resin beads is however limited, in part, by external mass transfer and intraparticle diffusion to active sites.^{2,3} Activity increases as the particle size decreases because the surface area to weight ratio is inversely related to particle diameter. Colloidal sized polymer particles, such as latex particles, are promising catalyst supports because of their high specific surface area and the ability to concentrate organic reactants in the active catalyst phase by absorption from water.⁴ Manufacturing processes involving aqueous colloids rather than organic solvents would also reduce the need for solvent recycling and disposal.⁵ Functionalized latex particles have proved viable catalysts⁶ for a variety of oxidation and hydrolysis reactions in which high electrolyte concentrations are not required. Functional groups have included sulfonic acids,^{7,8} a primary amine,⁹ and imidazoles¹⁰ for ester hydrolysis and cobalt complexes for autoxidation of organic compounds.¹¹⁻¹⁴ Catalysts are sought for environmental use, which would be capable of oxidising all organic compounds in industrial wastewater to carbon dioxide,¹⁵ as well as for use in chemical manufacturing processes. Chemical reactions in aqueous colloidal dispersions are related to important

reactions in living organisms;⁶ for example, metalloporphyrins have been used to mimic the action of natural oxygenases.¹⁶

Colloidal catalysts are more difficult to recycle than large beads, needing to be either ultrafiltered or coagulated and redispersed for repeat use,⁶ and under usual phase transfer catalytic conditions charged particles are impractical because of fast coagulation by electrolytes.¹⁷ These latter disadvantages of latex catalysts, with respect to ease of recovery and sensitivity to electrolyte addition, may be overcome if the functionalized latex is presented in the form of a film. Thin polymer latex films, with glass transition temperatures close to the physiological temperature, have been shown to offer better mechanical strength, chemical stability, and temperature stability than the more commonly employed soft gels, such as alginate or polyacrylamide, for use with trapped and immobilised viable microbial cells in biocatalytic applications.¹⁸ The problems of predominantly diffusive transport of reactants and products with the gels were also overcome.

Polymer films can be produced by evaporation of water from a latex dispersion. The film formation process is usually described as occurring in three idealized stages.^{19,20} It begins with a latex dispersion, which upon evaporation of water becomes so concentrated that the uniform latex particles arrange into a close packed structure. In the second stage as water is lost from between the polymer particles, they deform and fill interstices until no water is left and no voids are present in the film. The final step is termed "further gradual coalescence" or "autohesion" and involves the diffusion of polymer chain-ends into neighbouring particles, thus developing film strength.

Porosity may be developed in latex films by incorporation of suitable additives into the latex dispersion prior to film formation followed by subsequent removal of the additive when film formation is complete.^{21,22} It has been found that the pore characteristics of a film can be tailored by the choice and amount of additive used.²²

This study investigates the production of porous latex films prepared from a surface sulfonated poly(butyl methacrylate)

(1) Sherrington, D.C. *Chemistry & Industry* 1991, 7th Jan. 15-19.

(2) Hassanein, M.; Aly, El-S. A.; Abbas, Y.A.; El-Signey, S.M. *Makromol.Chem.* 1993, 194, 1817-1825.

(3) Ford, W.T.; El-Hamshary, H.; Stefanithis, I.; Spivy, H.O.; Hassanein, M.; Selim, A. *New J. Chem.* 1996, 20(5), 549-557.

(4) Hassanein, M.; Abdel-Hay, I.; El-Hefnawy El-Elawy, T. *Eur.Polym.J.* 1994, 30(3), 335-337.

(5) Lee, J.-J.; Ford, W.T. *J.Org.Chem.* 1993, 58, 4070-4077.

(6) Zhu, W.; Ford, W.T. *J. Polym. Sci.:Pt.A:Polym. Chem.* 1992, 30, 1305-1313.

(7) Fitch, R.M. In *Macromolecules*; Benoit, H.; Rempp, P. Eds.; Pergamon Press: Oxford, 1982; p.39.

(8) Arai, K.; Sugita, J.; Ogiwara, Y. *Makromol.Chem., Rapid Commun.* 1986, 7, 427.

(9) Hopkins, A.; Williams, A. *J.Chem. Soc., Perkin Trans.* 1983, 2, 891.

(10) Kinato, H.; Nakamura, K.; Ise, N. *J. Appl. Biochem.* 1982, 4, 34.

(11) Hassanein, M.; Ford, W.T. *Macromolecules* 1988, 21, 525-526.

(12) Turk, H.; Ford, W.T. *J.Org.Chem.* 1988, 53, 460.

(13) Ford, W.T.; Chandran, R.; Turk, H. *Pure Appl. Chem.* 1988, 60, 395.

(14) Chandran, R.S.; Srinivasan, S.; Ford, W.T. *Langmuir* 1989, 5(4), 1061.

(15) Ford, W.T.; Badley, R.D.; Chandran, R.S.; Babu, S.H.; Hassanein, M.; Srinivasan, S.; Turk, H.; Yu, H.; Zhu, W. *Am. Chem. Soc. Symp. Ser.* 1992, 492, 422-431.

(16) Jorgensen, K.A. *Chem. Rev.* 1989, 89, 431.

(17) Bernard, M.; Ford, W.T.; Taylor, T.W. *Macromolecules* 1984, 17, 812.

(18) Thiagarajan, V.S.; Huang, Z.; Scriven, L.E.; Schottel, J.L.; Flickinger, M.C. *J. Colloid Interf. Sci.* 1999, 215(2), 244-257.

(19) Steward, P.A.; Hearn, J.; Wilkinson, M.C. *Adv. Colloid & Interf. Sci.* 2000, 86, 195-267.

(20) Keddie, J.L. *Mater. Sci. Eng.* 1997, 21, 101.

(21) Steward, P.A.; Hearn, J.; Wilkinson, M.C.; Wilson, A.J.; Roulstone, B.J. *Am. Chem. Soc. Symp. Ser. No. 648, 1996, Chapter 23, 359.*

(22) Hodges, I.C.; Hearn, J. *Am. Chem. Soc. Symp. Ser. No. 790, 2001, Chapter 13.*

latex, to ascertain whether the sulfonate groups are still accessible within the porous films and to evaluate the resulting films' efficiencies as catalysts.

Experimental Section

Materials used were butyl methacrylate (BMA) (distilled under reduced pressure) (99%, Sigma-Aldrich Co. Ltd., Gillingham Dorset, UK), doubly distilled water (DDW) from an all Pyrex glass still, potassium hydrogen carbonate (KHCO_3) (>99% SLR Grade, Fisher Scientific UK, Loughborough, UK), potassium persulphate (KPS) (>98% SLR Grade, Fisher Scientific, UK, Loughborough UK), sodium styrene sulfonate (NaSS) (Polysciences Inc., Warrington PA USA), sucrose (GPR Grade, Merck, Poole Dorset, UK), glycerol (>99%, Avocado Research Chemicals Ltd., Heysham Lancashire, UK), and Eudragit® L30D (ethyl acrylate/methacrylic acid latex, 131 nm diameter) (30% aqueous dispersion, Röhm Pharma GMBH, Weiterstadt, Germany).

Latex films were formed from one base latex, which was a sulfonate functionalized poly(butyl methacrylate) (SLATEX) prepared, in house, by soap-free shot-growth polymerization.²³ A stirred mixture of 150 mL BMA, 1350 mL DDW, and 0.6 g KHCO_3 was initiated with 2.55 g of KPS at 60 °C. Between 90 and 95% monomer conversion, a shot consisting 18 mL BMA and 9 g NaSS (dissolved in 70 mL DDW) was added, along with 1.5 g of KPS, and allowed to react further. This resulted in a high concentration of functional groups on the surface of the particles. After reaction the latex was cleaned by repeated ultracentrifugation²⁴/decantation steps and sodium ions were exchanged for protons by acid-washing.

Water soluble additives investigated were sucrose and glycerol. The other additive investigated was the latex Eudragit® L30D, which is water soluble at pH>7.

The additive was mixed into the latex prior to film casting by gentle agitation. Films were cast at 60 °C in 75 mm diameter glass rings on plates sealed with silicone grease, producing 230 μm thick, coherent transparent films (although the films were not fully coalesced, the additives trapped within them did not have significantly differing refractive indices from the polymer so that light was not scattered). Films incorporating water-soluble additives were soaked in DDW to leach out the additive. Films containing L30D were washed with sodium hydroxide solution, at pH 12, followed by DDW. Washing was continued until no residue was detectable in the evaporated wash water. During the leaching process, the films turned opaque then white, as a consequence of light scattering from the pores as the additive was replaced with water. The sulfonate groups were converted to the acid form by washing in 0.5 M hydrochloric acid followed by rinsing in DDW until the wash water had the same conductivity as DDW. Surface charge characterization and catalytic activity were evaluated while the films were still immersed in water. Specific surface area and porosimetry measurements were carried out on films whose water was removed by freeze drying. Freeze drying eliminates any pore closure caused by drying the films by liquid water evaporation.²²

Films were prepared as shown in Table 1 with percentage of additive based on postcast dry film weight. Film NOADD was prepared additive free.

The concentrations of accessible sulfonate groups was evaluated by conductometric titration. The sample was titrated with 0.01M sodium hydroxide and back-titrated with 0.01 M hydrochloric acid²⁵.

The specific surface areas of the latex and films were measured by Brunauer-Emmett-Teller (BET) nitrogen desorption on a Quantasorb detector (Quantachrome Corp.). Nitrogen in a helium carrier stream was passed over the sample at various partial pressures by varying the flow rates of both gases

Table 1. Additives Used and Their Levels of Addition Based on Percentage Weight of PostCast Film

sample	glycerol (%)	sucrose (%)	L30D (%)	SSA (m^2/g)
GLY10	10			5.14
GLY15	15			6.52
GLY20	20			8.04
GLY25	25			9.02
SUC10		10		3.49
SUC15		15		6.75
SUC20		20		8.52
SUC30		30		10.1
L30D15			15	5.90
L30D20			20	6.67
L30D30			30	7.38
L30D40			40	8.71
NOADD				<0.5

Immersion of the sample in liquid nitrogen promotes adsorption on to the accessible surface of the film until equilibrium is reached. Warming of the sample after equilibrium desorbs the adsorbed nitrogen back into the carrier stream, which passes through a thermal conductivity detector where the amount of nitrogen was determined. Nitrogen adsorption at five partial pressures, between 0.1 and 0.3, were taken and incorporated into the BET equation, and the specific surface area of the sample was calculated. The Quantasorb continuous flow method of surface area determination has a high sensitivity allowing low specific surface areas to be determined.²⁶

Pore size distributions and pore volumes were determined by mercury porosimetry on a Porosimeter 2000 series mercury porosimeter (Carlo Erba Strumentazione). Film samples were placed in a dilatometer evacuated of air and then filled with mercury. Mercury is nonwetting and will not enter pores until a threshold pressure is reached relative to the pore diameter; smaller pores requiring higher pressures for mercury to enter them. The filled dilatometer was placed in an oil filled autoclave where the pressure was increased and the mercury intrusion volume noted for each pressure point. A plot of the pore radius against the change in volume of mercury intruded with change in pore radius gave the pore size distribution.

Electron micrographs of the films interior were obtained from gold-coated freeze-fractured samples on a Phillips XL30 scanning electron microscope.

The catalytic properties of the latex particles and films were evaluated by their ability to catalyse the hydrolysis of ethyl methanoate. The pseudo-first-order hydrolysis of ethyl methanoate to methanoic acid and ethanol is acid-catalyzed by the sulfonate groups on the polymer surface. The production of methanoic acid from the hydrolysis can be followed conductometrically and the relative rates of reaction found. One gram of polymer was mechanically stirred with 200 mL of DDW at 25 °C in a 250mL round-bottom flask. At thermal equilibrium 1 mL of ethyl methanoate was added and the change in conductance with time was recorded.

Results and Discussion

Sulfonated Latex Characterization. The latex surface as characterised by conductometric titration was found to be dominated by strong acid groups with no discernible weak acid contribution giving a total charge of (15.9 $\mu\text{mol/g}$). The average particle diameter measured by electron microscopy was found to be 500 nm (2 significant figures, 3% coefficient of variance), and the specific surface area was 12.7 m^2/g .

Film Characterization. Specific Surface Area. Films prepared using glycerol and sucrose additives, following leaching, show similar trends in specific surface area (SSA) with increasing additive content (Table 1). Films prepared using L30D, following

(23) Chainey, M.; Wilkison, M.C.; Hearn, J. *Ind. Eng. Chem. Prod. Res. Dev.* **1982**, *21*, 171.

(24) Chonde, Y.; Krieger, I.M. *J. Colloid Interface Sci.* **1980**, *77*, 138.

(25) Chainey, M.; Wilkison, M.C.; Hearn, J. *J. Colloid Interface Sci.* **1987**, *117*, 477.

(26) Lowell, S.; Shields, J.E. *Powder Surface Area & Porosity*, Chapman & Hall: London **1984**.

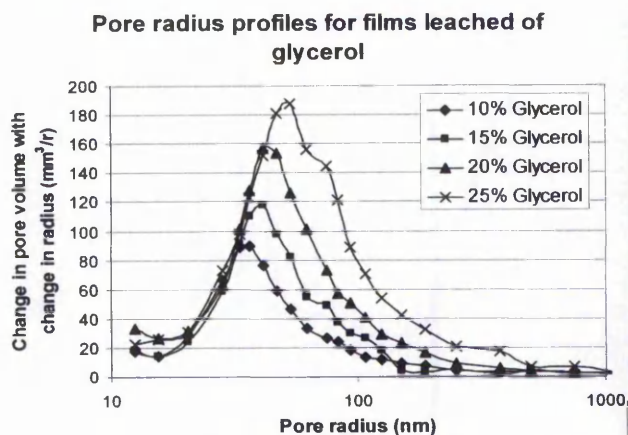


Figure 1. Pore radius profiles for films prepared using glycerol additive.

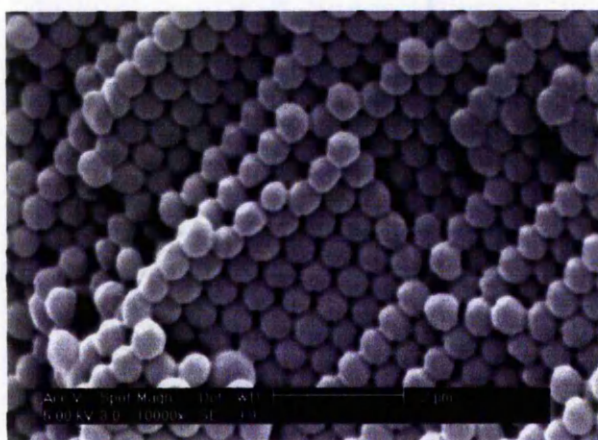


Figure 2. Scanning electron micrograph of film GLY20.

leaching, also show increasing SSA with additive content, but to a lesser extent. The films have less total surface area than the particles because of loss of surface from fusing of particles during casting. The SSA for film NOADD was too low for accurate determination using the Quantachrome apparatus.

Porosimetry. Pore radius profiles for films prepared using glycerol are shown in Figure 1. The profile trends show that with increasing additive content the total pore volume increased. The number average pore radius increased with additive content in all films. For films prepared using glycerol and sucrose the number of pores per gram increased with additive content, whilst films prepared using L30D showed a decrease in number of pores per gram with increasing additive.

Electron Microscopy. Micrographs of the freeze-fractured cross-section for films prepared using 20% weight of glycerol, sucrose, L30D and no additive are shown in Figures 2-5, respectively.

Films prepared using glycerol (Figure 2) and sucrose (Figure 3) show similar structural characteristics with particles close packed. The film prepared using glycerol has a higher degree of ordering than the sucrose film. A possible reason for this could be increasing viscosity of the sucrose solution as water leaves during film formation, hindering particle movement into the close packed arrangement. The film prepared using L30D (Figure 4) shows a disordered structure. This is due to the relatively large size of L30D, which cannot be pushed into interstices or exuded from the film, therefore stopping the development of the close-packed structure during drying. This results in the relatively open, random order seen in the micrograph. Films prepared using additives are held together by partial particle fusion with

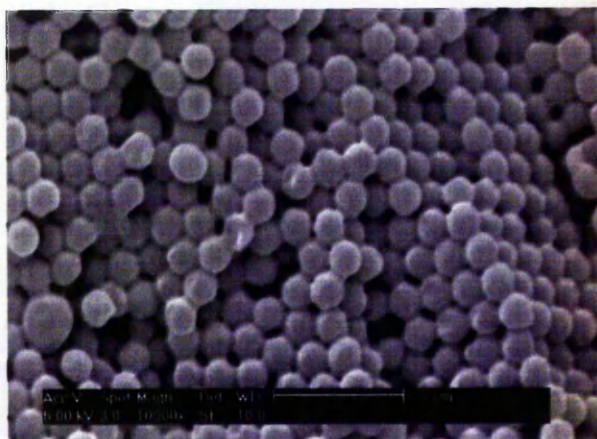


Figure 3. Scanning electron micrograph of film SUC20.



Figure 4. Scanning electron micrograph of film L30D20. Insert: film at higher magnification.



Figure 5. Scanning electron micrograph of film prepared with no additive.

neighbouring particles (Figure 4, insert). If no additive is used then no pores are formed in the sulfonated poly(butyl methacrylate) film (Figure 5).

Micrographs of films prepared using glycerol and sucrose are compatible with the idea that the additive becomes trapped in the interstices during film formation preventing full particle deformation. This produces a network of additive throughout the film, which is present in the final cast film. Leaching the additive leaves interconnecting pores spread throughout the whole film. At low amounts of additive, not all interstices between the

spherical particles form pores. Increasing the amount of additive in the film increases the number of interstices which are retained as pores and increases the average pore size because there is more trapped material. A different pore generation process is in operation for films prepared using L30D. L30D forms domains of particles within the film. Upon addition of more L30D these domains grow and join together forming larger and fewer domains, which in turn produce larger and fewer pores once L30D is removed from the film.

It has been shown previously that a successful pore-forming additive needs partial compatibility with the polymer.²² If the additive is too compatible, it will dissolve into the polymer; if too incompatible, it will be fully exuded to the surfaces and to islets within the film during the casting process.²⁷ L30D behaves differently; because of its large size in comparison to molecular additives, it will not get exuded out the film or dissolve into the film. This property makes L30D potentially more compatible for a wider range of latices as compared to the small molecular additives.

Surface Characterization. The charge density of the films is close to that of the original latex (SLATEX) across the additive range for all films (Table 2) except for film NOADD which had a charge density too low for determination by titration under the conditions used. At lower additive levels despite lower SSA the charge density is still high suggesting that during coalescence the polar groups tend to stay at the surface. This will enable the use of low amounts of additive, which would be favourable to film strength, while still retaining the majority of the functional groups. The fact that most of the functional groups are accessible is beneficial for improving reaction rates and would be helpful if the catalytic groups used were expensive to synthesise.

Catalytic Activity. All films prepared using an additive, give a rate of hydrolysis in the range 60-90% of the rate shown by the discrete latex particles (Table 2). The relative catalytic efficiency per μmole of sulfonate groups for all films and SLATEX are shown in Table 2. With increasing additive content, for all films an increase in rate is seen, and this can be attributed to the higher sulfonate group density available and to bigger pores reducing mass transfer restrictions. With increasing additive content, the relative efficiency of 1 μmole of sulfonate groups increases but never reaches that of SLATEX where mass transfer

Table 2. Charge Density, Relative catalytic Activity, and Relative Efficiency of 1 μmole of Charged Groups for All Samples

sample	charge density ($\mu\text{mol/g}$)	rel catalytic activity	rel efficiency of 1 μmol of charged groups
GLY10	13.7	67.7	78.6
GLY15	14.3	69.1	76.8
GLY20	14.4	70.6	77.7
GLY25	14.5	74.9	82.3
SUC10	13.4	62.0	73.6
SUC15	13.7	65.1	75.5
SUC20	14.4	71.1	79.1
SUC30	15.0	84.9	90.0
L30D15	14.5	67.4	73.6
L30D20	14.8	70.9	75.9
L30D30	15.0	78.9	83.6
L30D40	15.5	87.1	89.5
NOADD	<0.2	<2.0	
SLATEX	15.9	100.0	100.0

restrictions will be least, because of its dispersed state. This indicates that a proportion of catalytic activity in the films may be lost due to mass transfer restrictions.

Conclusion

Porous polymer films can be prepared from a functionalized latex by leaching of additives. The films retain 60-90% of the catalytic activity of the original latex particles, depending on the film preparation conditions.

The advantages of a catalytic polymer film compared with individual latex particles is the ease of removal from the reaction medium (literally lifted out) and subsequent cleaning, which can be achieved by repeated washing/decanting steps. In contrast, removal and cleaning of latex particles requires microfiltration or centrifugation, which are both time-consuming and potentially wasteful processes. Cleaning of the porous polymer films is a far simpler and quicker process.

(27) Zhao, C.L.; Dobler, F.; Pith, T.; Holl, Y.; Lambla, M. J. *Colloid Interface Sci.* 1988, 128, 437.

Chapter 13

Studies on Porosity in Polymer Latex Films

Ian C. Hodges, John Hearn, and Michael C. Wilkinson

Department of Chemistry and Physics, Nottingham Trent university,
Clifton Lane, Nottingham NG11 8NS, United Kingdom

Mechanisms for preparation of polymer latex films with permanent porosity in the dry state have been investigated. Leaching additives from cast films and exceeding the critical pigment volume fraction of a binder were assessed for their void generating characteristics. Leachable additives successfully used included sucrose, polyvinyl pyrrolidone, sodium diphenyl ether disulphonate, and pH dependent soluble polymer latex. Specific surface area and porosimeter studies were used to evaluate the effectiveness of each pore generating mechanism.

Initial studies on the transport properties of these porous latex films were evaluated via dynamic adsorption and advantages shown. Samples of a well characterized carbon adsorbent coated in non porous and porous latex films were compared to determine hindrance to vapour sorption.

Porous colloidal particles based on the principles of macroreticular resin synthesis, but utilizing emulsion polymerization have been produced. Incorporation of these porous particles into porous latex films to enhance surface area was investigated and proved reasonably efficient.

Differences in pore characteristics of porous films where interstitial water is removed by sublimation compared to evaporation were used to illustrate an effect of capillary forces on pore closure.

Introduction

The best barrier properties are usually obtained in latex films when the particles are well ordered prior to the final stage of film formation, when polymer chains interdiffuse, so as to achieve maximum density without voids or defects^{1,2}. Films with low porosity and low surface area have better film qualities such as scrub resistance³. The highest degree of ordering is usually

achieved when the latex particles have a monolayer coverage of surfactant with higher levels of addition resulting in an inferior performance⁴. When latex films are used as binders these same barrier properties can be a disadvantage where access to reactive or adsorptive sites is required. Transport pores are then desirable in a latex film⁵. Steward⁶ has shown that water leachable materials added to polymer latex films can be used to control solute permeability. This was attributed to water filled pores, but when films having Tg's below room temperature were allowed to dry, porosity was lost as a consequence of further film formation processes.

The aim of this study is to extend this approach to the creation of porosity in dried latex films by additive leaching and to explore other possible routes to pore creation by deliberate reductions in latex stability prior to film formation and by exceeding critical pigment volume fractions (CPVF). The latter is a method used in the coating industry to prepare 'breathable paint'. This involves adding excess pigment or filler so that there is enough binder to glue the particles together, but not enough to completely fill interstitial voids.

For successful production of porous films, leachable additives must neither be too compatible nor too incompatible. If too compatible with the polymer then it may dissolve into the particles producing a homogenous film, whereas an incompatible additive may be completely exuded from the film during coalescence. Work by Zhao⁷ *et al* measured surface concentrations of sodium dodecyl sulphate (SDS) and sodium diphenyl ether disulphonate (SDED) in coalesced acrylic latex films. It was found that SDS readily migrated to the films surfaces (film-air and film-casting substrate) and continued to be exuded to the surface during film maturation. However, SDED had a much less pronounced surface enrichment that did not change during film aging, indicating better polymer compatibility.

Successful pore generation can be evaluated by nitrogen adsorption and mercury porosimetry. These techniques evaluate the specific surface area and the pore size distribution respectively.

Barrier characteristics of prepared films can be evaluated via dynamic adsorption. This measures the ability of a packed bed of adsorbent to adsorb a vapour from an inert gas flowing through the bed. If the kinetics of vapour sorption are inhibited by the presence of the latex film then the adsorbent may not be able to utilise its full capacity before vapour breaks through the packed bed. Comparison of the dynamic adsorption profiles for the coated and uncoated adsorbent would then indicate the degree to which the polymer film hinders access of adsorbate to adsorptive sites.

Also of interest is production of colloidal porous particles, based on production of macroreticular resins, for potential use in reactive films. Macroreticular beads are commonly produced by suspension polymerization of styrene and divinyl benzene in the presence of a porogen (usually an organic solvent) producing millimetre size beads. Previous studies on emulsion polymerization of vinyl and divinyl monomers have been carried out, but without the incorporation of porogens⁸. During macroreticular resin synthesis the growing crosslinked polymers precipitate out of the porogen producing amalgams of polymer. Removal of porogen after reaction results in a permanent

porosity throughout the bead even when dry. Reaction of the monomers without a porogen results in a gel type resin that only has porosity when swollen with solvent. Adaptation of this process to emulsion polymerization was to be evaluated for the production of macroreticular particles with diameters in the nanometre range. This would facilitate their incorporation into a polymer film, which could then be utilized for its high surface area.

The aim of this paper is to report preliminary findings from ongoing research into pore development in latex films and in latex particles.

Experimental

Latex films were formed from four main base latices, which were soap free poly(styrene) (PS) ($\text{\O} 525\text{nm}$) and poly(butyl methacrylate) (PBMA) ($\text{\O} 320\text{nm}$) both prepared in-house, and Eudragit® L30D (ethyl acrylate/methacrylic acid), and Eudragit® NE30D (ethyl acrylate/methylmethacrylate) (Röhm Pharma). L30D is water soluble at $\text{pH}'\text{s} > 7$ and NE30D has a T_g below room temperature. Other water soluble additives investigated were, sucrose, hydroxypropyl methyl cellulose (HPMC), sodium dodecyl sulphate, Dowfax 2A1 (SDED), polyvinyl pyrrolidone, and sodium chloride. Films were cast at 40°C in glass rings and plates sealed with silicone grease. In the case of films incorporating water soluble additives the resulting cast films were soaked in distilled water until the additive was no longer detectable in the wash water.

Porous colloidal particle production was based on macroreticular resin preparation with modification of the polymerization type. The organic phase consisted of styrene (Aldrich), divinylbenzene (BDH Chemicals Limited), and toluene (Aldrich), which was emulsified in water containing the surfactant Aerosol OT-100 (Fisher Scientific U.K. Limited). Polymerization was initiated by potassium persulphate at a reaction temperature of 80°C for 6 hrs.

The specific surface areas of the final films were measured by BET nitrogen desorption on a Quantasorb detector (Quantachrome Corporation). Nitrogen in a helium carrier stream is passed over the sample at various partial pressures by varying both gases flow rates. Immersion of the sample in liquid nitrogen promotes adsorption on to the accessible surface of the film until equilibrium is reached. Warming of the sample after equilibrium desorbs the adsorbed nitrogen back into the carrier stream, which passes through a detector where the amount of nitrogen desorbed is determined. Nitrogen adsorption at five partial pressures, between 0.1 and 0.3, were taken and incorporated into the BET equation⁹ and the specific surface area of the sample was calculated. The Quantasorb continuous flow method of surface area determination has a high sensitivity allowing low areas to be determined.

Pore size distributions and pore volumes were determined by mercury porosimetry on a Porosimeter 2000 series mercury porosimeter (Carlo Erba Strumentazione). Films samples are placed in a dilatometer evacuated of air and

filled with mercury. Mercury is non-wetting so will not enter pores until a pressure is reached relative to the pore diameter, smaller pores require higher pressures for mercury to enter them. The filled dilatometer is placed in an oil filled autoclave where the pressure is increased and the mercury intrusion volume noted for each pressure point. A plot of the pore radius against the change in volume with change in pore radius gives the pore size distribution.

The barrier characteristics of the latex films were evaluated by dynamic adsorption of methanol as a model vapour on a base carbon adsorbent coated in latex film. The dynamic adsorption apparatus has been described previously¹⁰. 12-30 mesh granules of steam activated coal based carbon BPL (Chemviron) were dip coated in latex. Methanol was carried through a volume activity tube packed with granules by nitrogen carrier gas (1 l/min) at 1 mg/l, 0% relative humidity, and 25°C and the exhaust concentration monitored with time by infrared spectrometry (Miran model 1Acvf).

Results & Discussion

Porous Latex Films

Specific Surface Area

Of the methods tried, the most promising results were for the films obtained by leaching L30D, sucrose, PVP, and SDED from PBMA, and those obtained by exceeding the CPVF of NE30D with PS.

For L30D leaching experiments, PBMA films were cast with varying amounts of L30D based on the dry film weight with subsequent extraction of L30D by washing with 0.2M sodium hydroxide. For sucrose, PVP, and SDED leaching experiments, PBMA films were cast with varying amounts of each additive based on dry film weight with subsequent extraction by washing with distilled water. All films were freeze dried after additive leaching and their specific surface areas evaluated and the results are shown in figure 1. For the CPVF experiments, NE30D was cast with various loads of PS above its CPVF resulting in voids between PS particles. No further treatment was required after casting. The specific surface areas of these films are also shown in figure 1.

Study of the results reveals that L30D leached films show an increase in specific surface area with increasing L30D loading. This indicates that at the lower loadings there are large domains of film formed PBMA with limited access to the surface area of the original particles within the domain. With increasing L30D loadings these domains become smaller so more surface area is available for adsorption.

Films leached of sucrose, PVP, and SDED both show higher specific surface areas with increasing additive loading, in the same way as L30D. For sucrose films containing loadings greater than 35% no films were attainable, due to the washing step redispersing the polymer particles. This suggests that larger amounts of sucrose hinders particle-particle contact restricting coalescence of the film. PBMA films with PVP and SDED loadings greater than 25% and 45% respectively, also suffer from redispersion during the washing step. The film leached of 45% SDED shows no increase in surface area compared to leaching at 29%. This indicates that a certain point can be reached where the polymer domains will not get any smaller so no extra surface of the original particles can be accessed.

In CPVF experiments, a gradual decrease in specific surface area is seen with increasing NE30D loading. This is in accord with the assumption that larger NE30D loadings cover more of the polystyrene spheres and will begin to block interstices completely.

Visual examination of fracture cross-sections of the films shows opacity running all the way through the film from top to bottom. This indicates that the pores are interconnecting, else leaching additive completely from the film interior would not be possible. Examination of unsuccessful films shows opacity at the top and bottom only, with a transparent interior. This indicates the additives inability to form the continuous network required for leaching, resulting in the final films poor performance.

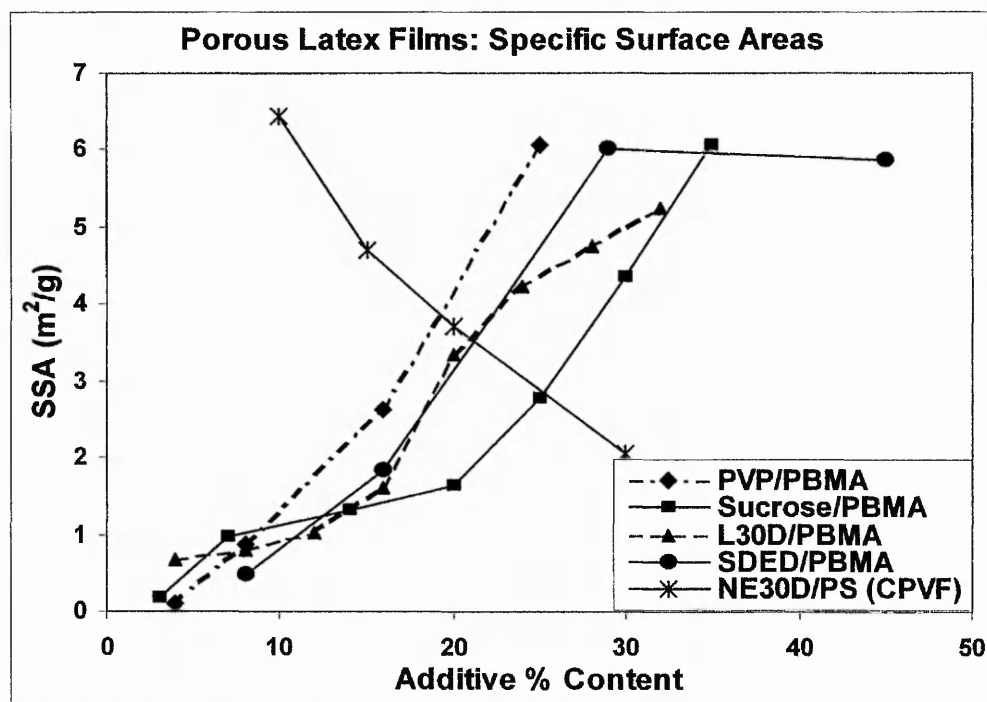


Figure 1. Comparison of specific surface areas for prepared films.

Porosimetry

The porous nature of all films was determined by mercury porosimetry for each pore generating process. Pore size profiles for PBMA films leached of L30D, and CPVF-exceeded NE30D are shown in figures 2 & 3 respectively. The trends in total pore volume for all films are shown in figure 4.

PBMA films leached of L30D show a general increase in pore radius and cumulative pore volume with increasing amount of L30D leached (fig 2 & 4). All films contain relatively the same amount of small pores, but with increasingly larger pores being added with increasing amounts of L30D. This indicates that with more L30D spheres present, larger agglomerates of L30D can be formed in the cast film which will produce larger pores once leached out.

PBMA films leached of sucrose show a decrease in pore radius and total pore volume with increasing amount of sucrose leached. This suggests that with higher sucrose loadings sugar is more easily expelled from the film possibly due to more complete migration channels to the surface formed during drying. This results in more sucrose exuded to the surface and less sucrose inside the dry film.

PBMA films leached of PVP show an increase in total pore volume with increasing amount of PVP leached, while the average pore radius stays relatively unchanged. This indicates that PVP separates out into domains of a single size. Addition of more PVP increases the number of pores while the pore radius stays constant.

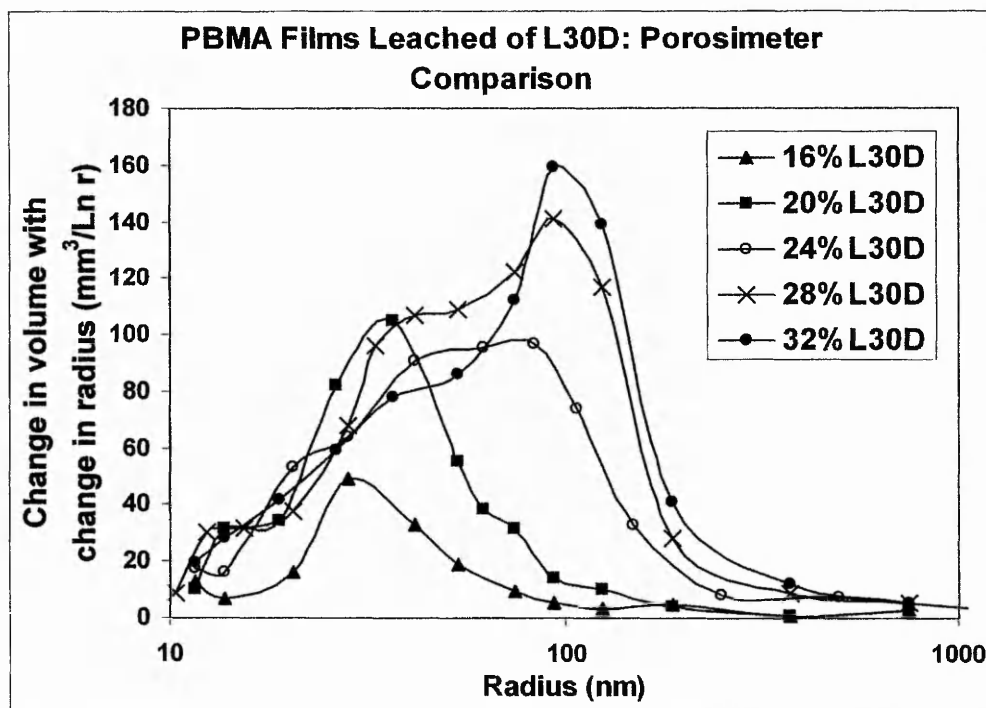


Figure 2. Comparison of pore radius profiles for films leached of L30D.

PBMA films leached of SDED show increasing total pore volume with increased loadings, while the average pore radius stays relatively unchanged. This indicates, like PVP, that SDED forms domains of a similar size and on addition of more additive increases the number of pores.

Films prepared by exceeding the CPVF of NE30D with PS have a relatively narrow pore size distribution and high total pore volumes (fig 3 & 4). At low amounts of NE30D there are two apparent pore size distributions close together. As NE30D loading is increased firstly the larger pore distribution is reduced leaving only the smaller, and then secondly the smaller distribution is reduced until no pores are present. The narrow pore radius distribution is due to the uniform interstices formed from the monodisperse PS latex. The reduction in total pore volume with increasing NE30D content is due to the filling of the interstices with polymer, which is also apparent in the specific surface area loss (fig 1).

Porous Latex Films: Exceeding CPVF of NE30D with PS

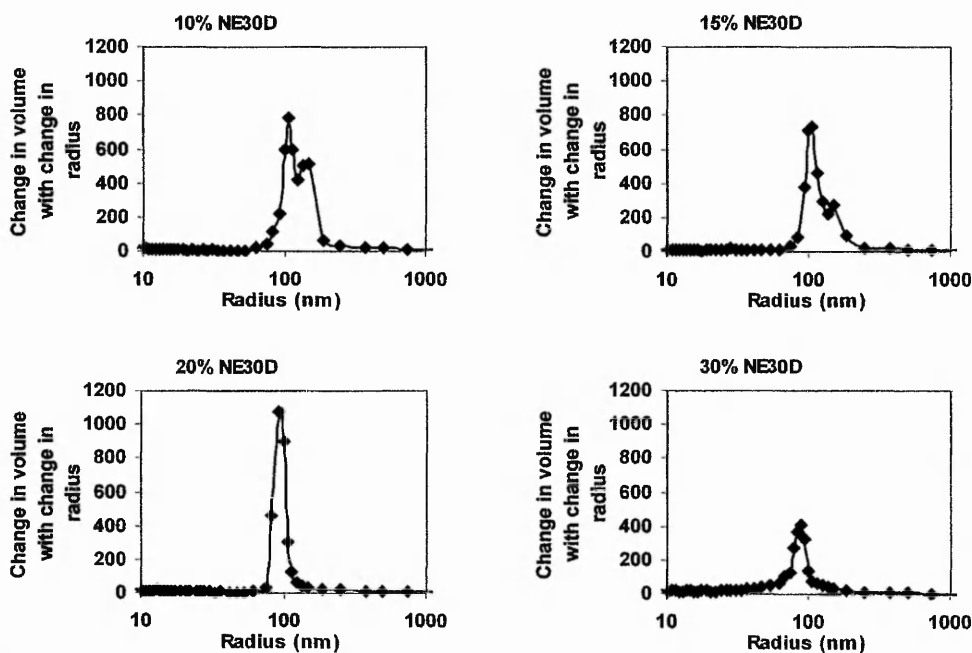


Figure 3. Comparison of pore radius profiles for films prepared by exceeding the CPVF of NE30D with PS.

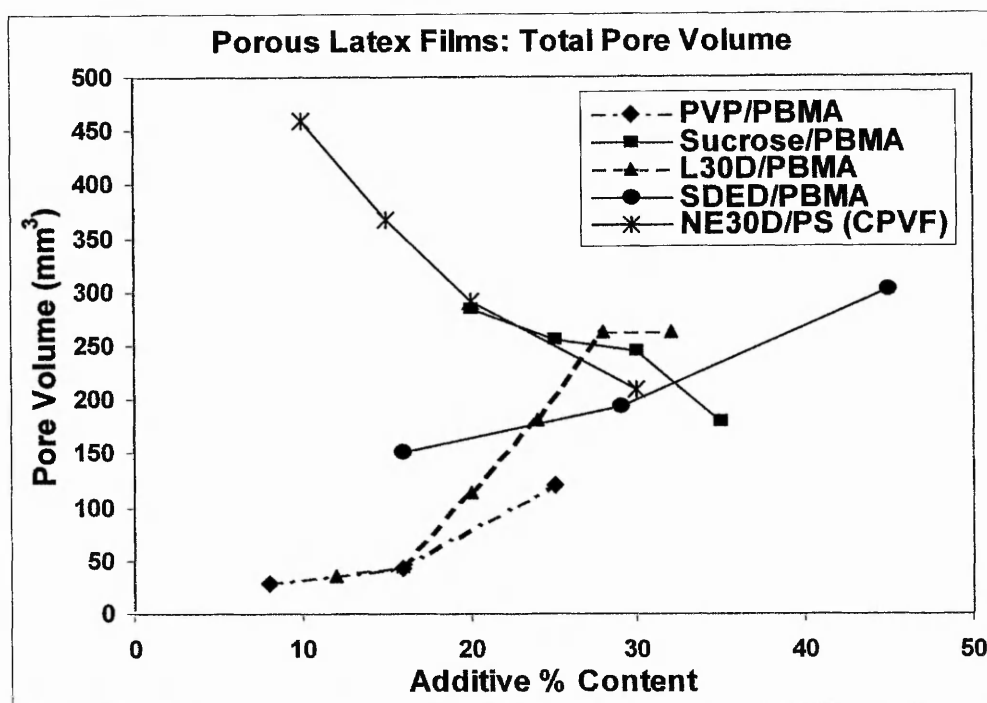


Figure 4. Comparison of total pore volume for prepared films.

Leaching HPMC, sodium dodecyl sulphate, and low concentrations of sodium chloride were ineffective in producing films with detectable specific surface areas under the casting conditions used. Limited solubility of HPMC in water, prevented films being formed with high enough quantities to form a porous film. After leaching only the surface of the film was opaque while the interior was still transparent. The degree of opacity is a good indication of porosity due to light scattering by a large number of small pores (unless the pores are significantly smaller than the wavelength of light).

Only small amounts of sodium chloride could be added to the latex without affecting stability. These small quantities were not effective for pore generation.

Sodium chloride was added to the latex in quantities so that some films were prepared from initially flocculated latex. Other films were cast from stable latex, but flocculation occurred at various stages of casting as the serum ionic strength increases during water evaporation. All films prepared by this method were very opaque and, in the case of higher sodium chloride contents, rough textured. Although pores were present in the film, indicated by the opacity, no surface area could be determined. This suggests that the majority of pores are inaccessible and are in the form of air pockets trapped within the polymer.

Films prepared by leaching SDS showed only surface opacity with a transparent interior. Du Chesne¹¹ *et al* showed that incompatible stabilizers migrate to the film surfaces and to islets within the polymer film. These islets may not be accessible to leaching so only the surface surfactant will be removed resulting in very little porosity. The successful pore generation by SDED compared to SDS illustrates the importance of partial additive-polymer compatibility for porous film production.

Good reproducibility of the pore radius profiles were found for films prepared under the same set of conditions, but on different dates.

Pore Closure

Films prepared for this study from poly(butyl methacrylate) with various loadings of leachable Eudragit® L30D show a different range of pore sizes between each film. The lower loadings form relatively small pores while higher loadings add larger pores to the profile (fig 2). After casting and leaching of L30D from the film a porous PBMA film is left with all pores filled with water. These films are effectively at film formation stage two as the particles are already ordered and partly coalesced. These films were divided into two halves, which were dried differently. One half was dried in a nitrogen gas stream at room temperature and the other half freeze dried so that water sublimed rather than evaporated from pores within the film. After freeze drying was complete, it too was kept at room temperature for an equal time as the nitrogen dried sample, before both halves being stored at 4°C ready for analysis.

The specific surface area results for freeze dried and nitrogen dried films are shown in figure 5. Nitrogen dried samples with low additive contents show complete loss of surface area compared to their freeze dried counterparts. As additive content increases the difference in surface area between nitrogen dried and freeze dried samples decreases until little difference is noted.

Comparison of the pore radius profile for films leached of 10% and 30% L30D both freeze and nitrogen dried are shown in figure 6.

Films prepared from 10% L30D show similar pore radii by both methods of drying, but the nitrogen dried sample shows a reduced number of pores suggesting pore closure. This pore closure is responsible for the differing specific surface areas seen for these two films.

Films prepared from 30% L30D by both drying regimes have similar pore radius profiles at similar heights indicating little difference in pore characteristics between the two. This is evident in the similar specific surface area obtained for both these samples. This indicates that films with only small pores further coalesce during nitrogen drying, but if larger pores are present less coalescence is seen. Pore closure can arise through viscoelastic deformation caused either by polymer-water interfacial tension (wet sintering)¹²; polymer-air interfacial tension (dry sintering)¹³ or from the water-air interfacial tension (capillarity)¹⁴. Both film halves experienced a similar period of leaching, so that wet sintering is unlikely to lead to a difference and both films experienced a

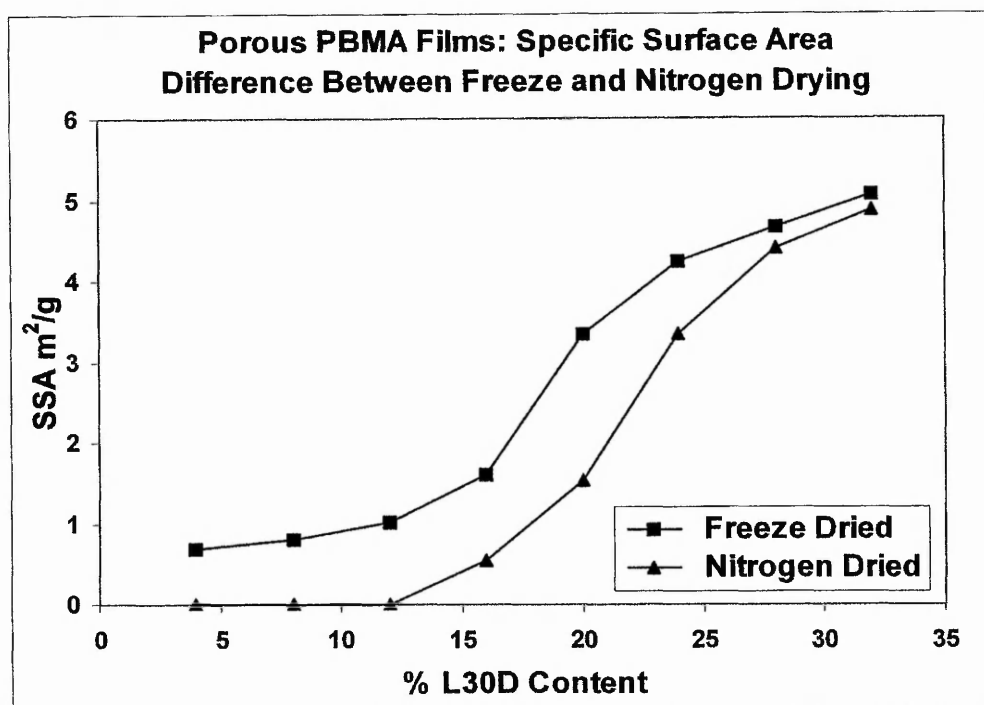


Figure 5. Comparison of the different specific surface areas found between freeze and nitrogen drying.

similar period in a dry state at room temperature, so that dry sintering is also an unlikely cause. It is thus tentatively suggested, since it is a matter of much debate¹⁵ whether water has a direct role to play in the mechanism of film formation from hydrophobic latex particles, that pore closure is driven by capillary forces as water evaporates from fine pores. These forces being proportional to pore radius, have the greatest effect on the population of small pores. Lin & Meier¹⁶ have also claimed a role for water and capillary forces in film formation from hydrophobic latex particles.

Macroreticular Colloid Particles

The preparation of porous particles based on macroreticular resin synthesis, but using emulsion polymerization has resulted in the production of stable colloidal latices with particle diameters of 100nm and specific surface areas of $\sim 200\text{m}^2/\text{g}$. The pore characteristics were evaluated via full nitrogen adsorption/desorption isotherms and two peaks were found between 2 and 4 nanometres indicating presence of pores in the microporous range.

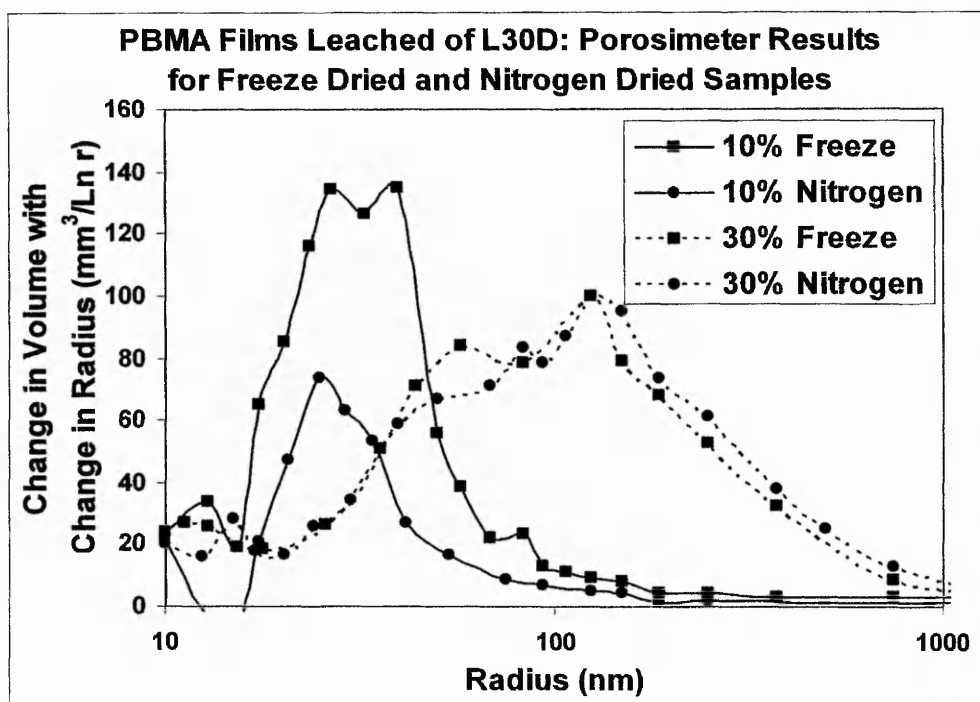


Figure 6. Comparison of the pore radius profiles for films leached of 10% and 30% L30D under different drying conditions.

Addition of this latex into NE30D (25% NE30D loading) above its CPVF resulted in a film with a specific surface area of 95 m²/g. The relatively high surface area of this film shows potential for development into a reactive film. Approximately half the surface area of the porous particles is lost. Study of the specific surface area graph for NE30D films exceeding CPVF with PS (fig 1) shows that there is scope to increase the surface area further.

Dynamic Adsorption

Dynamic adsorption profiles for plain BPL carbon, non-porous latex coated carbon, and porous latex coated carbon are shown in figure 7.

The latex coat consisted of PBMA and L30D at 50% loading. The non-porous coat involved no leaching and the porous coat required removal of L30D via washing. Plain BPL carbon shows a typical profile¹⁰ with an initial period (~10 minutes) where no vapour passes completely through the bed. The non-porous latex coated sample shows an immediate and rapid increase in methanol exhaust concentration indicating severe loss of performance. The porous latex coated sample has an initial period with no methanol in the exhaust stream (~3 minutes) and a slower rate of adsorption compared to the plain carbon sample.

Integration of the area above the curves gives the total amount of methanol adsorbed per sample and shows that the plain and porous coated carbons have adsorbed approximately the same amount. Although the porous coated sample showed poorer dynamic performance than the plain sample the results indicate that the adsorbent sites are still accessible, but at a slower rate.

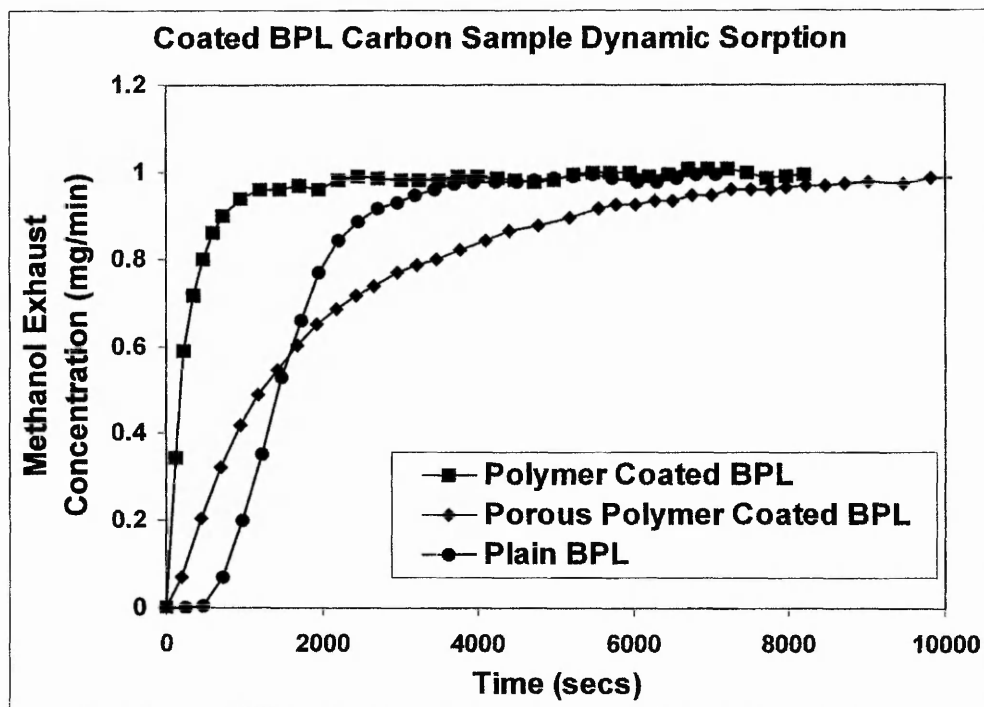


Figure 7. Comparison of dynamic adsorption profiles for polymer coated, porous polymer coated and plain BPL carbon.

Conclusions

Polymer films prepared from coalescence of polymer binder latex have been formed with permanent porosity in the dry state. Voids have been formed by leaching additives from cast films and by exceeding a binders critical pigment concentration. The number of small pores retained depends upon the method of drying used.

Initial studies on the transport properties of these porous latex films have been evaluated via dynamic adsorption. Carbon adsorbents coated in porous latex show their complete adsorption capacity for a vapour, but at a slower adsorption rate compared to plain carbon performance, whereas with a non porous film their capacity is lost completely.

Production of porous colloidal particles has been achieved based on macroporous resin synthesis utilizing emulsion polymerization. Incorporation of these porous particles into porous latex films to enhance available surface area has been successful.

The potential functionalization of these porous latex films to produce reactive films, offers the advantages of ready access to a high surface area of colloidal size particles whilst avoiding the difficulty of recovery from the reaction product. Functionalized lattices for example are deliberately destabilized and sedimented destroying their potential for further use. Porous binder films offer the prospect of improved adsorbent performance and its complement the potential for sustained release.

References

1. Roulstone B.J., Wilkinson M.C., Hearn J., *Polym. Int.*, 27, p43-50, (1992)
2. Okubo M., Takeya T., Tsutsumi Y., Kadooka T., Matsumoto T., *J. Polym. Sci., Polym. Chem. Ed.*, 19, p1-8, (1981)
3. Isaacs P.K., *J. Macromol. Chem.*, 1 (1), p163-185, (1966)
4. Juhué D., Lang J., *Colloids & surfaces A: Physico. Chem. Eng. Aspects*, 87 p177-185, (1994).
5. Lyngberg O.K., Scriven N.E., Flickinger M.C., Abstracts of papers of the American Chemical Society, Vol.216, No.Pt3, p35-BTEC, (1998).
6. Steward P.A., Hearn J., Wilkinson M.C., Wilson A.J., Roulstone B.J., Ch.23 in ACS Int. Symp. Ser. No. 648, p359-402, *Film Formation in Waterborne Coatings*, Eds. Provder, Winnick & Urban, (1996).
7. Zhao C.L., Dobler F., Pith T., Holl Y., Lambla M., *J. Colloid and Interface Science*, 128, 2, p437-449, (1988).
8. Tobita H., Hamielec A.E., *Polym. Int.*, 30, p195-201, (1993).
9. Brunauer S., Emmet P.H. Teller E., *J. Am. Chem. Soc.*, 60, p309, (1938).
10. Karpowicz F., Hearn J., Wilkinson M.C., *Carbon*, 33, 11, p1573-1583, (1995).
11. Du Chesne A., Gerharz B., Lieser G., *Polym. Int.*, 43, p187-196, (1997).
12. Vanderhoff J.W., Tarkowski H.L., Jenkins M.C., Bradford E.B., *J. Macromol. Chem.*, 1(2), p361-397, (1966).
13. Dillon R.E., Matheson L.A., Bradford E.B., *J. Colloid Sci.*, 6, p108-117, (1951).
14. Brown G.L., *J. Polym. Sci.*, 22, p423434, (1956).
15. Sperry P.R., Synder B.S., O'Dowd M.L., Lesko P.M., *Langmuir*, 10, p2619-2628, (1994).
16. Lin F., Meier D.J., *Langmuir*, 11, p2726-2733, (1995).